Spatiotemporal controls on nutrient source and transport in Puget Sound rivers

Elizabeth Elmstrom

A dissertation

submitted in partial fulfillment of the

requirements for the degree of

Doctor of Philosophy

University of Washington

2024

Reading Committee:

Gordon Holtgrieve, chair

Daniel Schindler

Mark Scheuerell

Program Authorized to Offer Degree:

School of Aquatic and Fishery Sciences

University of Washington

Abstract

Spatiotemporal controls on nutrient source and transport in Puget Sound rivers

Elizabeth Elmstrom

Chair of the Supervisory Committee:

Gordon Holtgrieve

School of Aquatic and Fishery Sciences

Understanding the factors controlling nitrogen (N) and phosphorus (P) in rivers is critical to preserve ecosystem functioning from land to the coast yet challenging given the complexity of climate and landscape interactions. These interactions operate across multiple spatial and temporal scales, often manifesting differently across rivers depending on watershed-scale controls, underscoring the need to study river N and P dynamics across diverse systems. My dissertation research investigates river N and P sources and transport in a human-influenced, mountainous region in western Washington state, aiming to disentangle the roles of climate and landscape variation in driving nutrient entry and delivery in coastal rivers. Using two large regional datasets at different temporal scales (i.e., seasonal, multi-decadal), I demonstrate the strong influence of regional and macro-scale climate patterns in driving seasonal river nutrient transport regimes, while highlighting the distinct role of watershed topography modifying river

nutrient responses to hydroclimatic change. Further, by using stable isotopes to trace N sources in rivers, I show the origins of N entering these human-influenced, coastal rivers are closely linked to upland soils in the forested landscape, the flushing of which is dependent on seasonal climate. To mitigate the effects of climate and landscape alterations on riverine ecosystems, there is a pressing need to understand how the interaction of ecological controls will play out across river systems. Findings from my dissertation research elucidate these interactions, demonstrating the strength of climate and the physical environment in driving river nutrient delivery to the coastal environment, and enhancing the predictability of river nutrient transport in mountainous regions facing increasing impacts from climate change and human activity.

Table of Contents

LIST OF FIGURES

LIST OF TABLES

ACKNOWLEDGEMENTS

My dissertation research was partially funded by the Department of the Interior's Northwest Climate Adaptation Science Center Graduate Fellowship and by the University of Washington School of Aquatic and Fishery Sciences (SAFS) Admissions and Finishing Fellowships. I also gratefully acknowledge funding from the NOAA National Estuarine Research Reserve Margaret Davidson Fellowship, which supported my professional development and research interests in riverine and coastal biogeochemistry. Additionally, I am thankful to SAFS for their support throughout my graduate career through two teaching assistantships and one reader/grader position.

I owe a special thanks to my advisor, Dr. Gordon Holtgrieve, for welcoming me into his lab and for challenging me to think more broadly and deeply as an ecologist and biogeochemist. Gordon, you are brilliant in your craft of bridging fundamental ecology with advanced methods and forward-thinking questions. I grew enormously as a scientist during my time working with you, and I am grateful to have watched you advance the field of ecosystems science throughout my PhD journey. Thank you for your mentorship, your friendship, and your abundant empathic support.

I also extend my gratitude to my other committee members, Drs. Daniel Schindler, Mark Scheuerell, Kathi Jo Jankowski, and Randie Bundy, who were all instrumental in my research and scientific growth in their own unique way. Daniel, thank you for challenging me to remain question-driven in my scientific pursuits and for pushing my science forward in depth and quality. I always left your office with my scientific questions at the forefront and a newfound sense of direction. Mark, this dissertation would not exist without the countless hours you spent guiding me through statistics and time series models. Thank you for always making time for me,

for making statistics approachable and exciting, and for the dedication you showed to my research. Whenever I felt most lost in the biogeochemical weeds, I knew I could reach out to Kathi Jo for her thoughtful and genuinely helpful feedback. Kathi Jo, thank you for being a mentor over so many years and for setting a powerful example of what to strive for as a biogeochemist. My GSR, Randie, brought a calming and supportive presence to every meeting. Randie, thank you for consistently showing up for me, offering valuable career advice, and asking thought-provoking questions that bridged oceanographic and riverine science.

I am deeply grateful to the Washington Department of Ecology for providing the water samples used in the nitrate stable isotope analysis for Chapters 1 and 3, as well as the long-term monitoring data on dissolved inorganic nitrogen and phosphorus for Chapter 2. Thank you to all the staff at the Washington Department of Ecology whose contributions to the Freshwater Information Monitoring Program over the past 30 years made this research possible. Additionally, the lab component of my research would not have been possible without the support of Andy Schauer, IsoLab's lead research engineer, as well as the laboratory assistance of Karrin Leazer and Sydney Clark. Andy, thank you for making my time in IsoLab a highlight of my early graduate career and for the many hours you spent troubleshooting Brave Irene and the denitrifier method. Although not included in this body of work, I also want to express my gratitude to those who supported my side project studying eelgrass ecosystem metabolism in Padilla and Samish Bays. To the Padilla Bay Research Reserve team—including Dr. Sylvia Yang, Heath Bohlmann, Nicole Burnett, Roger Fuller, Suzanne Shull, Dr. Jude Apple, and others—thank you for teaching me everything from sensor calibration in the lab to navigating the intertidal flats and deploying sensors in the field. You are an exceptional team, and I am grateful to have witnessed your success in educating others and advancing ecological research.

Graduate school is a journey, and I could not have reached this point without the support of my peer scientists, both at SAFS and at institutions elsewhere, who showed up for me both personally and professionally, ultimately becoming my closest friends. A huge thanks to these hidden mentors and friends in the SAFS community: Michaela Lowe, Ben Miller, Sam May, Marie Zahn, Jenny Stern, Katie McElroy, Megan Feddern, Eileen Bates, Lindsay Alma, and Grant Adams. I am equally grateful to my science companions and friends from Woods Hole: Kelsey Gosselin, Caroline Owens, Robin Littlefield, and Joy Belamarich. All of you have stood by me through so much, and your support has been one of the most rewarding aspects of my scientific career. I also want to thank all members of the Holtgrieve lab for listening to so many iterations of my work and for offering valuable feedback that pulled me out of the weeds. Finally, I most certainly would not have made it through the last year of graduate school without my writing group. Thank you for your accountability and camaraderie as we reached our final goal.

Above all, I owe my greatest appreciation and love to my family and my life partner. To my parents, Kurt and Ellen, thank you for instilling me with a love of the outdoors and a passion for conservation. I love you both as my parents and as my best friends. To my sisters, Anna, Sarah and Leah, thank you for all the phone calls, messages, and for supporting me through all my crazy science and outdoor adventures. And, finally, to my life partner, James, the love and laughter of our relationship carried me through the most challenging moments of this journey. Thank you for your constant encouragement of my curiosity and for always supporting me to pursue my dreams.

DEDICATION

To my dad, Kurt, who taught me to explore.

INTRODUCTION

Rivers and streams play a distinct role in regulating watershed ecosystem functioning through their ability to transform and transport nutrients from land to the coastal ocean (Aufdenkampe et al., 2011; Boyer et al., 2006). Dramatic increases in the transfer of nitrogen (N) and phosphorus (P) to freshwaters from human activities have stressed the bounds of river processes, fundamentally altering the delivery of N and P downstream and threatening freshwater and coastal water quality (Battye et al., 2017; Galloway et al., 2004; Vitousek et al., 1997). Understanding the source and delivery of N and P between watershed components and across river systems is critical to preserve ecosystem functioning but challenging given the complexity of landscapes (Goyette et al., 2019a; Jankowski & Schindler, 2019), and the temporal structure of river hydrologic regimes (Knapp et al., 2020; Perakis, 2002). Furthermore, climate-induced shifts in temperature and precipitation are altering river hydrologic regimes across the globe (Nijssen et al., 2001; Poff, 1992), while the broad ranging effects of land-use change continue to result in myriad water quality issues, such as eutrophication and hypoxia (Blaszczak et al., 2022; Hale et al., 2016). To understand how land use and climate-induced shifts interact across landscapes to influence aquatic ecosystem health, we need to identify the fundamental controls that govern river N and P biogeochemical fates across broad spatial and temporal scales (Heffernan et al., 2014; Soranno et al., 2014, 2019).

Traditional ecosystems science has long emphasized the importance of terrestrial and hydrologic controls on biogeochemical cycling at the watershed scale (Bormann et al., 1968; Bormann & Likens, 1967). In 1968, Hubbard Brook scientists tested the small watershed concept in which scientists manipulated entire watersheds to understand the controls on nutrient losses

from terrestrial ecosystems (Bormann et al., 1968). By clear-cutting the forest of a small watershed, this study showed deforestation decreased the watershed capacity's to retain water and nutrients, substantially increasing streamflow and N loads to streams in response to precipitation (Bormann et al., 1968). This approach inspired new ways of thinking and led to the foundational concept in aquatic ecosystems ecology that the structure and functioning of freshwater ecosystems are tightly linked to their terrestrial counterparts (Hynes, 1970; Likens, 1984). Since then, watershed-scale studies continue to show that terrestrial uplands are fundamental to riverine organization, and that variations in land use and land cover strongly influence water and nutrient fluxes from watersheds to rivers and streams (Barnes & Raymond, 2010; Lewis & Grimm, 2007). Notably, while medium to large rivers (discharge ranging from 10 to >100 m^3/s) are recognized as key players in biogeochemical cycles (Boyer et al., 2006), early research on watershed nutrient dynamics typically focused on smaller first- and second-order streams (discharge <0.1 m^3/s) (Mulholland et al., 2008; Strahler, 1952). As a result, our understanding of nutrient biogeochemistry at intermediate to large watershed scales remains relatively limited (Alexander et al., 2009; Mulholland et al., 2008; Wollheim et al., 2006), particularly in the context of climate and landscape interactions (Soranno et al., 2014).

Further, although river N and P cycles are often studied in the context of their surrounding land use and land cover, the source, quantity, and delivery of N and P are also closely related to watershed topographic features, such as elevation, slope, or valley form (Connolly et al., 2018a; Goyette et al., 2019a; Schiff et al., 2002). In watersheds with steep slopes, strong energy gradients and reduced plant and soil development promote rapid infiltration of precipitation and low uptake of N and P (Schiff et al., 2002; Sebestyen et al., 2019), such that nutrients quickly reach streams and are transported downriver (Bourgeois, Savarino, Némery, et

al., 2018a). Lower relief areas instead have longer water residence times and increased vegetation and soil organic matter, which enhances nutrient uptake and reactivity while decreasing precipitation-driven flushing of N and P to streams (Connolly et al., 2018a; Schiff et al., 2002). These processes, however, are often confounded by landform's influence on the spatial distribution of human activity. Lower sloped areas, for instance, are more amenable for human development and agricultural practices, promoting the accumulation of N and P sources, altering hydrologic flow paths, and enhancing potential for nutrient mobilization (Goyette et al., 2019a). Decades of human activity on flatter land have substantially increased the accumulation and leaching of N and P through soils (Van Meter et al., 2016), while the direct routing of nutrients through tile and storm drains has amplified precipitation-driven pulses of N and P to streams (Kaushal et al., 2014). Thus, watershed topography, combined with land use histories and precipitation patterns, may modify relative nutrient movement and source, but the balance of these controls in driving river N and P dynamics across watersheds of varying characteristics is often unclear (Goyette et al., 2019a).

Characterizing how different landscape and climatic controls retain or release nutrients from watersheds to streams is critical to understanding the future of river N and P exports, but difficult due to the multiple scales at which these drivers operate and the complex interactions they produce (Heffernan et al., 2014; Levin, 1992; Soranno et al., 2014, 2019). For instance, current ecological stressors, such as climate change and altered biogeochemical cycles, are global in scale with impacts that manifest differently across ecosystems (Jankowski et al., 2023; Mulholland et al., 2008; Nijssen et al., 2001; Rice & Emanuel, 2017). In riverine environments, climate-induced shifts to the quantity and source (rain vs. snow) of precipitation will alter the timing and magnitude of seasonal river discharge, resulting in substantially altered river

hydrologic regimes (Mauger et al., 2015; Poff, 1992). The anthropogenic enrichment of landscapes with nutrients, particularly reactive N, is also broad ranging (Bennett et al., 2001; Fowler et al., 2013; Galloway et al., 2004). For example, anthropogenic N emitted to the atmosphere can be deposited in even the most remote environments, altering the delivery of N to streams and rivers once considered largely pristine (Baron & Campbell, 1997; Holtgrieve et al., 2011). The processing and transport of river nutrients are fundamentally embedded within these large-scale hydroclimatic and biogeochemical shifts; however, the response of river nutrient concentrations and transport to change will likely vary across systems, making local variations in river N and P difficult to predict (Jankowski et al., 2023; McCluney et al., 2014; Smits et al., 2017).

While the impacts of climate and anthropogenic change may be expressed differently across rivers, summarizing variation among river systems that are spatially heterogenous and hydrologically diverse has the power to reveal the multiple interacting controls that drive hydrologic and biogeochemical change. For example, studies across rivers with contrasting land use and land cover have identified watershed forest cover as a critical modulator of streamflow responses to extreme precipitation (Kelly et al., 2016; Rice & Emanuel, 2017), while anthropogenic land use change has been shown to magnify the response of river N and P concentrations to seasonal and annual climate variation (Huang et al., 2021; Kaushal et al., 2014; Sobota et al., 2009). In relatively pristine, mountainous streams, research has further shown that the physical features of watersheds can act as master controls of physiochemical (Cline et al., 2020; Jankowski & Schindler, 2019; Lisi et al., 2015; Smits et al., 2017) and biological processes (Holtgrieve et al., 2010), and constrain the sensitivity of ecosystem responses to hydroclimatic change. For example, in northern Alaska, stream nitrate (NO_3^-) concentrations increased

predictably with catchment slope in response to seasonal permafrost thaw and snowmelt (Harms et al., 2016). Such relationships highlight the importance of both regional and local scale controls (e.g., climate, topography, and land use) on river N and P fates, and support the notion that by assessing nutrient dynamics across watershed subject to different controls, we can better understand the underlying processes that generate spatial and temporal variation (Levin, 1992; Lottig et al., 2017; Soranno et al., 2019).

Over the past few decades, the study of stable isotopes has increasingly demonstrated their potential to unravel larger spatiotemporal patterns in river nutrient sources and biogeochemical transformations (Bostic et al., 2022; Kendall et al., 2007; Matiatos et al., 2021). Specifically, the N and triple oxygen isotopes of nitrate (^{14}N, ^{15}N, ^{16}O, ^{17}O, ^{18}O), frequently the dominant form of reactive N, offer a direct means of terrestrial and atmospheric N source identification when the major sources of NO_3^- to surface waters are isotopically distinct (Kendall et al., 2007). Isotopic studies can also help identify gaseous losses or uptake of N in ecosystems, as fractionation processes such as denitrification and assimilation result in an apparent isotopic enrichment of NO_3^- (Aravena & Robertson, 1998; Sigler et al., 2022). Instream isotopic values typically represent a mixture of N-sources and these fractionations, which are largely driven by the land-use, geomorphology, and hydrographic stage of the surrounding catchment (Bourgeois, Savarino, Némery, et al., 2018b; Briand et al., 2017; Matiatos et al., 2021). Many applications of river isotopic NO_3^- studies have focused on the sources and transformations of NO_3^- within individual river reaches or at the watershed scale (S. Li et al., 2023; J. Lin et al., 2019; Rollinson et al., 2021a). However, recent studies have highlighted the potential of cross-system comparisons to elucidate the key environmental factors, such as land use, landform, and climate, that govern NO_3^- sources, uptake, and reactivity (Bostic et al., 2022; Matiatos et al., 2021).

While the study of stable isotopes can provide a useful link between the origins of NO_3^- and larger climatic and landscape processes, only a handful of studies have applied isotopes at broader scales to better understand the drivers of N sources and fates across river systems (Bostic et al., 2022; Burns et al., 2009; Matiatos et al., 2021; Sebestyen et al., 2019).

This dissertation explores the multiple spatial and temporal controls that interactively structure the source and transport of river nutrients (N and P). To do so, I investigate seasonal, annual, and decadal-scale patterns of river N and P concentrations, yields, and NO_3^- isotopic composition across a range of river and watershed types in the Puget Sound Basin, a spatially and climatologically complex region in Washington state. First, to better understand whether regional controls (like climate), or watershed variation (land-use or topography) play a larger role in driving the *seasonal* source and delivery of river N, I summarize monthly variation across Puget Sound river NO_3^- concentration, yield, and isotopic time series (*Chapter 1*). Second, to understand how climate and landscape variation has influenced *long-term* water quality across Puget Sound rivers, I investigate the influence of climate, landform, and hydrologic regime on multi-decadal patterns of river dissolved inorganic N and P concentrations, ratios, and transport across the Puget Sound Basin (*Chapter 2*). Finally, to understand how climate interacts with landscape to express spatial variation in river NO_3^- concentration and source across the Puget Sound Basin, I assess the influence of landscape gradients on atmospheric and terrestrially derived NO_3^- sources across rivers and within watersheds and examine how these relationships vary under different hydrologic and climate conditions (*Chapter 3*). By summarizing river N and P variability across broad spatiotemporal scales, I elucidate how large-scale anthropogenic and climatic stressors will differentially impact river ecosystems in the Puget Sound Basin and other mountainous regions, including the Pacific Northwest and elsewhere.

CHAPTER 1: Climate and landform interact to control the source and transport of nitrate in Pacific Northwest rivers

A version of this chapter was published as: Elmstrom, E. J., Holtgrieve, G.W., Scheuerell, M. D., Schauer, A. J., & Leazer, K. (2024). Climate and landform interact to control the source and transport of nitrate in Pacific Northwest rivers. *Nature Communications Earth and Environment*, **5**, 90. https://doi.org/10.1038/s43247-024-01235-8

1.1 ABSTRACT

The hydrological effects of climate change are documented in many regions; however, climate-driven impacts to the source and transport of river nutrients remain poorly understood. Understanding the factors controlling nutrient dynamics across river systems is critical to preserve ecosystem function yet challenging given the complexity of landscape and climate interactions. Here, we harness a large regional dataset of nitrate (NO_3^-) yield, concentration, and isotopic composition ($\delta^{15}N$ and $\delta^{18}O$) to evaluate the strength of hydroclimate and landscape variables in controlling the seasonal source and transport of NO_3^-. We show that hydroclimate strongly influenced the seasonality of river NO_3^-, producing distinct, source-dependent NO_3^- regimes across rivers from two mountain ranges. Riverine responses to hydroclimate were also constrained by watershed-scale topographic features, demonstrating that while regional climate strongly influences the timing of river NO_3^- transport, watershed topography plays a distinct role in mediating the sensitivity of river NO_3^- dynamics to future change.

1.2 INTRODUCTION

Rivers and streams play a critical role in regional nitrogen (N) cycles through the transport and *in situ* processing of dissolved reactive N as it moves from the land to the coast (Boyer et al., 2006). Dramatic increases in the load of N to freshwaters from human activities have stressed the bounds of riverine N processes, fundamentally altering patterns of riverine N transport, and exacerbating eutrophication in freshwaters and estuaries (Galloway et al., 2004; R. W. Howarth & Marino, 2006; Vitousek et al., 1997). Despite substantial investment to reduce watershed N loads to rivers, anthropogenic activity and land use change continue to elevate N sources across the landscape (Battye et al., 2017). Furthermore, as climate change strengthens precipitation patterns, hydro-climatic shifts are projected to alter the seasonal timing and delivery of NO_3^- (frequently the dominant form of dissolved N) from watersheds to rivers and streams (Sinha et al., 2017). Understanding the factors controlling seasonal river NO_3^- variation is critical to evaluate impacts downstream, but the balance of landscape and hydro-climatic variables in driving the N export dynamic remains unclear.

For any river system, landscape features represent a potentially dominant driver of instream NO_3^- concentrations and NO_3^- yields (Lewis & Grimm, 2007; R. Howarth et al., 2012; Goyette et al., 2019b; Schiff et al., 2002; Harms et al., 2016). Specifically, geomorphic attributes, such as watershed slope, channel morphology, and floodplain area, determine water residence times and hydrologic connectivity, ultimately governing watershed NO_3^- retention, loss (via biotic uptake or denitrification), and movement from watersheds to rivers and streams (Connolly et al., 2018a; Goyette et al., 2019b; Harms et al., 2016; Noe & Hupp, 2007; Schiff et al., 2002). Such catchment characteristics also influence the source composition and availability

of NO_3^- by determining the structure and composition of vegetation and soils, and by constraining the spatial distribution of human activity. In watersheds with steep slopes, catchment topography limits human activity, restricting NO_3^- source composition to nitrified soil ammonium (NH_4^+) and atmospheric deposition (Bourgeois, Savarino, Némery, et al., 2018b; Kendall et al., 2007). Lower sloped areas instead increase space for human development, agricultural activity, and the growth of N-fixing species (such as alders, *Alnus* spp.)(Kendall et al., 2007), promoting the accumulation of N in soils and groundwater, enhancing the transport potential of NO_3^- (Kumar et al., 2018; Van Meter et al., 2016). Spatial and temporal variation of river NO_3^- is further controlled by seasonal precipitation patterns and river flow, which mobilize NO_3^- from the landscape and drive the timing and magnitude of NO_3^- transport across systems (Compton et al., 2020; Sinha & Michalak, 2016).

Characterizing how different landscape and hydroclimatic controls transport or retain nutrients is important to improve the understanding of future river NO_3^- exports, but difficult due to the multiple scales at which drivers operate and the complex interactions they produce (Heffernan et al., 2014; Levin, 1992; Soranno et al., 2019). For instance, current ecological stressors, such as changing land-use and climate change, are global in scale with impacts that propagate differently across ecosystems (Sinha & Michalak, 2016; Smits et al., 2017). In riverine environments, climate-induced shifts to the quantity and form (rain vs. snow) of precipitation will alter the timing and magnitude of river discharge. Specifically, in northern latitudes like the Pacific Northwest, increases in flashy, event-driven runoff and decreases in spring snowmelt are projected to substantially alter seasonal hydrologic regimes (Mauger et al., 2015; Poff, 1992). The integration of landscape-level features, such as watershed slope or past land use histories, within these larger patterns will likely produce different ecosystem responses, making local

variations of river NO_3^- exports difficult to predict (Jankowski & Schindler, 2019; McCluney et al., 2014; Smits et al., 2017). The interaction of complex landscapes with altered climate patterns and river flows thus represents a key uncertainty in our understanding of riverine responses to ongoing climate and land-use change.

While the impact of large-scale stressors may manifest differently in rivers and streams, precipitation and river flow have been shown to synchronize seasonal patterns of river NO_3^- concentration and yield across watersheds that share similar characteristics (Basu et al., 2010; Van Meter et al., 2020). Flow-dependent nutrient regimes at the seasonal scale have been revealed, most recently in the Great Lakes, where monthly NO_3^- concentrations were shown to be synchronous with discharge in both agricultural and unmanaged catchments (Van Meter et al., 2020). Urban streams instead exhibited high concentrations during summer low-flow periods, creating out-of-phase nutrient regimes. In mountainous landscapes, research has shown that the physical features of watersheds can act as master controls of physiochemical (Cline et al., 2020; Jankowski & Schindler, 2019; Lisi et al., 2015; Smits et al., 2017) and biological processes (Holtgrieve et al., 2010), and constrain the susceptibility of ecosystem responses to climate and hydrologic variation. Such relationships highlight the importance of hydrologic connections and the role of both regional and local scale drivers (e.g., climate, land-use, and geomorphology) in the N export dynamic, and support the notion that by evaluating temporal patterns across rivers subject to different controls, we can better understand the underlying processes that generate shared or independent responses to hydroclimatic change (Levin, 1992; Lottig et al., 2017; Soranno et al., 2019).

Increasingly applied over the past decades, the stable isotopes of NO_3^- ($\delta^{15}N$ and $\delta^{18}O$) are tracers of N sources and biogeochemical transformations, with potential to unravel larger

spatiotemporal trends (Matiatos et al., 2021). Traditional applications of dual isotopic studies have focused on source identification using $\delta^{15}N$ and $\delta^{18}O$ biplots, however overlapping ranges of $\delta^{15}N$ and $\delta^{18}O$ of NO_3^- source values often limit direct source apportionment (Bourgeois, Savarino, Némery, et al., 2018b; Briand et al., 2017; Kendall et al., 2007). This overlap is further confounded by soil, aquifer, and stream processes (nitrification, denitrification, and assimilation) that fractionate $\delta^{15}N$ and $\delta^{18}O$ of NO_3^- values and alter isotopic signatures of NO_3^- pools (Briand et al., 2017; Matiatos et al., 2021; Venkiteswaran et al., 2019). Despite uncertainties in the assessment of sources, there is growing isotopic evidence that river NO_3^- concentrations are driven by hydrologic connections with different ecosystem compartments (e.g., direct water transfer through soils during storms events, groundwater inputs, or hyporheic exchange) (Briand et al., 2017; F. Chen et al., 2009; Lohse et al., 2013; Rollinson et al., 2021a; Wadnerkar et al., 2021). This has been shown in both temperate and tropical watersheds, where, at high river stages, NO_3^- concentrations have been isotopically linked to the transfer of soil N from the legacy of human activity or from forest organic matter (Briand et al., 2017; F. Chen et al., 2009; Jiang et al., 2022; Lohse et al., 2013; Rollinson et al., 2021a; Wadnerkar et al., 2021). Inputs from atmospheric NO_3^- are also linked to the hydrograph and have been shown to increase with spring and summer snowmelt in watersheds with higher elevation areas (Bourgeois, Savarino, Caillon, et al., 2018; Bourgeois, Savarino, Némery, et al., 2018b). This suggests that instream $\delta^{15}N\text{-}NO_3^-$ and $\delta^{18}O\text{-}NO_3^-$ values more accurately represent a mixture of seasonally dependent N-sources and fractionations, the proportions of which largely depend on the land-use history, geomorphology, and hydrographic stage of the catchment.

Whether seasonal NO_3^- dynamics are spatially coherent among rivers can help reveal the drivers of N sources and exports, however the evaluation of seasonal patterns across river $\delta^{15}N$

and $\delta^{18}O$ of NO_3^- time series has yet to be explored as an isotopic tool. Here, we took advantage of a unique two-year monthly data set of NO_3^- concentration and yield, combined with corresponding sample analysis of dual-isotopes of NO_3^- ($\delta^{15}N$, and $\delta^{18}O$) from 13 rivers that drain the Puget Sound basin in Washington State (see Fig. 1 for sample sites, see Fig. 2 for measured values). We applied a series of multivariate autoregressive state space models to quantify the degree to which monthly patterns of NO_3^- yield, NO_3^- concentration, $\delta^{15}N$-NO_3^-, and $\delta^{18}O$-NO_3^- (and therefore the inferred source of NO_3^-) were coherent across the basin. Through the inclusion of environmental covariates, we then characterized potential hydro-climate drivers shaping the timing, direction, and magnitude of monthly river NO_3^- dynamics, and quantified how their effects varied across systems. We aim to address three questions: (1) Are there shared monthly patterns in river NO_3^- yield, NO_3^- concentration, $\delta^{15}N$-NO_3^-, and $\delta^{18}O$-NO_3^- across Puget Sound rivers, and, if so, at what spatial or functional scale? (e.g., entire Puget Sound basin, among mountain ranges, or among land use or geomorphic groupings, Table 1), (2) What climate and hydrologic variables are best related to monthly variation in river NO_3^- yield, NO_3^- concentration, $\delta^{15}N$-NO_3^-, and $\delta^{18}O$-NO_3^-?, and (3) How does the response of river NO_3^- yield, NO_3^- concentration, $\delta^{15}N$-NO_3^- and $\delta^{18}O$-NO_3^- to hydro-climate variables vary with watershed-specific characteristics? By summarizing monthly variation at this regional scale, we sought to gain a better understanding of whether regional controls (like climate or hydrology), or individual watershed variation (land-use or geomorphic traits) played a larger role in driving seasonal patterns of yield, concentration, and source of river NO_3^-. Further, by looking at the individual river responses to hydro-climate variation, we sought to understand how the sensitivity of seasonal NO_3^- dynamics to hydro-climatic change might be modified by watershed-specific features, such as land-use cover, soil characteristics or watershed slope.

1.3 METHODS

1.3.1 Study area

The Puget Sound basin, located mostly in western Washington State, drains an area of approximately 13,700 km^2 (Fig. 1). Bounded by the Olympic Mountains to the west and the Cascade Range to the east, watersheds in the basin represent a gradient of geomorphic settings, with lowland and mountain valleys formed by continental glaciers, alpine glaciers, sediment deposition, and incision from rivers (Hall et al., 2018). Climate in the basin is seasonally variable, characterized by cool, wet winters, and warm dry summers. The average annual rainfall is 2147 mm, and the average annual air temperature is 8°C (PRISM Climate Group, 2015). During the hydrologic years of study, about 1947 mm and 2478 mm of precipitation fell within 2015 and 2016, respectively, and the average air temperature was 10°C in 2015 and 9°C in 2016 (PRISM Climate Group, 2015). For watersheds along both the Cascade and Olympic ranges, about 80% of the annual precipitation occurs from October to March (PRISM Climate Group, 2015). Within this setting, hydrologic regimes are governed by timing and form of precipitation and are characterized as rainfall-dominated (<600 m elevation with peak discharges in November-February) and mixed rain-and-snow hydrologies (>600 m elevation with peak discharges in February-June) (Hall et al., 2018; Reidy Liermann et al., 2012). Groundwater also sustains summer discharge in some rivers, as the unconsolidated glacial sediments of Puget Sound river channels are conducive to springs and hyporheic exchange (McGill et al., 2021). Notably, in 2015, substantial winter warming increased the proportion of precipitation falling as rain relative to snow, leading to declines in mountain snowpack and snowmelt-driven spring and summer discharge (Marlier et al., 2017). Though the effects of the snow drought were felt across

the entire basin, watersheds in the south Cascade Range and Olympic Mountains experienced the largest impacts to their snowmelt regimes (Marlier et al., 2017).

Land use histories and development in the region have resulted in a gradient of human disturbance and land cover across the basin. While the slopes of the Cascade Range and Olympic Mountains remain mostly forested, transitions to urban and agricultural land uses along with increased logging since the late 1800s have removed substantial areas of floodplain forest in the lower basin. The central Puget Sound region has seen rapid urbanization in recent years, gaining over a million people since 2000 (*Regional Data Profile*, 2017). The south and central valleys of the western Cascade Range are now mainly urban and rural residential land, with some pastureland and forage crops (hay and corn) located outside the urban fringe (*2015 WSDA Agricultural Land Use*, 2022; Hill et al., 2016). The majority of forage and specialty crop cultivation (including cereal grains, berries, and vegetables) is located in the northeastern part of the basin in the Nooksack, Skagit and Snohomish river watersheds (*2015 WSDA Agricultural Land Use*, 2022). Forested areas along the lower Cascade Range are a mix of deciduous and coniferous forest and include large stands of the early successional N-fixing tree species, red alder (*Alnus rubra*) (Wise & Johnson, 2011). Watersheds along the eastern Olympic Mountains remain mostly forested with coniferous trees, but with some logging, and sparse pastureland, forage cropped fields and residential development (*2015 WSDA Agricultural Land Use*, 2022; Hill et al., 2016). The combination of forested, mountainous areas, agricultural valleys, and sprawling cityscapes creates a variable landscape across the Puget Sound basin, and drives a diversity of N inputs that cover the full range of NO_3^- sources (Kendall et al., 2007).

1.3.2 Sample and data collection

We used two years of river monthly water quality samples collected by the Washington Department of Ecology's (DoE) River and Stream Water Quality Monitoring program from October 2014 to September 2016. The Washington DoE collects monthly water quality samples at nearly 100 river and stream stations across Washington state. For this study, we selected rivers that drain the Puget Sound Basin and range in their watershed physical and land use characteristics (Table 2, Fig. 6). This included 13 rivers, each with 1 DoE sampling station located near the Puget Sound outlet (Fig. 1). River order (i.e., Strahler number; Strahler, 1952) at the mouth ranged from 5 to 8, and sampling stations ranged from 4 to 300 m in elevation. We obtained subsamples of monthly water samples from each river site for NO_3^- stable isotope analysis ($\delta^{15}N$ and $\delta^{18}O$) and paired them with corresponding NO_3^- concentration data from the Washington's Department of Ecology's Freshwater Information Network database (Washington Department of Ecology, 2023). Details concerning the Washington Department of Ecology's water quality sample handling protocols and analytical methods can be found in (Von Prause, 2021).

To calculate river NO_3^- yields, we used the composite method within the loadflex R package (Appling et al., 2015) to calculate monthly river NO_3^- fluxes (estimated in kg day^{-1}), and subsequently divided monthly fluxes by watershed area for monthly estimates of river NO_3^- yield in kg km^{-2} day^{-1}. The composite method combines regression model predictions with model residuals to bring predictions closer to actual observations, thereby reducing model biases and increasing the accuracy of total flux estimates (Appling et al., 2015; Aulenbach, 2013; Aulenbach & Hooper, 2006). We therefore chose the composite method (in comparison to other methods, such as WRTDS or LOADEST models) as it provided the best estimate of actual river

NO_3^- yields across our rivers and our period of study. We provide plots of the monthly NO_3^- yields, NO_3^- concentrations, and NO_3^- stable isotopic values ($\delta^{15}N$ and $\delta^{18}O$) for each river site in Supplementary Figures 1 through 4.

1.3.3 Stable isotope analysis of NO_3^-

We analyzed river water subsamples for nitrogen and oxygen isotope ratios of NO_3^- ($^{15}N/^{14}N$ and $^{18}O/^{16}O$) using the bacterial denitrifier method (Kaiser et al., 2007; Sigman et al., 2001) at the University of Washington's Δ*IsoLab. Briefly, we used denitrifying bacteria (*Pseudomonas aureofaciens*) to convert NO_3^- and NO_2 to N_2O. The resultant N_2O was extracted, purified, and pyrolyzed to N_2 and O_2 in a heated gold tube held at 800°C. The isotopic ratios of each gas were then measured by a Finnigan Delta-Plus Advantage isotope ratio mass spectrometer after being separated by a gas chromatograph. We report the ratios of $^{15}N/^{14}N$ and $^{18}O/^{16}O$ of NO_3^- in the delta (δ) notation in per mil (‰), where $\delta = (R_{sample}/R_{standard} - 1)$ and R is the $^{15}N/^{14}N$ in N_2 normalized atmospheric air N_2 (Air) or $^{18}O/^{16}O$ normalized to Vienna Standard Mean Ocean Water (VSMOW). We calibrated $\delta^{15}N$ and $\delta^{18}O$ of NO_3^- using three international reference materials, USGS34: $\delta^{15}N = -1.8‰$, $\delta^{18}O = -27.8‰$, USGS35: $\delta^{15}N = +2.7‰$, $\delta^{18}O = +56.8‰$, and IAEA-NO3: $\delta^{15}N = +4.7‰$, $\delta^{18}O = +25.6‰$. We verified analytical accuracy using replicate measurements of USGS35 and IAEA-NO3 (for $\delta^{15}N$ and $\delta^{18}O$, respectively). The uncertainty was ±0.1‰ for $\delta^{15}N$ and ±0.5‰ for $\delta^{18}O$ (1SD, n = 84).

1.3.4 Regional climate and hydrologic covariates

We considered several climate and hydrologic predictors of river NO_3^- concentration, NO_3^- yield, $\delta^{15}N\text{-}NO_3^-$, and $\delta^{18}O\text{-}NO_3^-$ time series. We chose monthly precipitation, snowmelt, water temperature, and the Standardized Precipitation Index (SPI) as metrics of climatic

variability. SPI is a widely used drought index which captures how precipitation deviates from the climatological average across different timescales (Zargar et al., 2011). We used 12-month SPI, which is timescale indicative of long-term drought events (Zargar et al., 2011). To calculate precipitation and snowmelt values, we extracted gridded estimates of total daily precipitation, and snow water equivalent (SWE) data for each watershed boundary from Oak Ridge National Laboratory's Daymet dataset (Thornton et al., 2020) and summed the estimates per each month sampled. We then calculated monthly snowmelt for each watershed as the absolute value of negative differences in the cumulative SWE from each month to the next. We extracted monthly gridded estimates of 12-month SPI for each watershed boundary from the National Oceanic and Atmospheric Administration's nClimGrid-monthly dataset (*U.S. Gridded Standardized Precipitation Index (SPI) from nClimGrid-Monthly | Drought.Gov*, 2016). We obtained monthly water temperature measurements from the Washington's Department of Ecology's Freshwater Information Network database (Washington Department of Ecology, 2023), which were taken in the field alongside the provided river water quality samples.

To evaluate the influence of river hydrologic variation, we included both event-driven and seasonal components of each river's discharge hydrograph. By considering different components of the hydrograph in our analysis, we sought to reveal the role of flashy, runoff-driven flow vs. the sustained, seasonal pulse of river discharge in driving monthly river NO_3^- variation. To calculate seasonal and storm event-scale variations in discharge, we used recession analysis, a method that separates discharge hydrographs into short-term discharge variations driven by surface or interflow during storm events, and baseflow variations driven by slower water transit or eventual groundwater inputs (Lyne & Hollick, 1979; Nathan & McMahon, 1990; Xie et al., 2020). We extracted daily discharge data from the nearest U.S. Geological Survey

gaging station to each study site for the two years of study (no greater than 30 km from the sampling point) (*USGS Water Data for the Nation*, n.d.). To estimate the slow, seasonal (Q_{slow}), and quick, short-term (Q_{quick}) components of the hydrograph, we applied the baseflow recursive filter method (Minaudo et al., 2019; Nathan & McMahon, 1990) to each river hydrograph. To preserve the scale of individual storm events, we kept Q_{quick} as the raw daily value specific to the sample date. To incorporate the influence of river flow at the seasonal scale, we calculated Q_{slow} as the previous week sum of estimated baseflow values. Further details on the estimation and chosen time windows of Q_{quick} and Q_{slow} can be found in the supplemental material (Supplementary Note 1, Supplementary Fig. 5).

1.3.5 Watershed and landscape characteristics

We compiled watershed-scale landscape metrics for each of the watersheds corresponding to our 13 river sites using the Environmental Protection Agency's StreamCat data library (Table 2). These metrics included watershed area, mean watershed elevation, mean watershed soil depth, mean soil organic matter, watershed population density, and percent urban, wetland, agricultural, and forested land. We also included mean watershed slope in our analyses as it captures aspects of watershed topography and stream geomorphology that may influence NO_3^- accumulations or transfers, such as water residence times, floodplain area, and hydrologic connectivity (Connolly et al., 2018a; Goyette et al., 2019b; Schiff et al., 2002). We calculated watershed slope as the average of all slope raster pixels within the boundaries of each individual river's watershed using ArcGIS (v10.8).

1.3.6 Time series modeling approach

We used multivariate autoregressive state space (MARSS) models to examine temporal trends in NO_3^- concentration, NO_3^- yield, and NO_3^- isotopic composition ($\delta^{15}N$ and $\delta^{18}O$) across 13 major rivers in the Puget Sound basin (Holmes et al., 2021). MARSS models are a powerful class of time series models that can be used to evaluate hypotheses regarding synchrony among multiple time series (Jankowski et al., 2021; Smits et al., 2019; Webster et al., 2022). MARSS models consist of two equations. The process equation (1) is an estimate of changes in the true, but hidden, states of nature over time. The observation equation (2) relates actual observations to the unobservable process equation (1).

$$\mathbf{x}_t = \mathbf{B}\mathbf{x}_{t-1} + \mathbf{C}\mathbf{c}_{t-h} + \mathbf{w}_t;\ \mathbf{w}_t \sim \text{MVN}\ (\mathbf{0}, \mathbf{Q}) \quad (1)$$

$$\mathbf{y}_t = \mathbf{Z}\mathbf{x}_t + \mathbf{v}_t;\ \mathbf{v}_t \sim \text{MVN}\ (\mathbf{0}, \mathbf{R}) \quad (2)$$

In the process model (1), $\mathbf{x}_t$ is a j x 1 vector of hidden states in month t; j changes with each structure of **Z** tested in the observation equation. The j x j matrix **B** contains estimated parameters along the diagonal that determine the degree of mean-reversion of each state process, and zeros elsewhere. The $j \times k$ matrix **C** contains the model-estimated effects of environmental covariates measured at time $t - h$, where h represents the time lag between the covariate and the response. The $\mathbf{c}_{t-h}$ vector (k x 1) contains each of the measured hydro-climatic covariate values. The $j \times 1$ vector $\mathbf{w}_t$ contains process errors, which are distributed as a multivariate normal with mean vector **0** and covariance matrix **Q**. The off-diagonals of the **Q** matrix measure covariance in the process errors after accounting for shared trends, thus providing an estimate of independence or correlation between the modelled trends, $\mathbf{x}_t$.

In the observation model (2), $\mathbf{y}_t$ is an i x 1 vector of measured data (log NO_3^- concentration, log NO_3^- yield, or $\delta^{15}N$ and $\delta^{18}O$ of NO_3^-) at time t from each watershed (i = 13). The **Z** matrix maps each of the measured river time series (i = 13) onto the hidden states in $\mathbf{x}_t$ (the term state refers to the true, but unobserved temporal pattern of NO_3^- concentration, yield, or isotopic value). The $i \times 1$ vector $\mathbf{v}_t$ contains the observation errors, which are distributed as a multivariate normal with mean vector **0** and covariance matrix **R**.

1.3.7 Testing for seasonal patterns in NO_3^- dynamics

By specifying different structures of the **Z** matrix, we evaluated the data support for synchrony among NO_3^- concentration, NO_3^- yield, $\delta^{15}N$ and $\delta^{18}O$ of NO_3^- time series at different spatial and functional scales ranging from the entire Puget Sound basin to individual watersheds (Table 2). We modeled each response variable separately and tested five options for the **Z** matrix, which represented the following river groupings: 1) All rivers follow the same state ("Basin model"), 2) There are two states defined by mountain range, one for rivers located in the Cascade Range, and one for rivers located in the Olympic Mountains ("Mountain model"), 3) There are three states defined by watershed land use ("Land use model"), 4) There are three states defined by watershed topographic and soil characteristics ("Geomorphology model"), and 5) Each river follows its own independent state or trend through time ("Watershed model"). To define the Land use and Geomorphology model groupings, we used *k*-means clustering analyses to group the Puget Sound rivers based on the similarity and closeness of their watershed land use and geomorphic characteristics (Table 1, Supplementary Note 2). To evaluate the possible variance and covariance among state processes, we tested data support for four options of the **Q** matrix including: equal variance and equal covariance, independent variance and independent covariance, independent variance but no covariance, and equal variance but no covariance.

Because the collection and laboratory analysis of all samples was the same, we modeled the observation errors as independent and identically distributed (IID), such that **R** had a single estimated value along the diagonal and zeros elsewhere. In this piece of analysis, we set both the **C** and **c** matrices to zero.

1.3.8 Testing covariates as drivers of monthly variation

To evaluate the data support for different climate and hydrologic drivers of temporal variation in NO_3^- concentration, NO_3^- yield, $\delta^{15}N$ and $\delta^{18}O$ of NO_3^-, and to test whether the effects of hydro-climate variables were shared across different spatial or functional scales, we used our "Watershed" scale model and adjusted the **C** matrix of the process model (1) to apply the covariate data in the **c** matrix to each watershed state process. We compared models that included 6 potential covariates: water temperature, precipitation, Q_{quick} (as a measure of event-scale discharge), Q_{slow} (as a measure of seasonal-scale baseflow), snowmelt, and SPI. To reduce the number of model parameters, we fit each model with a single covariate, but compared five coefficient or "effect" options. This included (1) a Basin effect where state processes among all rivers responded identically to hydroclimate (one **C** coefficient per covariate); (2) a Mountain range effect where state processes among all rivers in a given mountain range (i.e., Cascade Range vs. Olympic Mountains) responded identically to hydroclimate (**C** = 2); (3) a Land use effect where state processes among rivers that share similar watershed land use responded identically to hydroclimate (**C** = 3); (4) a Geomorphology effect where state processes among rivers that share similar watershed topography and soil characteristics responded identically to hydroclimate (**C** = 3), and (5) a Watershed effect where state processes for each river responded uniquely to hydroclimate (**C** = number of state processes (13); Table 1). To avoid double

counting, we did not include discharge (Q_{quick} or Q_{slow}) as a covariate for our NO_3^- yield models.

To facilitate model comparisons and interpretation across river groupings and covariates, we standardized all response variable and covariate data to have a mean of 0 and standard deviation of 1. In our test for spatial synchrony, we used Akaike Information Criterion adjusted for small sample size (AICc)(Burnham & Anderson, 2004) to rank models with varying numbers of states as determined by the **Z** matrix and different forms of **Q**. In our covariate analysis, we again used AICc to rank different models that varied by which covariate was included (**c** matrix) and the extent to which the effect of the coefficient was shared or unique (**C** matrix). We also included a null "Watershed" model with no covariates. For both analyses, we selected the model with the lowest AICc value as the best model. We considered models with a ΔAICc of less than 10 to show moderate statistical support.

Post hoc, we used Pearson correlation coefficients to examine if variation in river-specific covariate effect sizes (**C**) could be explained by watershed geomorphic or land-use attributes (including watershed area, elevation, slope, soil depth, soil organic matter, and percent urban, wetland, agricultural, and forested land).

1.4 RESULTS

1.4.1 Shared monthly patterns in river NO_3^- dynamics

We found that temporal patterns in monthly river NO_3^- dynamics were strongly coherent across the Puget Sound basin at the mountain range scale. For all four response variables (NO_3^- yield, NO_3^- concentration, $\delta^{15}N\text{-}NO_3^-$, and $\delta^{18}O\text{-}NO_3^-$), the model with states defined by

mountain range resulted in the greatest support compared to either individual watershed, or land-use, geomorphology, and basin-wide grouping structures (Supplementary Tables 1-4). The next best model in terms of river grouping was the geomorphology grouping structure, which was also consistent across all four response variables. However, none of the geomorphology models had particularly high statistical support (ΔAICc < 2), with ΔAICcs of 8.7, 3.2, 8.3, and 9.3 for NO_3^- yield, NO_3^- concentration, $\delta^{15}N\text{-}NO_3^-$, and $\delta^{18}O\text{-}NO_3^-$, respectively. This suggests that monthly variation in NO_3^- yield, NO_3^- concentration, $\delta^{15}N\text{-}NO_3^-$, and $\delta^{18}O\text{-}NO_3^-$ was best defined by two river state processes, one for rivers located in the Cascade Range, and one for rivers located in the Olympic Mountains (Fig. 3).

Models with correlated process errors were best supported by all response variable data (Supplementary Tables 1-4). For NO_3^- yield, NO_3^- concentration, and $\delta^{18}O\text{-}NO_3^-$, the best process error structure had equal variance and covariance among the two state processes (Supplementary Tables 1, 2, and 4), indicating that states across the two mountain ranges were temporally correlated and shared similar magnitudes in the peaks and troughs of their curves through time. For $\delta^{15}N\text{-}NO_3^-$, the best model included an unconstrained **Q** matrix structure (Supplementary Table 3), indicating that states were temporally correlated across mountain ranges, but the magnitude of monthly variation differed between the Cascade Range and Olympic Mountain rivers.

1.4.2 Hydro-climate drivers of monthly river NO_3^- variation

For all response variables, the best covariate model included a shared coefficient among rivers within each mountain range (Supplementary Tables 5-8). That is, rivers in the Cascade Range shared similar effects of hydro-climate variables, while the effects of hydro-climate

variables shared by rivers in the Olympic Mountains were distinctly different. For example, for both NO_3^- yield and concentration, the model including precipitation had the most data support (Supplementary Tables 5-6), but the magnitude and directionality of the precipitation effect varied for rivers in each mountain range. In the Cascade Range rivers, precipitation had a positive effect on NO_3^- concentration and yield (Fig. 4a, b), indicating that during periods of heavy rainfall, the amount and export of river NO_3^- increased. In the Olympic Mountain rivers, however, precipitation's effect on NO_3^- yield was smaller than rivers in the Cascade Range, and the effect on river NO_3^- concentrations was strongly negative (though not statistically significant from 0, Fig. 4a, b). For both NO_3^- concentration and yield, the next best covariate model included an effect of water temperature at the mountain range scale (NO_3^- concentration ΔAIC_c = 1.9, NO_3^- yield ΔAIC_c = 9.8). In the Cascade Range rivers, water temperature had a negative effect on NO_3^- yield but was unrelated to NO_3^- concentrations. Conversely, in the Olympic Mountain rivers, the effect of water temperature was unrelated to NO_3^- yields but exhibited a strong positive effect on NO_3^- concentrations (Fig. 4a, b).

Event-scale discharge and precipitation best explained variation across $\delta^{15}N\text{-}NO_3^-$ patterns (Q_{quick} ΔAIC_c = 0, Precipitation ΔAIC_c = 6.7, Supplementary Table 7). In the Cascade Range rivers, Q_{quick} had a strong, negative effect on the $\delta^{15}N\text{-}NO_3^-$ time series (Fig. 4c), indicating that depleted $\delta^{15}N\text{-}NO_3^-$ values were highly correlated with winter runoff or storm events. The effect of Q_{quick} on $\delta^{15}N\text{-}NO_3^-$ was, however, not present in the Olympic Mountain rivers, as indicated by an effect size that was not statistically distinguishable from 0 (Fig. 4c). Precipitation was the second-best explanatory covariate for $\delta^{15}N\text{-}NO_3^-$ and further enforced these differences between the two mountain ranges. In the Cascade Range rivers, $\delta^{15}N\text{-}NO_3^-$ values

decreased when precipitation increased (Fig. 4c), and again, in the Olympic Mountain rivers the effect of precipitation on $\delta^{15}N\text{-}NO_3^-$ was not statistically distinguishable from 0 (Fig. 4c).

For $\delta^{18}O\text{-}NO_3^-$, snowmelt was the best descriptor of isotopic variation (Supplementary Table 8). Snowmelt had a strong, positive effect on $\delta^{18}O\text{-}NO_3^-$ in the Olympic Mountain rivers (Fig. 4d), but no effect on $\delta^{18}O\text{-}NO_3^-$ in rivers in the Cascade Range (Fig. 4d). The second most parsimonious model for $\delta^{18}O\text{-}NO_3^-$ at the mountain range scale included Q_{quick} (ΔAICc = 7.7). Positive values of Q_{quick} were strongly related to depleted $\delta^{18}O\text{-}NO_3^-$ values in the Cascade Range (negative effect sizes, Fig. 4d). In the Olympic Mountain rivers, Q_{quick} had a positive, but insignificant, effect (Fig. 4d).

For all response variables, no other explanatory covariate had a high ($\Delta AIC_c < 2$) or moderate ($\Delta AIC_c < 10$) degree of support. However, the second most parsimonious model for all the best explanatory covariate models included a common response to hydroclimate at the geomorphic grouping scale (Supplementary Tables 5-8).

1.4.3 Landscape controls of river NO_3^- responses to hydroclimate

The sensitivity of NO_3^-, NO_3^- yield, $\delta^{15}N\text{-}NO_3^-$, and $\delta^{18}O\text{-}NO_3^-$ among rivers to hydro-climate drivers (i.e., covariate effect sizes) covaried strongly with mean watershed slope (Fig. 5). For both NO_3^- concentration and yield, steep watersheds were less sensitive to the positive effects of precipitation. As mean watershed slope increased, the effect of precipitation on NO_3^- yield diminished (Fig. 5a) or became negative for NO_3^- concentration (Fig. 5b). Similarly, the negative effect of Q_{quick} on $\delta^{15}N\text{-}NO_3^-$ was greater in rivers draining relatively flat watersheds with more floodplain area and the effect lessened as watershed slope increased (Fig. 5c). Rivers

draining steeper watersheds had the strongest effect of snowmelt on $\delta^{18}O\text{-}NO_3^-$, and this effect did not exist or was negative in less-steep watersheds (Fig. 5d).

1.5 DISCUSSION

Using a unique regional dataset, we show the monthly riverine NO_3^- dynamics were coherent across watersheds within individual mountain ranges, despite wide variation in land use and hydrologic regimes across watersheds in the Puget Sound Basin. Our findings demonstrate the overarching importance of regional-scale climate drivers such as precipitation on N transport in rivers, while simultaneously identifying different components of the hydrograph as an important control of monthly NO_3^- source variation in both human-influenced and in more pristine catchments. Furthermore, we found that not all rivers were equally sensitive to hydroclimate variables, and that variation in this sensitivity was largely determined by a simple geomorphic feature - mean watershed slope. These results suggest that while regional-scale climate controls seasonal NO_3^- delivery in Puget Sound rivers, watershed topography plays a distinct role in influencing landscape-level drivers of NO_3^- source and transfer, which together modify the response of riverine NO_3^- dynamics to hydroclimatic change.

1.5.1 Seasonal patterns at the mountain-range scale

Monthly coherence in NO_3^- dynamics at the mountain-range scale suggests that regional-scale processes have stronger controls on seasonal patterns of NO_3^- concentration, yield, and isotopic signatures than finer watershed-scale variation. Given known links between river discharge, solute concentration, and flux (Basu et al., 2010; Sinha & Michalak, 2016; Van Meter et al., 2020), we anticipated some degree of coherence in NO_3^- concentration and yield time series among rivers, but the exact extent of that coherence was unknown. The separation of NO_3^-

yield and NO_3^- concentration patterns in the Cascade Range and Olympic Mountain rivers likely reflects the cumulative differences in landscape composition that exist between the two mountain ranges. The lower sloped watersheds of the Cascade Range have sprawling valley floors, with larger wetland and riparian areas, deeper soils, and varied degrees of agricultural activity and human development. Watersheds in the Olympic Mountains are instead spatially constrained in relief, generally high elevation, and remain mostly forested with little to no agriculture and sparse human development (Table 2, Fig. 1c). Our results thus agree with previous work that seasonal-scale nutrient regime curves can be driven by regional-scale variation, such as seasonal flow and precipitation patterns, but become asynchronous with varying physical traits and land-use histories due to differences in source type and availability (Van Meter et al., 2020).

With large variation in watershed land-use and hydrogeomorphic characteristics among the Puget Sound basin rivers (Table 2, Fig. 1c), we expected watershed-specific traits to drive varied source proportions and processing rates and to diminish the coherence in monthly values of $\delta^{15}N$ and $\delta^{18}O$ of NO_3^-. Instead, despite broad variation in watershed characteristics, rivers in the Cascade Range experienced notable coherence $\delta^{15}N\text{-}NO_3^-$ and $\delta^{18}O\text{-}NO_3^-$ over time, and rivers in the Olympic Mountains shared strong monthly patterns of $\delta^{18}O\text{-}NO_3^-$, but little change in $\delta^{15}N\text{-}NO_3^-$ (Fig. 3). The observed degree of coherence found across $\delta^{15}N$ and $\delta^{18}O$ of NO_3^- time series, along with the divergent patterns between the Cascade Range and Olympic Mountain rivers, suggests that the two isotopic states depict a region-specific mixture of seasonally dependent NO_3^- sources, or perhaps show cumulative fractionation processes that are similar in each river group.

1.5.2 Hydroclimate drivers in the Cascade Range and Olympic Mountain rivers

The support for seasonal coherence at the mountain range scale was further corroborated by our covariate analysis, where correlations between hydroclimate drivers and NO_3^- response variables highlighted fundamental differences in NO_3^- source availability, transport potential, and transformation processes across the Cascade Range and Olympic Mountains. In the Cascade Range rivers, we found that precipitation had positive effects on both NO_3^- concentration and yield, and that NO_3^- yields decreased seasonally as the hydrograph fell and river waters warmed (as indicated by the negative effect of water temperature; Fig. 4a.). This finding supports the notion that in these moderately to highly disturbed catchments, river nutrient export is "transport limited", and that NO_3^- yields are primarily driven by the seasonal mobilization of NO_3^- sources with increased precipitation and resultant river flow (Basu et al., 2010; Sinha & Michalak, 2016). In anthropogenically modified watersheds, N accumulates within soils and groundwater from fertilizer and manure applications (Basu et al., 2010; Van Meter et al., 2016), septic waste (Jankowski et al., 2012; Weitzman et al., 2021), N-fixing species (such as legumes or alder (Compton et al., 2003, 2020)), or from altered atmospheric deposition patterns across the watershed (Bourgeois, Savarino, Caillon, et al., 2018; Bourgeois, Savarino, Némery, et al., 2018b; Hundey et al., 2016a). Consistent relationships between hydro-climate variables and NO_3^- loads across human-modified catchments have thus been attributed to the mobilization of accumulated NO_3^- pools in soils and groundwater (Basu et al., 2010; Van Meter et al., 2016), rather than direct runoff from surface point sources.

In the Olympic Mountain rivers, the effect of precipitation on NO_3^- yield was positive, but smaller than in the Cascade Range rivers, signaling a reduced response of monthly NO_3^- transport to increased precipitation in rivers draining relatively intact watersheds. Snowmelt had

a negative effect on NO_3^- yields in Olympic Mountain rivers, which reflects a decrease in NO_3^- export during spring freshets in rivers with snow-driven hydrologies. This, combined with the uniformly negative effects of hydro-climate variables on NO_3^- concentrations, suggests that Olympic Mountain rivers were highly sensitive to the effects of seasonal dilution with increased river volume. Negative concentration-discharge relationships have been shown in other forested and undeveloped watersheds (J. M. Duncan et al., 2017; Goodale et al., 2009), and have been described as "source limited" due to the absence of excess watershed N supplies. In these systems, NO_3^- concentrations peak in the summer and during the rising limb of the hydrograph from increased stream or nearby soil nitrification pools, then decrease with the exhaustion of sources (J. M. Duncan et al., 2017). The increase in NO_3^- concentrations with warm summer flows supports this hypothesis (positive effect of water temperature; Fig. 4b). Collectively, this indicates that the Olympic Mountain rivers are "source limited" in their NO_3^- patterns and that NO_3^- source pools are quickly depleted with the onset of fall precipitation.

Our isotopic results reinforce this distinction between "transport" and "source limited" NO_3^- regimes in the Cascade Range and Olympic Mountain rivers and highlight the importance of hydrologic connections between different ecosystem compartments, such as soil N pools. After the addition from fertilizers, atmospheric deposition, snowmelt, or mineralization within soils, NH_4 can be nitrified to NO_3^-, resulting in high NO_3^- concentrations with relatively low $\delta^{15}N$-NO_3^- and $\delta^{18}O$-NO_3^- values (Briand et al., 2017; Kendall et al., 2007; Rollinson et al., 2021a; Sebilo et al., 2013; Venkiteswaran et al., 2019). This is especially relevant in watersheds with historical and current land use change, where additions of N to the landscape enhance soil mineralization and subsequent nitrification rates (X. Lin et al., 2020). Higher net nitrification has also been shown to occur under N-fixing red alder trees (Hart et al., 1997; Perakis et al., 2012), a

species prevalent along the Cascade Range valley floors due to both human and riparian disturbance. In the Cascade Range rivers, the observed negative relationship between storm event-scale variations in river flow (Q_{quick}) and precipitation and $\delta^{15}N\text{-}NO_3^-$ thus implies that heavy winter rains and flooding may uniformly and rapidly mobilize nitrified soil NH_4^+, decreasing river $\delta^{15}N\text{-}NO_3^-$ during high flow events. The decrease in river $\delta^{15}N\text{-}NO_3^-$ with winter rains could also be attributed to the delivery of atmospheric NO_3^- or direct runoff from NO_3-based fertilizers. However, if that were the case, $\delta^{18}O\text{-}NO_3^-$ would have increased with precipitation. Instead, Cascade Range $\delta^{18}O\text{-}NO_3^-$ values decreased with increased event-scale flow and precipitation (negative effect sizes; Fig. 4), supporting a link between wintertime NO_3^- yields and inputs of nitrified soil NH_4^+ from the legacy of human activity in the region.

The Cascade Range rivers experienced noticeable enrichment of $\delta^{15}N\text{-}NO_3^-$ during the spring and summer months as NO_3^- exports fell (Fig. 3c). While we lack a covariate that adequately captures this seasonal variation, this could be explained by the drainage from a relatively ^{15}N enriched NO_3^- pool, such as septic and manure waste, or by NO_3^- that has undergone denitrification or biological uptake (assimilation). During denitrification and assimilation, the lighter isotopes of $\delta^{15}N$ and $\delta^{18}O$ are preferentially processed, resulting in the dual isotopic enrichment of residual NO_3^- (Aravena & Robertson, 1998; Böttcher et al., 1990; Briand et al., 2017; Kendall et al., 2007). In fact, we do see a shared seasonal enrichment of the $\delta^{15}N\text{-}NO_3^-$ and $\delta^{18}O\text{-}NO_3^-$ states in Cascade Range rivers (Fig. 3c, d), suggesting that summertime NO_3^- concentrations could be influenced by nutrient retention processes that occur instream or elsewhere within watersheds. Notably, the Cascade Range watersheds have increased riparian and wetland areas, which promote anoxia and denitrification (Hanson et al., 1994) (Table 2), and the river channels themselves are conducive to groundwater springs and exchange with the

reactive hyporheic zone (McGill et al., 2021). As discharge volumes and velocities decline, it is possible that increased connections with biogeochemically reactive sites or increased proportions of denitrified NO_3^- from external pools could seasonally enrich the Cascade Range $\delta^{15}N\text{-}NO_3^-$ and $\delta^{18}O\text{-}NO_3^-$ river values (Briand et al., 2017; Gomez-Velez et al., 2015; Marcé et al., 2018). However, summertime values of $\delta^{18}O\text{-}NO_3^-$ across the Cascade Range rivers were distinctly more variable (Fig. 3d) and could also be enriched by unprocessed atmospheric NO_3^- (Bostic et al., 2022; Bourgeois, Savarino, Némery, et al., 2018b). Furthermore, processes such as respiration and O-isotopic exchange between NO_2 and H_2O molecules during nitrification can significantly alter $\delta^{18}O\text{-}NO_3^-$ values (Venkiteswaran et al., 2019), making nutrient retention patterns difficult to surmise at this regional scale.

In the Olympic Mountain rivers, the observed effects of hydroclimate variables on the isotopic states suggest that NO_3^- concentrations were derived mostly from a combination of soil or instream nitrification processes and contributions from atmospheric deposition. Average $\delta^{15}N\text{-}NO_3^-$ values were low (Fig. 2), and correlations with seasonal hydro-climate variables were insignificant (Fig. 4c). The lack of significance of $\delta^{15}N\text{-}NO_3^-$ with temporal variables in Olympic Mountain rivers indicates that $\delta^{15}N\text{-}NO_3^-$ values were relatively unchanged through time, and there was limited mixing among isotopically distinct sources, or isotopic enrichment from human waste or agricultural inputs. Increased snowmelt in the Olympic Mountains had a positive effect on $\delta^{18}O\text{-}NO_3^-$, and the singular peak of $\delta^{18}O\text{-}NO_3^-$ in Olympic Mountain rivers coincided with local climate conditions, rising during a normal hydrologic year in 2016, but absent during 2015, which was a record drought in terms of snowpack for Washington State (Marlier et al., 2017). The positive effect of snowmelt, and the timing of increased $\delta^{18}O\text{-}NO_3^-$, implies that spring and

early summer snowmelt washes unprocessed atmospheric NO_3^- downstream, increasing measurable atmospheric contributions to the Olympic Mountain river NO_3^- pools.

1.5.3 Landform influence on river responses to hydroclimate

The final piece of our analyses identifies watershed-scale differences in landform as a strong underlying control of the contrasting responses of the Cascade Range and Olympic Mountain rivers to hydro-climatic change. We found that a significant amount of the variation in the individual river NO_3^- responses to hydroclimate variables was explained by a simple geomorphic metric, mean watershed slope (Fig. 5). NO_3^- yields, NO_3^- concentrations, and $\delta^{15}N\text{-}NO_3^-$ values in rivers draining flatter watersheds were distinctly more sensitive to changes in precipitation and storm-event scale flows. In contrast, $\delta^{18}O\text{-}NO_3^-$ in rivers draining mid- to high-sloped watersheds were less sensitive to runoff-related hydrologic conditions, and highly sensitive to changes in snowmelt (Fig. 5). This relationship between river NO_3^- sensitivities and watershed slope illuminates the broad-scale influence of topography on river ecosystem function. Watershed topography can directly influence the source, transfer, and transport of NO_3^- directly through both physical and chemical mechanisms. For example, in watersheds with steep slopes, strong energy gradients rapidly route water and snowmelt to stream channels, quickly transferring available NO_3^- (Connolly et al., 2018a; Harms et al., 2016; Schiff et al., 2002). Lower relief areas instead increase residence times and rates of N reactivity (Connolly et al., 2018b; Goyette et al., 2019b; Harms et al., 2016), and also promote river connections to N sources and sinks across high flow (i.e., floodplain soils (Bechtold et al., 2003; Noe & Hupp, 2007)) and low flow conditions (i.e., hyporheic and channel storage zones (Briand et al., 2017; Lohse et al., 2013; Marcé et al., 2018)). Terrain relief can also indirectly affect NO_3^- dynamics through its control on the distribution of human activity. In flat watersheds, humans populate and

modify the landscape to larger degrees, enhancing the accumulation of NO_3^- on land and in soils (Basu et al., 2010; Van Meter et al., 2016), while often altering hydrologic flow paths (Kaushal et al., 2014). Together, this can saturate or bypass biogeochemical retention opportunities, and ultimately increase the potential for NO_3^- transfers and transport downstream (Kumar et al., 2018; Mulholland et al., 2008).

Our results highlight that while regional-scale variation exhibits large controls on monthly NO_3^- sources and exports across the Puget Sound Basin, watershed characteristics still influence river sensitivity to hydroclimate variables. Specifically, our results imply that differences in landform, and therefore availability, source, and transfer of NO_3^-, alters NO_3^- inputs across rivers in the two mountain ranges, as well as the sensitivity of river NO_3^- transport to hydro-climatic change. This finding is similar to recent work from Alaskan watersheds (Cline et al., 2020; Connolly et al., 2018b; Harms et al., 2016; Jankowski & Schindler, 2019; Lisi et al., 2015; Smits et al., 2017) and is meaningful in that it supports the notion that watershed slope can act as a master variable for predicting biogeochemical processes, ultimately modifying the response of river ecosystem function to climate across watersheds of varying relief. In the Pacific Northwest, climate change is predicted to increase the proportion of precipitation falling as rain relative to snow (Hamlet et al., 2013; Marlier et al., 2017). With more precipitation falling as rain, instances of flooding and storm-event scale flow are likely to increase, particularly in low and mid-sloped watersheds. The results of our analyses imply that the sensitivity of river NO_3^- transport to hydro-climatic changes may be strongest in watersheds with lower slopes where excess NO_3^- can be stored and remobilized in response to precipitation and high river flows. While further research is needed to understand climate-driven perturbations to river nutrient dynamics across human modified catchments, this work demonstrates the strong influence of topography on river

NO_3^- dynamics and reveals watershed slope as a potential predictor of river responses to hydroclimatic change.

1.5.4 Conclusions

This work contributes to the understanding of spatiotemporal patterns of river NO_3^- source and transport, including insight into seasonal patterns, as well as the identification of physical mechanisms at finer scales. We provide evidence that regional climate exhibits strong controls on monthly isotopic composition, concentration, and yield of river NO_3^-, forming distinct source and transport-driven NO_3^- regimes across two local mountain ranges. Within these broad-scale patterns, we also show that watershed landform influences the availability and transfer of NO_3^-, ultimately controlling the sensitivity of river NO_3^- dynamics to climate. Climate change is likely to have important effects on river NO_3^- transport, with impacts that will play out differently across watersheds (Sinha et al., 2017; Soranno et al., 2019). The clear linkage between NO_3^- regimes, hydroclimate, and landform has broad implications for river nutrient management and suggests that topographic features, such as watershed slope, could be used to improve scenarios of NO_3^- transport at the scale of regions, which will become increasingly important as climate, hydrology, and land use continues to change.

1.6 TABLES

Table 1. Description model structures considered in the MARSS time series models. Models compared groupings of NO_3^- concentration, NO_3^- yield, $\delta^{15}N$, and $\delta^{18}O$ of NO_3^- time series and the effects of hydroclimate on state processes at different spatial and functional scales (see Methods for details).

Model name	Model descriptions	# of state processes
Basin	All rivers in the Puget Sound basin follow the same hidden state or trend through time.	1
Mountain	There are two hidden states defined by mountain range, one for rivers located in the Cascade Range, and one for rivers located in Olympic Mountains.	2
Land-use	Rivers that share similar watershed land-use and degree of human disturbance follow the same hidden state (i.e., urban *vs.* agriculture *vs.* forest).	3
Geomorphology	Rivers that share similar watershed topographic and soil characteristics follow the same hidden state. *Groupings as follows:* 1) Small watershed area, high slope and elevation, lower soil depths and organic matter (OM), 2) Large watershed area, high slope and elevation, lower soil depths and OM, 3) Intermediate watershed area, lower slope and elevation, and higher soil depths and OM.	3
Watershed	Each river follows its own independent state or trend through time.	13

Table 1-1 Model descriptions

Table 2. River and watershed characteristics ordered by decreasing monthly mean NO_3^- concentration. Other descriptors include watershed area, mean watershed elevation, mean watershed slope, stream order, percent urban, agriculture, wetland, and forest cover by area of the watershed, mean watershed soil depth, and mean watershed soil organic matter (OM). Water quality sampling sites are labeled on Figure 1 using the italicized abbreviations in the first column of the table.

Table 1-2 Watershed characteristics

River name (Map abbreviation)	Local mountain range	NO_3^- (mg L-1)	Watershed area (km^2)	Watershed elevation (m)	Watershed slope (°)	% Urban by area	% Agriculture by area	% Wetland by area	% Forest by area	Soil Depth (cm)	Soil OM (% by weight)
Deschutes (*De*)	Cascade	0.75 ± 0.1	409	288	8	15.4	8.4	5	51.5	139.8	2.2
Samish (*Sa*)	Cascade	0.74 ± 0.2	225	268	8	9.2	7.5	5.8	65.8	143.2	2.4
Green (*Gr*)	Cascade	0.39 ± 0.2	1116	546	11	22.6	4.8	2.4	59.4	140.8	2.2
Nooksack (*No*)	Cascade	0.33 ± 0.2	2046	674	14	4.8	12.4	2.9	62.5	139.3	3
Nisqually (*Ni*)	Cascade	0.25 ± 0.1	1853	556	9	8.4	6.4	5.6	59.4	143.8	2
Cedar (*Ce*)	Cascade	0.24 ± 0.1	457	611	13	15.8	0.6	1.5	74.1	143	1.9
Puyallup (*Pu*)	Cascade	0.23 ± 0.1	2439	921	15	9.1	2.7	2.4	65.9	145.8	1.8
Snohomish (*Sno*)	Cascade	0.22 ± 0.1	4450	688	16	7.1	2.7	2.4	72.1	137.2	1.9
Stillaguamish (*St*)	Cascade	0.21 ± 0.1	1457	604	14	4.3	2.9	1.7	79.3	139.8	2
Skagit (*Ska*)	Cascade	0.09 ± 0.05	8035	1128	22	2	1.3	0.9	69.7	133.5	2
Skokomish (*Sko*)	Olympic	0.06 ± 0.03	592	609	21	5.5	1	1.3	72.9	112.6	2.3
Elwha (*El*)	Olympic	0.03 ± 0.02	757	1089	24	0.3	0	0.4	81.6	118.3	1
Duckabush (*Du*)	Olympic	0.03 ± 0.02	179	1047	27	0.8	0	0.3	76.1	95.7	2

1.7 FIGURES

Figure 1.1. Map and characteristics of the Puget Sound Basin watersheds of study. **a)** The watersheds of study shaded with their local slope in degrees. Black points represent the river water quality sampling stations. Italicized abbreviations refer to the river names, which are provided in full in Table 2. **b)** Location of the Puget Sound Basin within Washington state and British Columbia. **c)** Ordination plot showing principal component analysis (PCA) of watershed characteristics from the Puget Sound Basin rivers. Green points represent rivers located in the Cascade Mountains. Purple points represent rivers located in the Olympic Mountains. Length and direction of arrows on the ordination are proportional to vector loading of watershed characteristics into each principal component (PC).

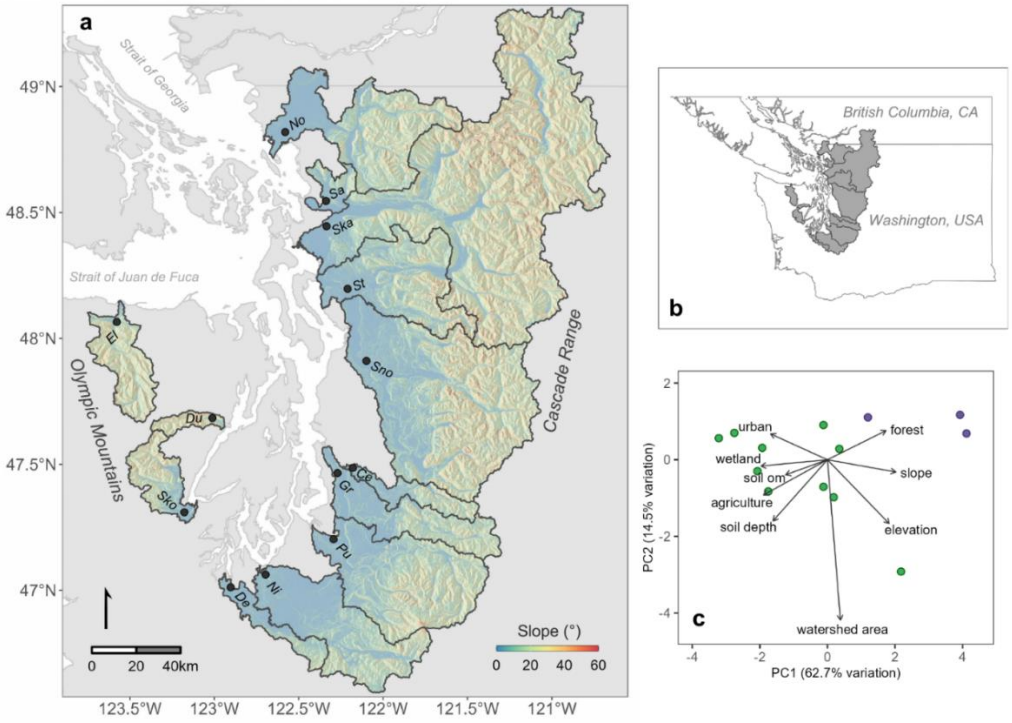

Figure 1-1 Study map

Figure 1.2. NO_3^- concentrations, $\delta^{15}N\text{-}NO_3^-$, and $\delta^{18}O\text{-}NO_3^-$ measured in the Puget Sound rivers. **a)** $\delta^{15}N\text{-}NO_3^-$ plotted versus NO_3^- concentrations. **b)** $\delta^{18}O\text{-}NO_3^-$ plotted versus $\delta^{15}N\text{-}NO_3^-$. Green points are values measured in the Cascade Range rivers. Purple points are values measured in the Olympic Mountain rivers. Typical ranges of the different nitrate end-members are also presented (Kendall et al., 2007), as well as the two typical trends (1:1 and 2:1) observed in literature(Kendall et al., 2007) for denitrification.

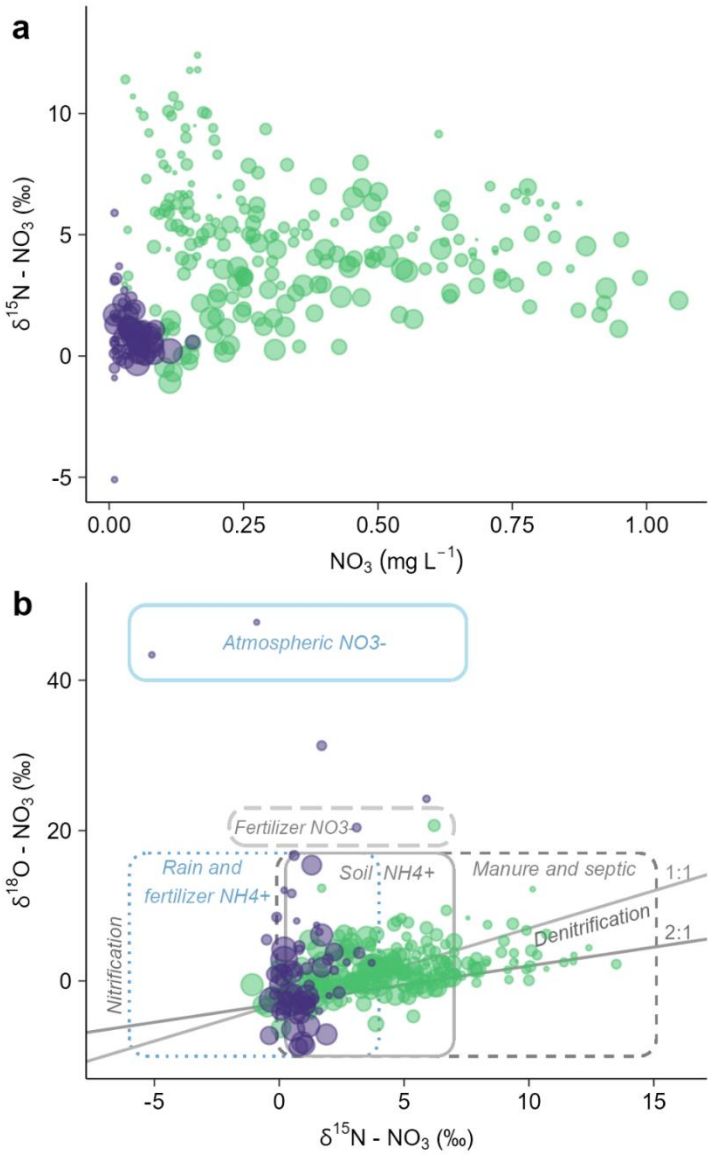

Figure 1-2 d15N vs. NO3

Figure 1.3. Modeled states for each response variable at the "Mountain range" scale (our most supported model). Green lines are the Cascade-level modeled state for each response variable (**a-d**). Purple lines are the Olympic-level modeled state for each response variable (**e-h**). Estimates are shown with their standard error, shaded in green and purple respectively. Gray circles represent the measured water quality sample data for the individual watersheds. Blue lines represent mean daily discharge across each mountain range river group. All data are standardized by mean and variance.

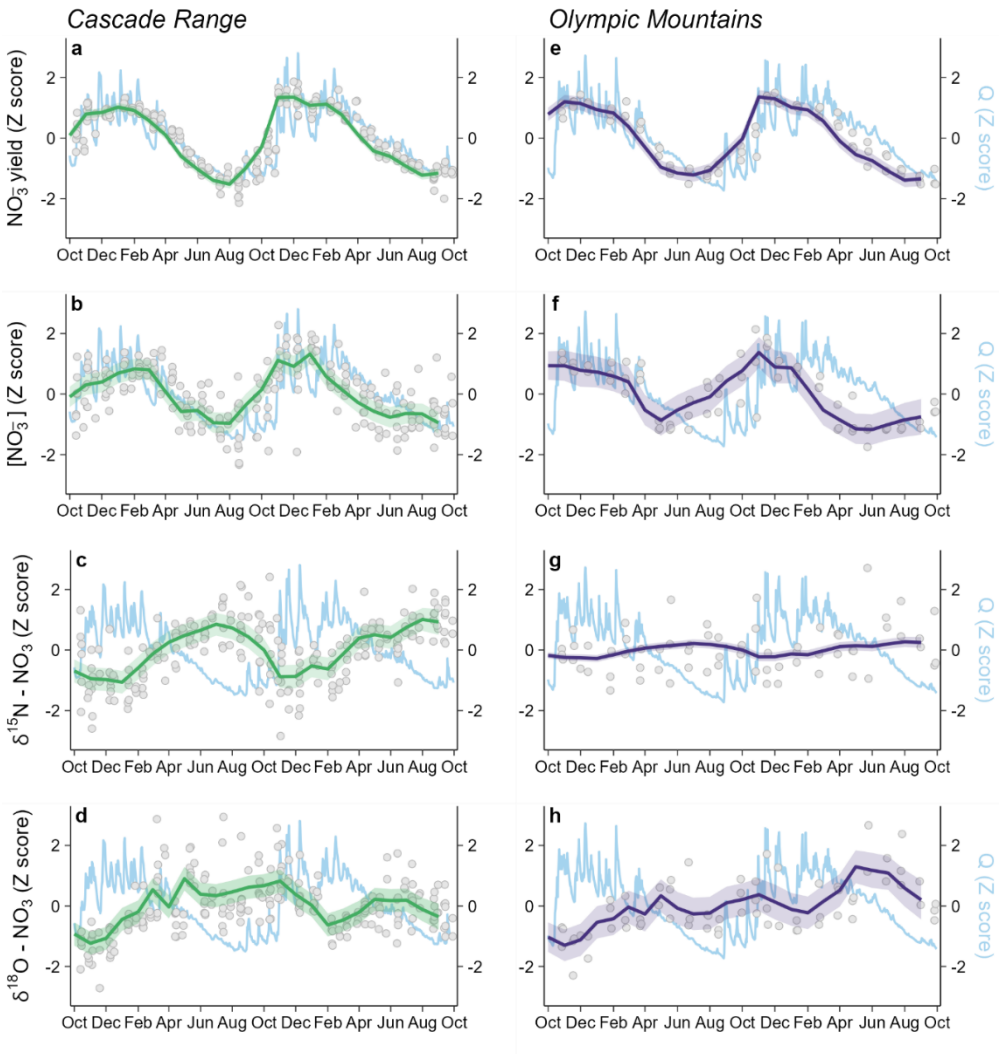

Figure 1-3 Mountain states

Figure 1.4. Estimated MARSS model coefficients for each covariate model considered at the mountain range scale. **a)** Effects of water temperature, precipitation, snowmelt and Standardized Precipitation Index (SPI) on NO_3^- yield at the mountain range scale. **b-d)** Effects of water temperature, precipitation, snowmelt, event-driven discharge (Q_{quick}), seasonal discharge (Q_{slow}), and SPI on NO_3^- concentration, $\delta^{15}N\text{-}NO_3^-$, and $\delta^{18}O\text{-}NO_3^-$ at the mountain range scale. Green points are the covariate effects shared among Cascade Range rivers. Purple points are the covariate effects shared among Olympic Mountain rivers. Points are maximum likelihood estimates for each coefficient with horizontal bars indicating the 95% confidence intervals around that estimate.

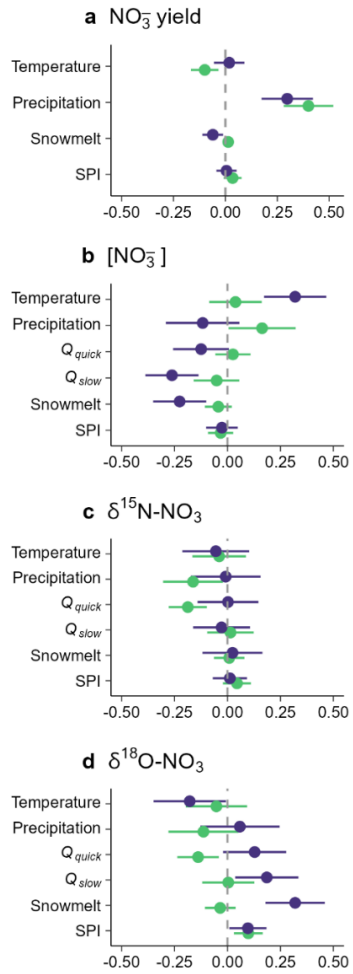

Figure 1-4 Climate effects

Figure 1.5. Watershed-scale MARSS covariate coefficients plotted versus mean watershed slope for each of our best covariate models. **a-b)** Watershed-scale effects of precipitation on NO_3^- yield and NO_3^- concentration plotted versus mean watershed slope. **c)** Watershed-scale effects of event-driven discharge (Q_{quick}) on $\delta^{15}N\text{-}NO_3^-$ plotted versus mean watershed slope. **d)** Watershed-scale effects of snowmelt on $\delta^{18}O\text{-}NO_3^-$ plotted versus mean watershed slope. Green points represent the covariate effect for each of the Cascade Range rivers. Purple points represent the covariate effect in the Olympic Mountain rivers. Pearson correlation coefficients are given in the lower left or upper left corner of each plot.

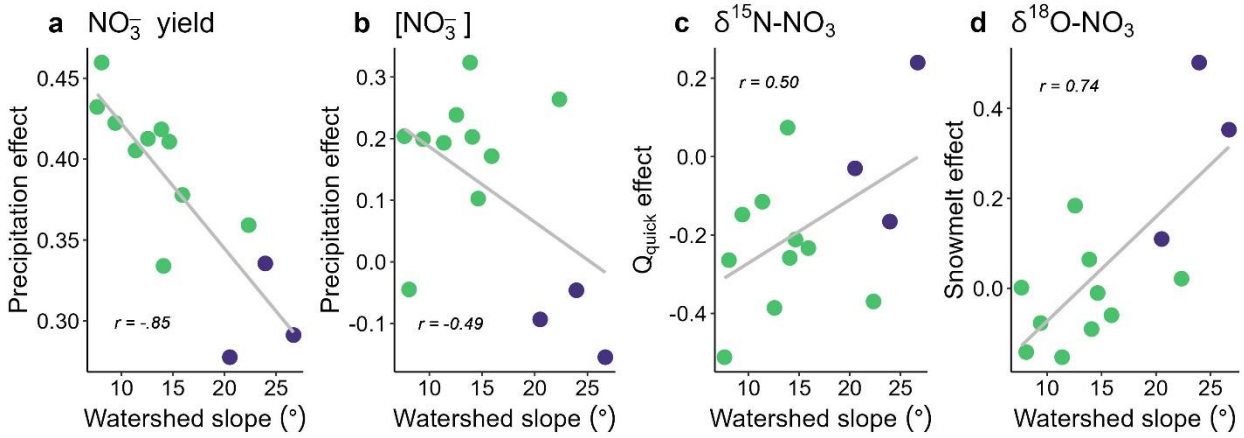

Figure 1-5 Climate vs. slope

CHAPTER 2: North Pacific climate modes and landform interact to drive multi-decadal patterns of nutrient concentration and transport in Pacific Northwest rivers

2.1 ABSTRACT

Evaluating interactions between climate, land use, and landscapes in driving river nitrogen (N) and phosphorus (P) dynamics is critical to understanding long-term changes in aquatic ecosystem functioning and downstream nutrient fluxes. These drivers, however, operate across multiple time scales and include seasonal, annual, and decadal climate fluctuations, which can obscure our understanding of long-term trends. Here, we assess the role of climatic and landscape-level variables in driving long-term (20-30+ years) changes in monthly river inorganic N and P concentrations and yields in 14 coastal rivers in western Washington State. We show that N and P concentrations, their ratio, and yields decreased or remained stable over time from 1988 to 2022, and that multi-decadal changes in river N and P dynamics were strongly influenced by shifts in North Pacific climate modes, particularly the Pacific Decadal Oscillation (PDO). Furthermore, we found that the response of N and P to PDO shifts varied among seasons and rivers, and this variation was best explained by a simple topographic feature, watershed slope. These results demonstrate the strong of climate variation on long-term river nutrient patterns, while also highlighting the distinct role of watershed topography in modulating the sensitivity of river N and P dynamics to hydroclimatic change.

2.2 INTRODUCTION

Interactions between climate and human-modified landscapes represent a key uncertainty in our understanding of the response of river nitrogen (N) and phosphorus (P) dynamics to anthropogenic and climate-driven change (Lewis & Grimm, 2007; McCluney et al., 2014; Soranno et al., 2014). In many river ecosystems, the enrichment of landscapes with N and P from human activities has stressed the bounds of river nutrient processing, fundamentally altering the delivery of N and P from land to sea and increasing primary production along the freshwater-to-marine continuum (R. Howarth et al., 2012; Ockenden et al., 2017; Turner, 2024; Vitousek et al., 1997). Climate is also changing globally, resulting in substantial shifts to temperature, precipitation, and river hydrologic patterns across freshwater landscapes (Arnell & Gosling, 2013; Hattermann et al., 2017). The transformation and transport of riverine nutrients are fundamentally embedded within these hydroclimatic shifts, yet we only have a limited understanding of how climate, anthropogenic change, and complex landscapes will interact to drive river N and P concentrations and the delivery of these nutrients from land to the coastal ocean (Seybold et al., 2022; Sinha & Michalak, 2016).

Understanding the long-term trajectories of N and P dynamics in rivers can provide important perspective to management efforts at landscape and regional scales, particularly in the context of climate and anthropogenic perturbations (Murphy & Sprague, 2019; Stets et al., 2020). Long-term change in and across rivers, however, is influenced by multiple controls that operate and interact across a wide range of spatial and temporal scales (Van Meter et al., 2018; Wilkinson et al., 2020). Anthropogenic changes to land use, management, or climate, for example, can progress slowly through time, resulting in gradual ecosystem shifts and directional, non-stationary patterns of N and P concentrations and loads (Metson et al., 2020; Murphy &

Sprague, 2019; Stackpoole et al., 2021; Wilkinson et al., 2020). Temporal changes in nutrient concentrations and transport at seasonal or annual time scales have instead been linked to interannual variability in precipitation (Sinha & Michalak, 2016), which mobilizes nutrients from the landscape and can generate shared or alternate responses to climate across rivers depending on local river and watershed-scale controls (Elmstrom et al., 2024; Smits et al., 2019). To effectively manage and conserve river ecosystems in the face of nutrient pollution, there is a pressing need to understand how anthropogenic and environmental controls interact across multiple scales to drive long-term patterns of change (Wilkinson et al., 2020).

Large scale climate phenomena such as the El Niño–Southern Oscillation (ENSO) and the Pacific Decadal Oscillation (PDO) introduce further variability to the long-term trajectories of river N and P concentration and transport (Hao & Lu, 2021; Smits et al., 2019). The influence of these climate phenomena manifests over multiple timescales, controlling and interacting with seasonal, annual, and decadal-scale variation in river discharge and nutrient loads (Fleming et al., 2007; Keener et al., 2010). The alternate phases of ENSO and PDO, for example, are associated with changes in air temperature, the magnitude and form of precipitation (rain vs. snow), and soil moisture, leading to annual and seasonal-scale variability in biogeochemical transformations, nutrient mobilization, and river flow (Rice & Emanuel, 2017; Smits et al., 2019). This finer-scale temporal variation ultimately scales up to decadal changes across river hydrologic and biogeochemical times series, which can mask or amplify directional change and obscure our understanding of anthropogenic or climate-driven shifts to river nutrient biogeochemistry and hydrologic regimes (Z. Chen & Grasby, 2009; Wilkinson et al., 2020).

Further complicating the response of ecosystems to temporal environmental variability is the spatial heterogeneity of landscapes, which filters the effects of regional-scale processes like

climate on river ecosystems. This has been exemplified across rivers in mountainous landscapes, where topographic relief exerts control over river hydrologic regimes (i.e., rain vs. snow-driven regimes) and watershed composition (e.g., vegetation, soils, land use), ultimately producing spatial variation in the climate sensitivity of river physical and chemical processes to climate (Cline et al., 2020; Elmstrom et al., 2024; Fleming et al., 2007; Lisi et al., 2015). Watershed land use and land cover can also alter the influence of climate on hydrology and biogeochemistry across river systems and at large spatial scales. For example, streamflow responses to El Niño events across the United States have been shown to be partially mediated by watershed forest cover (Rice & Emanuel, 2017), whereas the response of N and P concentrations to seasonal climate variation in the Great Lakes region has been shown to be altered by anthropogenic land use change, particularly increased agricultural and urban land cover (Van Meter et al., 2020).

While the impacts of anthropogenic change and climate may be expressed differently across rivers and through time, summarizing temporal variation among river systems that are spatially heterogenous and hydrologically diverse has the power to elucidate the multiple interacting controls that drive long-term biogeochemical change (Jankowski et al., 2021; Smits et al., 2019). Here, we harness a long-term (20-30+ years), regional dataset of dissolved inorganic N and P concentrations, yields, and N:P from 14 coastal rivers in western Washington State to examine how anthropogenic-driven changes, climate modes, and complex landscapes interact to control river N and P dynamics across space and through time. To distinguish discharge-driven temporal patterns in river N and P dynamics, we also assess long-term patterns of river discharge alongside our investigation of the long-term trajectories of river N and P. Specifically, we aim to address three questions: (1) How have river discharge, N and P concentrations, yields, and N:P changed across multiple decades?, (2) What climate and hydrologic variables are most related to

long-term changes in river discharge, N and P concentrations, yields, and N:P?, and (3) How does the response of river discharge and nutrient variables to changing climate conditions vary with watershed-specific factors, such as land use, topography, and hydrologic regime? By summarizing multiple decades of temporal variation at this regional scale, we examine the importance of regional controls (like climate or regional landscape change) and variation across individual watersheds (such as river hydrology, watershed land use and topography) in driving the long-term trajectories of river N and P dynamics. Strong contrasts in watershed land use, topography, and hydrologic regimes across our rivers of study allowed us to quantify the sensitivity of individual river nutrient dynamics to hydro-climatic change.

2.3 METHODS

2.3.1 Study area:

The Puget Sound Basin, located mostly in western Washington state, comprises a series of hydrologically complex and heterogeneous watersheds drained by intermediate to large rivers (Fig. 1, Table 1). The basin is bounded by the Olympic Mountains to the east and the Cascade Mountains to the west, with elevations exceeding 1,800 meters including several volcanic peaks surpassing 3,000 meters (Beechie et al., 2006). Intra-annual fluctuations in atmospheric circulation patterns over the North Pacific Ocean drive seasonal climate variability, which interacts with basin topography to produce heavy precipitation during the winter months (October – March), while summers (July – September) are generally warm and dry (Fleming et al., 2007). Within this setting, river hydrologic regimes are governed by timing and form of precipitation and are characterized as rainfall-dominated (low elevation with rain-driven winter freshets), snowmelt-dominated (high elevation with snow-driven summer freshets), and

transitional (intermediate elevation with mixed winter and spring freshets) (Beechie et al., 2006; Reidy Liermann et al., 2012). We expect that each of these river hydrologic regimes has a unique sensitivity to long-term changes in climate, with multi-annual variability driven by large-scale ocean and climate patterns (Fleming et al., 2007, 2016).

Land-use histories and development in the region have resulted in a gradient of human disturbance and land cover across the basin. While the slopes of the Cascade and Olympic Mountain ranges remain mostly forested, transitions to urban and agricultural land uses along with increased logging since the late 1800s have significantly reduced lower elevation and floodplain forests. The south and central valleys of the western Cascade Range are now mainly urban and rural residential land, with some pastureland and crop fields located outside the urban fringe (Hill et al., 2016). Most agricultural activity, including forage and specialty crop cultivation, occurs in the northeastern part of the basin (*2015 WSDA Agricultural Land Use*, 2022). Lower elevations along the Cascade Range feature a mix of second-growth and regenerating forest, and include large stands of the early successional N-fixing species, red alder (*Alnus rubra*) (Wise & Johnson, 2011). Some areas retain pockets of primary forest, particularly at higher elevations and in protected regions like national forests. Watersheds along the eastern Olympic Mountains remain mostly forested with coniferous trees, but with some logged areas and sparse pastureland, crop fields and residential development (*2015 WSDA Agricultural Land Use*, 2022; Hill et al., 2016). Primary forests remain intact in areas like the Olympic National Park, which has been protected from logging since its establishment. The combination of complex topography, multiple hydrologic regimes, and altered land use history creates a variable landscape across the Puget Sound basin, making it a valuable system for studying the role of

climate vs. human activity in driving multi-decadal patterns of river N and P transport regimes and their implications for coastal oceans.

2.3.2 Nutrient and discharge data:

We obtained time series of monthly dissolved ammonium, nitrate, nitrite, and orthophosphate (DIP) data (October 1988-2022 for N; May 2001-2022 for P) from the Washington Department of Ecology's Freshwater Information Network database. Because the majority of inorganic N in Puget Sound rivers is nitrate, we summed dissolved ammonium, nitrate, and nitrite prior to analysis (hereafter called total dissolved inorganic N or DIN). We focused on dissolved inorganic nutrient forms due to their prevalence in Puget Sound rivers and the consistency of available records and laboratory methods. We selected 14 rivers that drain into the Puget Sound, which exhibited a range of watershed physical and land use characteristics (see Table 1), and which had a DoE sampling station located at the watershed mouth (Fig. 1). For more information on the Washington DoE's freshwater monitoring program and methods, refer to Von Prause, 2021.

Daily discharge data for the USGS gaging station nearest to each water quality sampling station were obtained from the USGS National Water Information System database using the dataRetrieval package in R (De Cicco et al., 2024; USGS, 2023). We estimated monthly river DIN and DIP loads (kg month^{-1}) using the Weighted Regression on Time, Discharge, and Season model with the Kalman filter (WRTDS-K; Q. Zhang & Hirsch, 2019) in the Exploration and Graphics for RivEr Trends (EGRET) R package (Hirsch et al., 2023). To generate DIN and DIP yields (kg km^{-2} month^{-1}) for our analysis, we divided these monthly fluxes by watershed area.

Plots of monthly river discharge, DIN and DIP yields, DIN and DIP concentrations, and DIN:DIP molar ratios for each river site can be found in Supporting Information Figs. S1–S6.

2.3.3 Regional and watershed-scale climate covariates:

We considered the Pacific Decadal Oscillation (PDO) and the Multivariate El Niño–Southern Oscillation Index (MEI) as metrics of large-scale climate variability in our time series models. The PDO represents a long-term climate pattern characterized by spatial patterns and fluctuations in sea surface temperatures in the North Pacific Ocean. It involves alternating phases of warm and cool conditions, with each phase typically lasting for one to two decades (Y. Zhang et al., 1997). The MEI uses multiple variables to monitor cyclic variability associated with the El Niño-Southern Oscillation (ENSO), a climate phenomenon characterized by sea surface temperature anomalies in the equatorial Pacific Ocean. The warm (El Niño) and cool (La Niña) phases of ENSO can vary in duration, ranging from months to a few years (T. Zhang et al., 2019). Though they represent different climate phenomena, both the PDO and the ENSO exhibit strong controls on atmospheric circulation and weather patterns in western Washington state. We downloaded monthly PDO and MEI index values using the rsoi package in R (Albers, 2023).

Average monthly temperature and total monthly precipitation were included to represent monthly climatic variability at the watershed scale. We extracted gridded estimates of total daily precipitation and daily air temperature data for each watershed boundary from Oak Ridge National Laboratory's Daymet dataset (Thornton et al., 2020) and summed the estimates per each month sampled. For our DIN and DIP concentration and ratio models, we also considered mean monthly discharge as a covariate.

2.3.4 Watershed and landscape characteristics

We compiled watershed-scale landscape metrics for each of the watersheds corresponding to our 14 study rivers using the Environmental Protection Agency's StreamCat data library (Table 1). These metrics included watershed area, mean watershed elevation, and percent urban, wetland, agricultural, ice, and forested land. We also included mean watershed slope in our analyses as it captures aspects of watershed topography and stream geomorphology that may influence nutrient retention, loss, or transfer, such as water residence times, floodplain area, and hydrologic connectivity. We calculated watershed slope as the average of all slope raster pixels within the boundaries of each individual river's watershed using ArcGIS (v10.8).

2.3.5 Principal component analysis

To summarize the dominant gradients of environmental variability among river sites and their watersheds, we used principal component analysis (PCA) to reduce the dimensionality of watershed land use, land cover, and topographic features, which were highly colinear across our study sites. Data constrained to irregular, restricted ranges were scaled to [0-1] and arcsine-square root transformed, along with all proportional data (the logit transform was avoided to prevent generation of infinite values.). All multivariate data analyses were conducted using the **vegan** and **biostats** packages in the program R (R Core Team, 2023).

2.3.6 Time series analysis

We used a series of multivariate linear mixed effect models with different combinations of shared or independent random walks through time and time-varying covariates to 1) characterize the long-term, multi-annual pattern of river discharge and nutrient time-series, and

2) estimate the strength of different climate and hydrologic variables in explaining temporal variation at the multi-decadal scale. Specifically, the model structure is as follows:

$$\mathbf{x}_t = \mathbf{x}_{t-1} + \mathbf{u} + \mathbf{w}_t;\ \mathbf{w}_t \sim \text{MVN}\ (\mathbf{0}, \mathbf{Q})\ \ (\mathbf{1.1})$$

$$\mathbf{y}_t = \mathbf{Z}\mathbf{x}_t + \mathbf{D}\mathbf{d}_t + \mathbf{v}_t;\ \mathbf{v}_t \sim \text{MVN}\ (\mathbf{0}, \mathbf{R})\ \ (\mathbf{1.2})$$

In the process model (1.1), the shared or independent latent state ($\mathbf{x}_t$), is modeled as a random walk through time such that the value at time *t* is equal to its value at time $t - 1$ plus a bias term (**u**) and some random normally distributed error (w_t) with a mean (**0**) and variance (**Q**). The off-diagonals of the **Q** matrix measure covariance in the process errors after accounting for shared or independent random walks, thus providing an estimate of independence or correlation between the latent states, $\mathbf{x}_t$. In the observation model (1.2), $\mathbf{y}_t$ is an *i* x 1 vector of measured data (i.e., river discharge, nutrient yield, concentration, or ratio) at time *t* from each river station (*i* = 14). $\mathbf{y}_t$ is modeled as a linear combination of the latent states ($\mathbf{x}_t$), a *j* x 1 vector of explanatory variables ($\mathbf{d}_t$; *j* refers to different number of covariates), and an $i \times 1$ vector of observation errors ($\mathbf{v}_t$), which are distributed as a multivariate normal with mean 0 and variance-covariance matrix (**R**). The $i \times m$ vector **Z** maps each of the measured river time series (i = 14) onto the shared or independent latent states (*m* = 1 or 14) in $\mathbf{x}_t$. The $i \times j$ matrix **D** contains the coefficients of the covariate effect sizes.

We modeled each response variable separately (i.e., river discharge, DIN and DIP yields, DIN and DIP concentrations, and DIN:DIP) and first tested the fit of candidate models that included all possible covariates (i.e., our global model) and contained either one shared state among rivers or independent, river-specific states through time using Akaike Information Criterion adjusted for small sample size (AICc; Burnham & Anderson, 2004). To evaluate the

possible variance and covariance in our observation errors and among the independent state processes ($\mathbf{x}_t$), we tested data support for two options of the **R** and **Q** matrices: (1) equal variance and equal covariance, and (2) equal variance but no covariance. To calculate the monthly rate of change in river discharge and nutrients across our 20 to 30-year period of study, we set **u** to be unique for each of the states. Using the most parsimonious model for the model states, **R**, and **Q** matrices as determined by AICc, we then evaluated the data support for different climate and hydrologic drivers of river discharge and nutrient dynamics by adjusting covariate time series (i.e., river discharge, precipitation, temperature, MEI and PDO) in the **d** matrix. Additionally, to address the strong autocorrelation in our monthly observation time series, we included a fixed effect of month in each model. We evaluated correlations among individual covariates and, to avoid multicollinearity, correlated covariates were never included in the same model.

To further assess how the alternating phases of the ENSO and PDO influenced river seasonal hydrologic and nutrient regimes, we manipulated the **D** and **d** matrices to test two models for season-specific climate phenomena effects: (1) One where the effects of MEI and PDO were separate for fall (October-December), winter (January-March), spring (April-June), and summer (July-September), and (2) another where the effects of MEI and PDO on the wet, winter months were shared (October-April), and separate for the transitional, spring (May-June), and dry, summer (July-September) months.

The response data were log-transformed to meet the assumptions of normality. Both the response and covariate data were standardized to a mean of zero and standard deviation of one (Z-score) to account for the differences in means and variances and standard effect sizes. Candidate models (models with different number of states and covariate terms) were treated as different hypotheses and compared using AICc (Burnham & Anderson, 2004). Models were

programmed using the MARSS and marssTMB (Holmes et al., 2021) package in R (R Core Team, 2023).

Finally, we examined if variation in river-specific covariate effect sizes (**D**) could be explained by differences in watershed geomorphic or land-use attributes, specifically, watershed area, elevation, slope, and percent urban, wetland, agricultural, and forested land.

2.4 RESULTS

2.4.1 River and watershed characteristics covary with watershed slope:

PCA summarized a large proportion of variance (85%) in the river and watershed characteristics (PC1 = 61.1%, PC2 = 23.9%). PC1 was statistically significant according to a Monte Carlo randomization test (PC1, p = 0), and all variables except watershed area and ice cover had significant loadings on PC1 (Table SI 1, Fig. 1c). Notably, watershed slope had an exceptionally high loading on PC1, with a linear correlation between the PC1 vector loadings of 0.96 (Table SI 1). Rivers with increased human activity and wetland areas were found in low-elevation, low-gradient watersheds (Fig. 1c). Conversely, rivers with greater forest cover were grouped in watersheds with higher elevations and steeper gradients (Fig. 2a). These river groupings also corresponded to average mean annual temperatures, likely reflecting precipitation form and river hydrologic regimes. This indicates that rain-dominant rivers are prevalent in low-elevation, low-gradient watersheds with increased human activity, while snow-dominant rivers are more common in higher, steeper watersheds with greater forest cover. The second PCA axis was primarily explained by watershed area and percent ice cover and was not statistically significant (PC2, p = 0.193).

2.4.2 Long-term trajectories of river discharge and nutrients:

Long-term trajectories of river discharge and nutrients were largely independent among rivers that drain the Puget Sound Basin, but river discharge and nutrient dynamics exhibited some degree of correlation at the multi-decadal scale. For all six response variables (river discharge, DIN and DIP yields, DIN and DIP concentrations, and DIN:DIP), models that allowed time series to follow separate state processes resulted in better fits than models including a single shared state among rivers (Figure 2, Table SI 2). However, we also found that models with correlated error structures were best supported for all six response variables (Table SI 2), indicating that, although rivers followed separate long-term trajectories, rivers still shared some degree of variation in their long-term patterns of discharge and nutrients (Fig. 2).

The estimated bias terms for the state processes represent the trend or drift component for each individual river, providing an average rate of change per time step (in this case, per month) for each river discharge and nutrient time series. The monthly rate of change in discharge varied among rivers, but on average most rivers showed increases in mean annual discharge since 1988. Notably, decreases in DIN concentrations and yields were found across almost all of the Puget Sound rivers, with the exception of the Deschutes River, which exhibited a positive rate of change through time for both response variables (Figure 2). Although changes to DIP concentrations were less pronounced than those in DIN concentrations, most rivers showed decreases while the Puyallup, Nooksack, Snoqualmie, and the Elwha rivers exhibited increasing concentrations since 2001. Rates of change in river DIP yields were also comparably small and variable across rivers (Fig. 2a, e). The net impact of changes to DIN and DIP concentrations resulted in declining DIN:DIP trends, with the exception of the Deschutes and Duckabush rivers, which had positive rates of change through time. (Fig. 2).

When considering rates of change in units of total river nutrient load (km^2 $month^{-1}$), the largest contributors to the total Puget Sound Basin-scale net decrease in river DIN load were the Skagit, Puyallup, Nooksack, and Snoqualmie Rivers, the first three of which have the largest watersheds in our study system (Fig. 3a, Fig 1a). The Skagit, Puyallup, and Nooksack rivers were also the largest contributors to the basin-scale net change in total DIP load, but instead contributed a Puget Sound Basin-scale increase in total river DIP loads (Fig. 3b).

2.4.3 Climate effects on river discharge and nutrients:

For all response variables, our best-supported models ($\Delta AIC < 2$) included an effect of precipitation and season-specific effects of the PDO (Supplemental Tables 3-8). River discharge and DIN and DIP yields responded positively to precipitation across all rivers (Fig. 4), demonstrating that during years with heavy rainfall and snow, the export of freshwater and nutrients broadly increased across the Puget Sound Basin. The responses of river DIN and DIP concentrations and DIN:DIP ratios to increased precipitation were smaller and more variable (Fig. 4). In most rivers, precipitation had a positive effect on DIN concentrations, whereas the response of DIP concentrations to precipitation varied across rivers, with some rivers increasing and others decreasing in DIP concentration in response to increased rainfall and snow (Fig. 4). The net impact of precipitation on river DIN and DIP concentrations resulted in a positive or neutral response of river DIN:DIP to precipitation, with the exception of the Deschutes, Green, and Elwha rivers, where DIN:DIP decreased during wet years.

In contrast to precipitation, responses of river discharge and nutrients to PDO-driven climate shifts were distinct across rivers but varied predictably across the hydrologic season in association with one simple topographic feature, mean watershed slope. When PDO values were positive (i.e., phases associated with higher air temperatures and precipitation falling as rain vs.

snow), rivers draining steeper watersheds exhibited stronger winter and summertime responses in discharge compared to rivers draining lower sloped terrain. In mid-sloped watersheds, the greatest response of river discharge to PDO-related climate shifts was found in the spring, resulting in a notable decrease in spring-time river flow (Fig. 5a).

For DIN concentrations and DIN:DIP ratios, the strongest effects of the PDO were expressed in the spring, with contrasting responses across rivers again depending on topography. In low-sloped rivers, DIN concentrations and DIN:DIP increased under warming conditions, and, in high-sloped rivers, DIN concentrations and DIN:DIP decreased (Fig. 5b, d). Similar to our precipitation model effects, the sensitivity of DIP concentrations to PDO-phase shifts was comparably variable among rivers, with the largest effects found in the summer and in rivers draining intermediate sloped watersheds (Fig. 5e). The response of DIN and DIP river yields to PDO-driven shifts closely mirrored the effects of PDO on river discharge, but with a decrease in springtime DIN yields in high sloped rivers (Fig., 5c, f).

2.5 DISCUSSION

Using a long-term, regional dataset with monthly resolution, we found evidence of widespread, directional change in river nutrient dynamics across the Puget Sound Basin, alongside climate-driven, oscillatory variation in seasonal river hydrologic and nutrient regimes. Our findings reveal that concentrations, ratios, and yields of DIN and DIP in Puget Sound rivers have largely decreased or remained stable over the past two to three decades, and that multi-annual patterns in river discharge and nutrient regimes are strongly influenced by the large-scale climate oscillations, particularly by the PDO. Furthermore, we found that the seasonal response of N and P concentrations, ratios, and yields to PDO shifts varied among rivers, and that this variation was best explained by a simple topographic feature, mean watershed slope.

Specifically, rivers in steep-sloped watersheds exhibited the greatest sensitivity in their nutrient transport regimes to climatic changes, compared to rivers draining low-relief watersheds. These results demonstrate the influence of climate oscillations on long-term river nutrient patterns, while also highlighting the distinct role of watershed topography in mediating the sensitivity of river N and P dynamics to hydroclimatic change.

2.5.1 Long-term changes are by driven by large-scale, regional processes

Given the strength of regional-scale climate patterns in the Pacific Northwest and the varied landscape and land use history of the Puget Sound Basin, it was unclear whether shared climate forces would drive coherence across rivers or if watershed-scale variation in landform and human influence would produce independent patterns of river discharge and nutrients. Here, we found that rivers statistically followed separate long-term trajectories, but that rivers still exhibited a high degree of coherence in their directionality of change and patterns of variance over multiple years. DIN concentrations declined in all but one river, and all rivers displayed similarities in their multi-annual patterns of discharge, DIN and DIP yields, concentrations and DIN:DIP molar ratios (Fig. 2). The independent, yet correlative nature of the river states aligns with recent work from the Mississippi River Basin, where river basins responded similarly to inter-annual and multi-annual scale climate variation, but followed separate, long-term patterns of river discharge and nutrient loads (Smits et al., 2019). Together, this exemplifies how long-term patterns of river nutrient transport are influenced by large-scale climate forces but become disparate due to watershed-scale differences in land use and hydro-geomorphic river controls.

The broadly shared declines in DIN concentration and yield found across most Puget Sound rivers further point to regional-scale processes as potential drivers of long-term change, but instead at the spatial, landscape-level scale. An example of such a process could arise from

regional-scale water quality management efforts, shifting atmospheric N deposition patterns, or changes in regional economies. Notably, the rise and decline of timber harvest over the past century has created a large-scale land use experiment across mountainous western North America, with potential implications to river water quality. Reduced harvest volumes and improved logging practices, for example, have been linked to declining runoff and sediment inputs to rivers in both the Cascade Range and the Olympic Mountains (Jaeger et al., 2023; Reiter et al., 2009). Additionally, in northern Sierra Nevadan streams, long-term declines in NO_3 concentrations and loads have been attributed to forest aggradation and the replacement of N-fixing alder stands with nitrification-inhibiting coniferous trees. It is plausible that these same mechanisms could drive declines in DIN across the Puget Sound rivers, as soils and red alder have been identified as key sources of nitrogen in these watersheds (Elmstrom et al., 2024; Wise & Johnson, 2011). However, monitoring data from the National Atmospheric Deposition Program indicates that atmospheric N deposition has declined across the Cascade Range since the late 1980s (Supplemental Figure 7), suggesting that deposition patterns are likely also contributing to the DIN concentration and yield declines.

The Skagit, Nooksack, Puyallup, and Snoqualmie rivers were the largest contributors to the Puget Sound Basin-scale change in total DIN and DIP loads ($kg^2\ month^{-1}$), indicating that while most rivers exhibited changes over time, not all were considered equal contributors to the net change in total nutrient load to the Puget Sound estuary (Fig. 3). Notably, while these rivers contributed to a basin-scale decrease in DIN load since 1988 (Fig. 3a), they conversely contributed to a basin-scale increase in DIP load since 2001 (Fig. 3b). The Skagit, Nooksack, and Puyallup rivers have the largest contributing watersheds to the Puget Sound estuary in our study, suggesting that their large contributions to the basin-scale decrease in DIN loads were likely

influenced by both watershed DIN inputs and their total discharge volume. Larger rivers typically carry larger total loads, so even modest percentage decreases in load can translate into substantial decreases in absolute terms. These watersheds also have increased agricultural activity relative to other locations within the Puget Sound Basin. For instance, the Nooksack and Skagit watersheds are located in the northern part of the basin, where the majority of forage and row crops are grown and harvested (Wise & Johnson, 2011). The contrasting decreases in DIN and increases in DIP loads in these rivers suggests that changing land cover and agricultural practices in these watersheds likely altered river DIN and DIP loads to the Puget Sound estuary. Regardless of land use effects or physical controls, the changes in river DIP loads were relatively small (ranging from 0 to less than 200 kg^2 $month^{-1}$) (Fig. 3b), indicating that the largest changes in total nutrient load to the Puget Sound estuary were in DIN, whereas river DIP loads remained relatively stable over time.

2.5.2 Large-scale changes in climate as drivers of river discharge and nutrient regimes

Our modeled effects of precipitation and the PDO further distinguish large-scale climate forces as key drivers of long-term river hydrological and biogeochemical change, while providing detail critical to our understanding of changing climate conditions and river biogeochemistry at the seasonal scale. We found that precipitation and the PDO best explained multi-decadal patterns in river discharge and nutrients, but that the effects of PDO-driven climate shifts on river hydrologic and nutrient regimes manifested differently across seasons (Fig. 4). This highlights the sensitivity of river hydrologic and nutrients to both the total amount of precipitation (as described by our precipitation covariate), as well as finer-scale, seasonal sensitivity to changes in air temperature and precipitation form (as described by the PDO). Hydrologic regimes shift under alternate PDO phases in the Pacific Northwest through changes

to runoff and snow-driven flow (Fleming et al., 2007, 2016). Large-scale climate phenomena have also been linked to biogeochemical processes and river constituent transport in other parts of the globe through hydrologic regime shifts and climate controls on soil temperature and moisture (Hao & Lu, 2021; Jankowski et al., 2021; Johnston et al., 2022; Keener et al., 2010; Smits et al., 2019). Here, we show that climate phenomena also affect in-stream nutrients and transport regimes in the Pacific Northwest, specifically that seasonal-scale changes in river DIN and DIP yields, concentrations and DIN:DIP molar ratios are associated with PDO-driven shifts to air temperature and the proportion of precipitation falling as rain vs. snow.

In hydrology, ecology, and oceanography, it well established that extracted trends can be influenced by climate-driven oscillations within the natural dataset, potentially obscuring true directional changes (Z. Chen & Grasby, 2009; Litzow et al., 2020; Y. Zhang et al., 1997). Our results extend this understanding to riverine nutrient dynamics in the Pacific Northwest—Not only do river nutrient concentration and transport change seasonally, but these seasonal patterns shift with macro-scale climate drivers like the PDO, producing longer-term oscillations at the multidecadal scale. This highlights the importance of multi-annual dynamics in river biogeochemical time series and underscores the necessity of accounting for large-scale climate oscillations in river nutrient trend analyses before attributing long-term changes to management or climate change alone (Wilkinson et al., 2020).

2.5.3 Topography controls the climate sensitivity of river discharge and nutrient regimes

The final piece of our analyses indicates that variation in the response of river discharge and nutrient regimes to PDO-driven climate shifts was largely explained by watershed-scale differences in topography, specifically by watershed slope. These results suggest that for rivers that drain the Puget Sound Basin, the sensitivity of discharge and nutrient regimes to changing

climate conditions is strongly influenced by the slope and elevation of watersheds, which interact with large-scale climate patterns to control the contribution of rain vs. snow that shape river hydrologic regimes (Fleming et al., 2007). For example, we found that in warmer years when PDO was positive, discharge and nutrient yields in rivers draining steeper watersheds increased in the winter but declined in the summer, demonstrating a shift from snowmelt to rain-driven nutrient transport in rivers with snow-dominant hydrologic regimes (Fig. 5a). Conversely, in rivers draining lower sloped watersheds with rain-dominant hydrologic regimes, altered air temperature and precipitation patterns under positive PDO-phases left the seasonality of river discharge and nutrient transport regimes largely unchanged (Fig. 5). The alternate responses of discharge and nutrient yield in rivers with rain- and snow-dominant flow suggest that the seasonal shift in N and P yield in high-sloped rivers is largely driven by physical mechanisms, particularly the transition from snowmelt to rain-driven runoff at higher elevations, which enhances the physical transport of water and nutrients across the landscape and out to sea (Sinha & Michalak, 2016).

In rivers draining intermediate-sloped watersheds, spring-time flow experienced notable declines during positive PDO years, indicating that, in rivers characterized by earlier and lower volume snowmelt, the snow freshet all but diminished (negative effects, Fig. 5a). The contrasting responses of spring nutrient concentrations with watershed slope (Fig. 5b, e) can be directly related to these changes in snow-driven flow and highlight the nuanced control of topography on hydrologic regime and on instream nutrient biogeochemistry— particularly through nutrient transfers, watershed composition (e.g., vegetation and soil development), and sources. Notably, in the Puget Sound Basin, watershed topography also is related to the spatial arrangement of human activity (Fig. 1c) and land use is subsequently correlated with topographic controls on

instream nutrients and their response to hydroclimatic change (Elmstrom et al., 2024). Although we cannot disentangle the role of land use vs. topography in driving the sensitivity of instream nutrients to climate, we surmise much of the variation in the response of river DIN and DIP concentrations to the PDO was driven by simple physical controls on discharge volume and nutrient supply. For example, in lower to mid-sloped rivers, springtime DIN and DIP concentrations increased under warmer conditions (positive PDO effects; Fig. 4), suggesting DIN and DIP simply concentrated in response to snow-driven discharge declines. Further, although spring discharge appeared unchanged in high sloped rivers in our model results during warm PDO years (Fig. 5), plots of the raw discharge data indicate that volume of the spring snow-freshet did in fact decline (Fig. S7). The decrease in springtime nutrient concentrations in high sloped rivers under low flows demonstrates the reliance of snow-dominant rivers on snow-driven hydrologic connections and the associated delivery of external nutrient supplies.

Taken together, these results show that the hydroclimatic shifts dominate the response of winter and summer DIN and DIP yields across rivers, whereas changes to springtime nutrient concentrations, yields, and DIN:DIP are driven by complex interactions between snow-driven flow and the influence of topography on instream nutrient concentrations, sources, and supply. While the coherence of nutrient yields with altered hydrologic regimes is largely to be expected (Sinha & Michalak, 2016), the translation of climate-altered flows to instream nutrient concentrations and stoichiometric ratios in the Pacific Northwest is relatively new. Snow-driven flow has been established as a critical, but unstable component of fluvial constituent regimes in other Mediterranean and in sub-arctic environments (Johnson et al., 2024). Here, we link snow-driven flow to interannual variation in seasonal concentration regimes and DIN:DIP, but with a common underlying controlling feature across watersheds (i.e., watershed slope). The contrasting

responses of nutrient concentrations and DIN:DIP with watershed slope indicate that rivers draining high sloped watersheds may increase in their N limitation during warmer PDO phase conditions, with the most pronounced effects seen in the spring. While further research is needed to understand climate-altered nutrient concentrations and stoichiometric ratios in the Puget Sound rivers, our work provides evidence to show that the sensitivity of instream nutrients and N:P to hydroclimatic change is controlled by the influence of topography on instream nutrient supply and on seasonal hydrologic regime.

2.5.4 Conclusions

Establishing this connection between large-scale climate oscillations and watershed topography provides mechanistic insight into drivers of interannual variability in seasonal nutrient transport by rivers, while providing new information to help predict future patterns of river N and P transport. Our results ultimately show that rivers draining steeper watersheds had hydrologic and nutrient transport regimes that were more sensitive to variation in PDO phases (i.e., transient and snow dominant regimes), compared to rivers draining lower sloped terrain (i.e., rain dominant regimes) (Fig. 5). The homogenization of river hydrologic regimes due to reductions in snow-driven flow is projected to be one of the major outcomes of climate change in the Pacific Northwest (Hamlet et al., 2013; Marlier et al., 2017). Our results suggest that as snowpack declines, rivers draining intermediate and steeper slopes will also lose seasonal complexity in their nutrient exports, leading to an overall increase in winter-time nutrient transport at the Puget Sound Basin scale. This study builds upon two areas of previous work in river biogeochemical and ecosystems science. The first is the connection between climate-altered precipitation patterns and the changing seasonality of river nutrient transport. Increased winter-time nutrient transport, for example, has been projected to be a major outcome of climate-altered

runoff patterns and increased rain-on-snow events in the Midwest U.S. (Hrycik et al., 2024; Seybold et al., 2022). More broadly, in boreal and temperate watersheds across the globe, winter has seen greater increases in nutrient transport compared to other seasons (Jankowski et al., 2023). The second area of focus is the is the link between watershed topography and the response river ecosystem function to changes in climate. This has been previously established across the Pacific Northwest and in other mountainous landscapes, where the sensitivity of multiple other river physical and biogeochemical parameters to climate has been shown to vary as a function of watershed slope (Cline et al., 2020; Connolly et al., 2018b; Harms et al., 2016; Jankowski & Schindler, 2019; Lisi et al., 2015). Altogether, this work underscores the value of exploring multi-annual climate dynamics across river systems, and suggests that topographic features, including watershed slope, could enhance predictive modeling of nutrient transport across rivers at regional scales, which will be increasingly important under future climate scenarios that involve losses in snow and substantially altered river hydrologic regimes.

2.6 TABLES

Table 1. River and watershed characteristics of the Puget Sound Basin rivers of study. River and watershed characteristics are ordered by decreasing monthly mean DIN concentration. Other descriptors include mean DIP concentration, stream order, watershed area, mean watershed elevation, mean watershed slope, and percent urban, agriculture, wetland, forest, and ice cover by area of the watershed. Water quality sampling sites are labeled on Figure 1 using the italicized abbreviations in the first column of the table.

Table 2-1 Watershed characteristics

River name (*Map abbreviation*)	DIN (mg L^{-1})	DIP (mg L^{-1})	Stream Order	Watershed area (km^2)	Watershed elevation (m)	Watershed slope (°)	% Urban	% Agriculture	% Wetland	% Forest	% Ice
Samish (*Sa*)	0.69 ± 0.2	0.007 ± 0.003	4	225	268	8	9.2	7.7	5.8	68.3	0
Deschutes (*De*)	0.68 ± 0.1	0.015 ± 0.004	3	409	288	8	15.4	8.3	5	55.2	0
Green (*Gr*)	0.40 ± 0.1	0.013 ± 0.005	5	1116	546	11	22.8	4.8	2.4	62.6	0
Nooksack (*No*)	0.39 ± 0.2	0.009 ± 0.005	5	2046	674	14	4.9	12.4	2.9	65.5	1.3
Snoqualmie (*Sn*)	0.27 ± 0.1	0.005 ± 0.002	5	1780	638	16	6.5	2.7	2.7	75.5	0.05
Cedar (*Ce*)	0.26 ± 0.1	0.007 ± 0.002	4	457	611	13	15.8	0.6	1.5	76.4	0
Puyallup (*Pu*)	0.24 ± 0.1	0.018 ± 0.007	6	2439	921	15	9.3	2.6	2.4	67.3	1.5
Nisqually (*Ni*)	0.24 ± 0.1	0.010 ± 0.003	5	1853	556	9	8.5	6.4	5.6	64	0.9
Stillaguamish (*St*)	0.22 ± 0.1	0.006 ± 0.004	5	1457	604	14	4.4	2.9	1.7	81.5	0.05
Skykomish (*Sky*)	0.14 ± 0.08	0.003 ± 0.001	5	1987	905	21	2.4	0.9	1.1	80.9	0.3
Skagit (*Ska*)	0.11 ± 0.06	0.004 ± 0.001	6	8035	1128	22	2	1.3	1	70.9	2
Skokomish (*Sko*)	0.07 ± 0.04	0.007 ± 0.002	5	592	609	21	5.5	1	1.3	77.9	0.02
Duckabush (*Du*)	0.04 ± 0.02	0.003 ± 0.001	3	179	1047	27	0.8	0.01	0.3	76.9	0.2
Elwha (*El*)	0.04 ± 0.03	0.004 ± 0.001	4	757	1089	24	0.4	0.03	0.5	81.8	0.5

2.7 FIGURES

Figure 2.1. Map of the Puget Sound watersheds of study. **a)** Study watersheds shaded by land surface slope in degrees. Black points indicate the river water quality sampling station locations. Italicized abbreviations refer to the river names, which are provided in full in Table 1. **b)** Location of the Puget Sound Basin within Washington state and British Columbia. **c)** Ordination plot showing principal component analysis (PCA) of watershed characteristics from the Puget Sound Basin rivers. Length and direction of arrows on the ordination are proportional to vector loading of watershed characteristics into each principal component (PC). Points are colored by the watershed 30-year average annual air temperature (PRISM Climate Group, 2015).

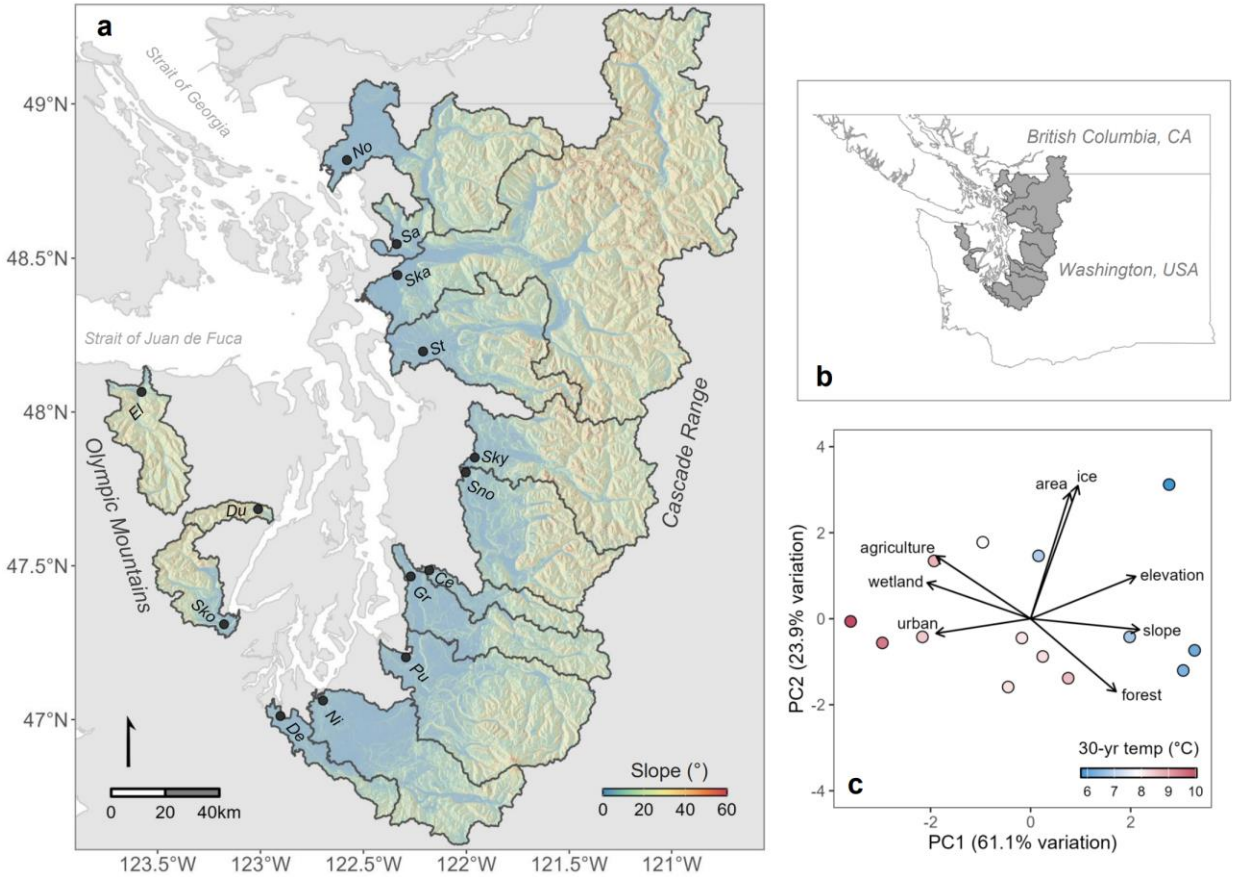

Figure 2-1 Study map

Figure 2.2. Modeled states for each response variable plotted alongside the bias component of each river's long-term trajectory. All response variable data are standardized by mean and variance and are dimensionless, including the model biases, which represent the average trend over time or "rate of change" for each river state. Sites are arranged from top to bottom along the *y* axis by watershed slope (low to high). The shared state among rivers is overlaid to help visualize the long-term state of river discharge and nutrients dynamics across the Puget Sound Basin.

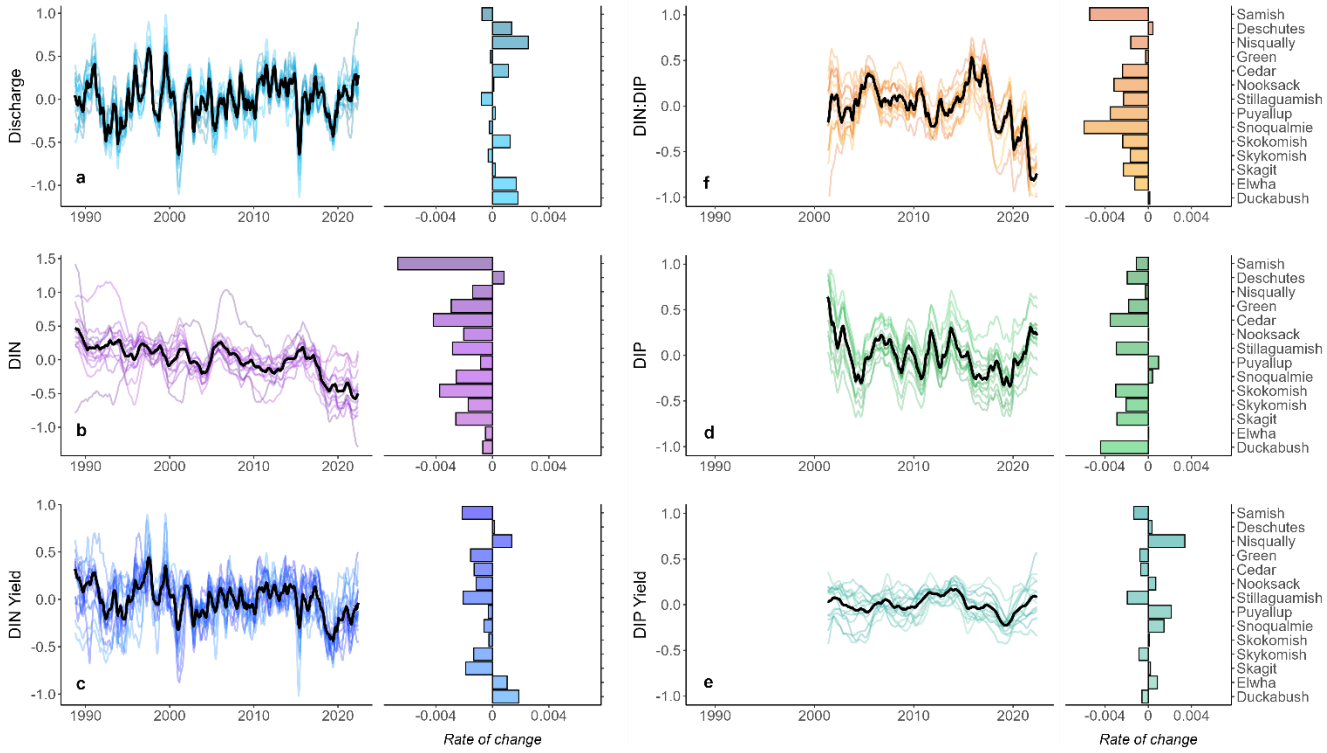

Figure 2-2 Model states

Figure 2.3. a) Estimated rate of change for DIN loads in kg month^{-1}. **b)** Estimated rate of change for DIP loads in kg month^{-1}. Sites are arranged from top to bottom along the *y* axis by watershed area (large to small). The total net rate of change at the Puget Sound Basin-scale is indicated in grey at the top of the plot for each nutrient load.

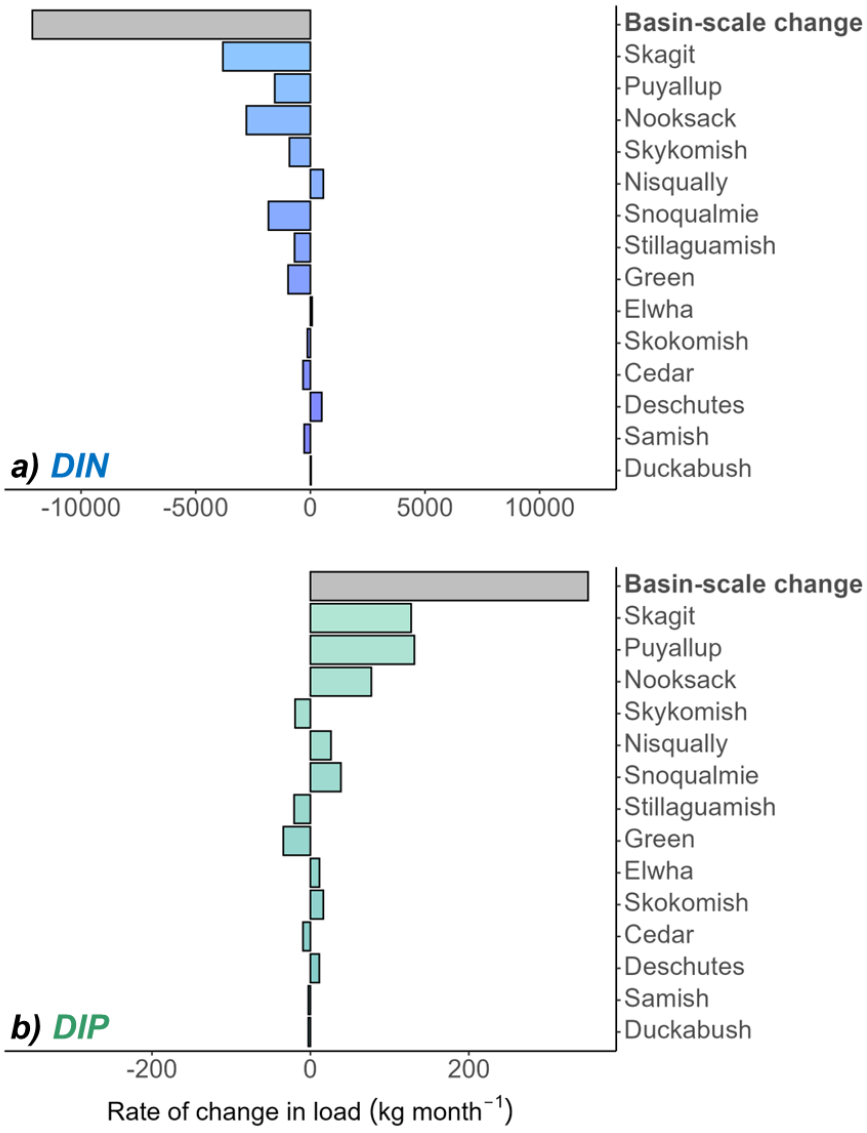

Figure 2-3 Basin-scale change

Figure 2.4. Estimated model coefficients for the effect of precipitation on each individual river's **a)** discharge, **b)** DIN concentration, **c)** DIN yield, **d)** DIN:DIP molar ratio, **e)** DIP concentration, and **f)** DIP yield. Sites are arranged from top to bottom along the vertical axis by watershed slope (low to high).

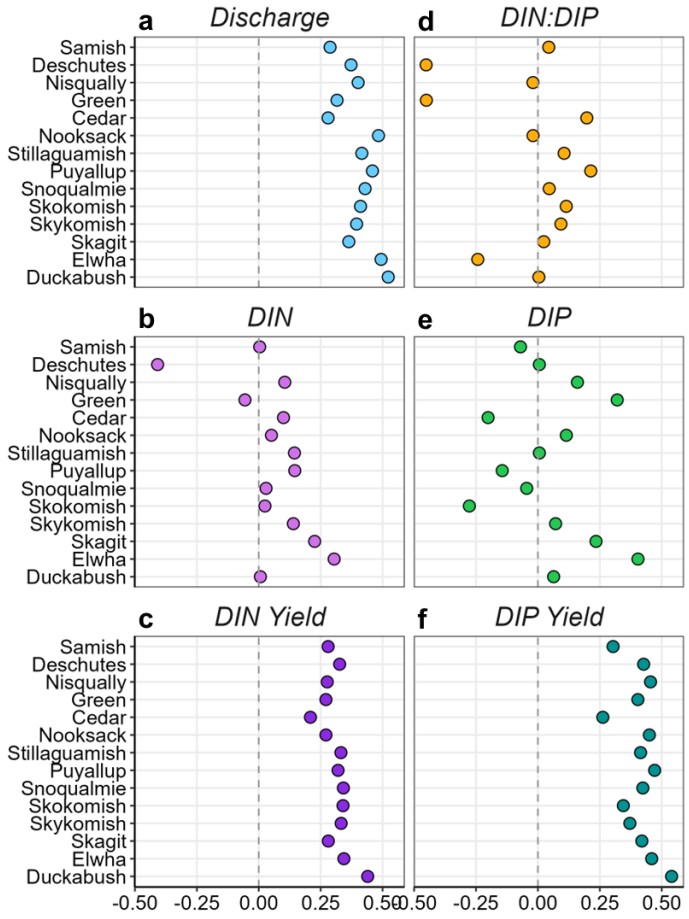

Figure 2-4 Precipitation effects

Figure 2.5. Estimated model coefficients for the PDO plotted versus mean watershed slope for each of our response variables. Each point represents the estimated effect of the PDO on each individual river's **a)** discharge, **b)** DIN concentration, **c)** DIN yield, **d)** DIN:DIP molar ratio, **e)** DIP concentration, and **f)** DIP yield for the winter, spring, and summer seasons. The open circles represent the Skokomish River, whose river flow is regulated by a dam.

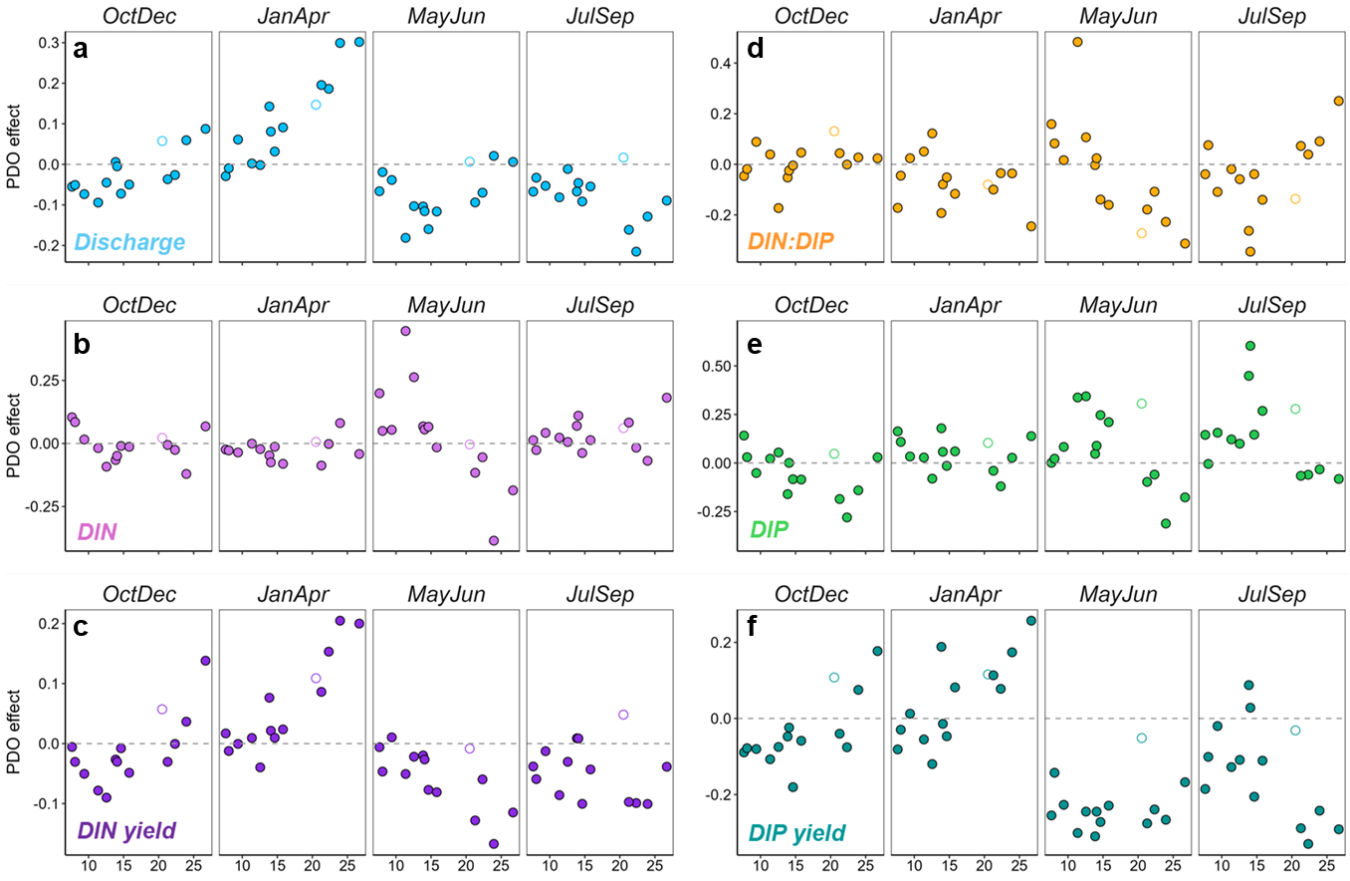

Figure 2-5 PDO vs. slope

CHAPTER 3: Landscape properties and changing climate conditions interact across watersheds to drive atmospheric and terrestrially derived sources of nitrate in Pacific Northwest rivers

3.1 ABSTRACT

Changing climate conditions interact with landscapes to modify the delivery of reactive nitrogen (Nr) to rivers, often obscuring our understanding of how landscape properties retain or release different sources of Nr pollution. In this study, we measured nitrogen and oxygen stable isotopes of dissolved nitrate (a tracer of both terrestrial and atmospherically derived nitrate; NO_3^-) in monthly river water samples from 13 watersheds with varied land use and topographic features in western Washington state. This study occurred across two highly contrasting hydrologic years and included a record drought for the region. Using these data, we assessed the influence of landscape variation on NO_3^- source dynamics among rivers in two separate ways (that is, across rivers and within watersheds), and examined how these relationships varied under different hydrologic and climate conditions. Our findings reveal that spatial variation in NO_3^- concentrations and sources across rivers, whether terrestrial or atmospheric, was strongly associated with a gradient of watershed land use and topography, and river sampling position. Additionally, we found seasonal hydrologic conditions either obscured or amplified differences in NO_3^- sources dynamics across rivers, and the relative delivery of terrestrial and atmospheric NO_3^- sources to rivers varied significantly between the two highly contrasting water years.

3.2 INTRODUCTION

Understanding the factors controlling nitrogen (N) inputs to rivers is critical for evaluating anthropogenic impacts to water quality yet remains challenging due to the diffuse nature of N pollution and the multiple controls that interact across watersheds to drive different N source contributions. Although N transfer to rivers primarily occurs through fertilizer applications, human development, and soil processes on land, a substantial portion of anthropogenic N is also emitted to the atmosphere as NOx ($NO + NO_2$), where it can be transformed, transported, and deposited to both human-dominated and remote watersheds and their receiving rivers (Fowler et al., 2013; Holtgrieve et al., 2011). Increased contributions of atmospheric nitrate (NO_3^-; frequently the dominant form of dissolved N) have been consequently found across a diversity of river and watershed types, including high-elevation montane streams as well as low-lying urban and agricultural rivers (Bostic et al., 2022; Bourgeois, Savarino, Némery, et al., 2018a). The influence of terrestrial vs. atmospheric NO_3^- on total N loads, however, can vary across river types and is partially dependent on interannual climate variability, such as seasonal changes to runoff or snowmelt, which interact with landscapes to affect the timing and delivery of different NO_3^- sources to rivers, as well as their downstream transport (Bourgeois, Savarino, Némery, et al., 2018a; Jiang et al., 2022).

In mountainous landscapes, watershed topography can act as a strong underlying control of atmospheric vs. terrestrially derived NO_3^- source contributions across and within river systems (Bourgeois, Savarino, Caillon, et al., 2018; Bourgeois, Savarino, Némery, et al., 2018b; Elmstrom et al., 2024). The seasonal transfer and availability of atmospheric NO_3^- within watersheds, for example, is strongly influenced by elevational controls on snowpack and glacier

coverage, which store and directly release atmospheric NO_3^- in spring and summer meltwaters (Clark et al., 2021). Slope and relief also play a distinct role in mediating different NO_3^- sources by modifying water residence times and hydrologic connectivity along river networks. For example, in watersheds with steep slopes, strong energy gradients promote the rapid transfer and potentially long-reaching transport of NO_3^- sources downstream (Bourgeois, Savarino, Caillon, et al., 2018; Elmstrom et al., 2024). Conversely, in low relief areas, increased residence times slow water and constituent movement and enhance the terrestrial retention (via assimilation) or loss (via denitrification) of NO_3^- sources (Harms et al., 2016; Schiff et al., 2002). These topographic controls, however, are increasingly confounded by human development and agricultural activity in mountain lowlands, which increase the total amount of NO_3^- on land and consolidate watershed drainage (Kaushal et al., 2014). Together, these alterations can saturate or divert NO_3^- from terrestrial retention and loss processes, ultimately increasing the delivery of both atmospheric and terrestrially derived NO_3^- sources from watersheds to streams and rivers (Bostic et al., 2022).

Evaluating spatial variation in atmospheric and terrestrially derived NO_3^- across rivers can help determine the relative influence of landscape controls on NO_3^- sources, though this is increasingly complicated by climate-altered precipitation patterns which interact with landscapes to drive NO_3^- source contributions. Specifically, in riverine environments, changes in the intensity and form of precipitation (rain vs. snow) are projected to alter seasonal patterns of runoff and snow-driven flow (Hamlet et al., 2013; Nijssen et al., 2001), both of which influence the atmospheric and terrestrially derived NO_3^- sources of river N loads. The intensity and duration of drought periods are also expected to increase, likely introducing further variability in the timing and magnitude of NO_3^- source inputs (Marlier et al., 2017). Extended drought periods,

for example, have been shown to reduce hydrologic connectivity and increase landscape N retention, which can later amplify the pulse of NO_3^- from land at the onset of heavy precipitation (Greaver et al., 2016; Kaushal et al., 2014). Past work illustrates that these hydroclimatic shifts will likely manifest differently across river systems depending on local hydrologic regime (rain vs. snow-dominant) and watershed-scale physical and biogeochemical controls (Elmstrom et al., 2024; Van Meter et al., 2020). Earlier snowmelt and increased runoff, for instance, has been linked to contrasting responses of dissolved inorganic N and phosphate yields in rain vs. snow-dominant rivers in the Pacific Northwest (Elmstrom et al., *in prep*). Understanding how climate-driven alterations to land-river connectivity will impact the seasonal transfer of NO_3^- sources across rivers systems is crucial for determining future N loads (L. Li et al., 2024). However, how changes in precipitation form and intensity affect atmospheric vs. terrestrially derived NO_3^- source inputs across rivers with varying hydrologic regimes, watershed topography, and land use remains largely unexplored.

Stable isotopic ratios of nitrogen (N) and oxygen (O) in NO_3^- ($\delta^{15}N$, $\delta^{18}O$, and $\Delta^{17}O$) can be used to estimate the dominant sources of river NO_3^- by enabling the exclusive quantification of atmospheric vs. terrestrially-derived sources of NO_3^- (Kaiser et al., 2007; Michalski et al., 2004). $\delta^{15}N$-NO_3^- values, for example, have been used extensively to differentiate human-derived NO_3^- sources, as sewage and manure are more enriched in ^{15}N than precipitation, soil, and synthetic fertilizers (Barnes & Raymond, 2010; Divers et al., 2014; Jankowski et al., 2012; Liu et al., 2013). Similarly, many previous studies have used $\delta^{18}O$-NO_3^- values to distinguish atmospheric NO_3^- from microbially produced NO_3^- in watershed soils (Barnes & Raymond, 2010; Divers et al., 2014). The preferential uptake of lighter isotopes (^{14}N and ^{16}O) during denitrification and assimilation, however, can substantially alter $\delta^{15}N$ and $\delta^{18}O$ values of residual

NO_3^- pools, leading to inaccurate source apportionment of NO_3^- when using these isotopic ratios alone (Aravena & Robertson, 1998; Venkiteswaran et al., 2019; Weitzman et al., 2021). $\Delta^{17}O$ values avoid these complications by taking advantage of both $\delta^{18}O$ and the ^{17}O isotope anomaly in atmospheric NO_3^-. Specifically, because NO_3^- produced in the atmosphere is enriched in ^{17}O relative to ^{18}O, it positively deviates from the typical terrestrial $\delta^{18}O$ vs. $\delta^{17}O$ relationship (i.e., the terrestrial fractionation line: $\delta^{17}O \approx 0.52 \times \delta^{18}O$) (Kaiser et al., 2007; Michalski et al., 2004). $\Delta^{17}O$ quantifies this deviation ($\Delta^{17}O = \delta^{17}O - 0.52 * \delta^{18}O$) and provides an explicit tracer of atmospheric NO_3^- in aquatic ecosystems that has been unaltered by terrestrial fractionations, such as nitrification, assimilation, and denitrification (Bostic et al., 2022; Bourgeois, Savarino, Caillon, et al., 2018; Clark et al., 2021; Sebestyen et al., 2019).

Assessing how landscape and climatic changes affect the dominant NO_3^- sources of river N loads requires accurate accounting of atmospheric and terrestrial NO_3^- inputs across watersheds with varied land use, physical controls, and hydrologic conditions, but this remains a major challenge. Here, we took advantage of a unique two-year monthly data set of NO_3^- concentrations and NO_3^- stable isotopic values ($\delta^{15}N$, $\delta^{18}O$, and $\Delta^{17}O$) from 13 rivers that drain the Puget Sound Basin, a spatially complex region in Washington State. By chance, this study occurred across two highly contrasting hydrologic years, and captured the 2015 hydrologic year – a record drought in terms of snowpack in the Pacific Northwest (Marlier et al., 2017). To understand how landscape variation influenced the sources of NO_3^- across the Puget Sound rivers, we quantified the association between watershed characteristics (i.e., land use and topographic features) and river NO_3^- concentrations and the $\delta^{15}N$, $\delta^{18}O$, $\Delta^{17}O$ values of NO_3^-. Further, by examining how these relationships varied across hydrologic conditions (i.e., seasons and contrasting hydrologic years), we characterized how rivers responded to altered hydrologic

conditions in terms of their atmospheric and human-derived NO_3^- inputs and corresponding NO_3^- concentrations. Finally, in a subset of rivers which included upstream sampling sites, we investigated how river network position influenced the relative contribution of NO_3^- sources and whether hydrologic connectivity, and the consequent delivery of upland NO_3^- sources downstream, varied in strength across rivers depending on climate conditions and watershed-scale characteristics. Ultimately, by summarizing variation across this spatially and climatologically diverse dataset, we sought to determine how spatial variation in different river NO_3^- sources inputs is controlled by heterogeneous landscapes, seasonal hydrologic regimes, and climate-altered precipitation conditions.

3.3 METHODS

3.3.1 Study area

The Puget Sound basin, located mostly in western Washington State, drains an area of approximately 13,700 km^2 (Fig. 1). Bounded by the Olympic Mountains to the west and the Cascade Range to the east, watersheds in the basin represent a gradient of geomorphic settings, with lowland and mountain valleys formed by continental glaciers, alpine glaciers, sediment deposition, and incision from rivers (Hall et al., 2018). Climate in the basin is seasonally variable, characterized by cool, wet winters, and warm dry summers. The average annual rainfall is 2147 mm, and the average annual air temperature is 8°C (PRISM Climate Group, 2015). During the hydrologic years of study, about 1947 mm and 2478 mm of precipitation fell within 2015 and 2016, respectively, and the average air temperature was 10°C in 2015 and 9°C in 2016 (PRISM Climate Group, 2015). For watersheds along both the Cascade and Olympic ranges, about 80% of the annual precipitation occurs from October to March (PRISM Climate Group,

2015). Within this setting, hydrologic regimes are governed by timing and form of precipitation and are characterized as rainfall-dominated (<600 m elevation with peak discharges in November-February) and mixed rain-and-snow hydrologies (>600 m elevation with peak discharges in February-June) (Hall et al., 2018; Reidy Liermann et al., 2012). Groundwater also sustains summer discharge in most rivers, as the unconsolidated glacial sediments of Puget Sound river channels are conducive to springs and hyporheic exchange (McGill et al., 2021). Notably, in 2015, substantial winter warming increased the proportion of precipitation falling as rain relative to snow, leading to declines in mountain snowpack and snowmelt-driven spring and summer discharge (Marlier et al., 2017). Though the effects of the snow drought were observed across the entire basin, watersheds in the southern Cascade Range and Olympic Mountains experienced the largest impacts to their snowmelt regimes (Marlier et al., 2017).

Land use histories and development in the region have resulted in a gradient of human disturbance and land cover across the basin. While the slopes of the Cascade Range and Olympic Mountains remain mostly forested, transitions to urban and agricultural land uses along with increased logging since the late 1800s have removed substantial areas of floodplain forest in the lower basin. The central Puget Sound region has seen rapid urbanization in recent years, gaining over a million people since 2000 (*Regional Data Profile*, 2017). The south and central valleys of the western Cascade Range are now mainly urban and rural residential land, with some pastureland and forage crops (hay and corn) located outside the urban fringe (*2015 WSDA Agricultural Land Use*, 2022; Hill et al., 2016). The majority of forage and specialty crop cultivation (including cereal grains, berries, and vegetables) is located in the northeastern part of the basin in the Nooksack, Skagit and Snohomish river watersheds (*2015 WSDA Agricultural Land Use*, 2022). Forested areas along the lower Cascade Range are a mix of deciduous and

coniferous forest and include large stands of the early successional N-fixing tree species, red alder (*Alnus rubra*) (Wise & Johnson, 2011). Watersheds along the eastern Olympic Mountains remain mostly forested with coniferous trees, but with some logging, and sparse pastureland, forage cropped fields and residential development (*2015 WSDA Agricultural Land Use*, 2022; Hill et al., 2016). The combination of forested, mountainous areas, agricultural valleys, and sprawling urbanization creates a variable landscape across the Puget Sound basin, and drives a diversity of N inputs that cover the full range of NO_3^- sources (Kendall et al., 2007).

3.3.2 Sample and data collection

We used two years of river monthly water quality samples collected by the Washington Department of Ecology's (DoE) River and Stream Water Quality Monitoring program from October 2014 to September 2016 (Elmstrom 2024). The Washington DoE collects monthly water quality samples at nearly 100 river and stream stations across Washington state. For this study, we selected rivers that drain the Puget Sound Basin and range in their watershed physical and land use characteristics (Table 1, Fig. 1c). This included 13 rivers, each with 1 DoE sampling station located near the Puget Sound outlet (Fig. 1a), as well as corresponding upstream stations for 6 rivers located along the Cascade Range (n = 21). River order (i.e., Strahler number (Strahler, 1952) at the mouth ranged from 5 to 8, and sampling stations ranged from 4 to 700 meters in elevation. We obtained subsamples of monthly water samples from each river site for NO_3^- triple oxygen isotope analysis ($\delta^{15}N$, $\delta^{18}O$, and $\Delta^{17}O$) and paired them with corresponding NO_3^- concentration data from the Washington's Department of Ecology's Freshwater Information Network database (Washington Department of Ecology, 2023). Details concerning the Washington Department of Ecology's water quality sample handling protocols and analytical methods can be found in Von Prause (2021).

To calculate local atmospheric deposition isotopic values, we procured monthly samples of wet-only deposition from two National Atmospheric Deposition Program (NADP) National Trends Network sites located in the north and south Cascade Range from May 2015 until September 2016. All river water and precipitation samples were shipped to the University of Washington and frozen until isotopic analysis.

3.3.3 Stable isotope analysis of NO_3^-

We analyzed river water subsamples and NADP deposition samples for the nitrogen and oxygen isotope ratios of NO_3^- using the bacterial denitrifier method (Kaiser et al., 2007; Sigman et al., 2001) at the University of Washington's Δ*IsoLab. Briefly, NO_3^- in the samples was converted to N_2O by the denitrifying bacteria *Pseudomonas aureofaciens*. The resultant N_2O was extracted, purified, and pyrolyzed to N_2 and O_2 in a heated gold tube held at 800°C. The isotopic ratios of each gas ($^{15}N/^{14}N$ for N_2, $^{18}O/^{16}O$ and $^{17}O/^{16}O$ for O_2) were measured by a Finnigan Delta-Plus Advantage isotope ratio mass spectrometer after separation by a gas chromatograph. Isotopic mass ratios are reported in the delta (δ) notation in per mil (‰), where $\delta = (R_{sample}/R_{standard} - 1) \times 1000$ ‰ and R is the $^{15}N/^{14}N$ in N_2 normalized to atmospheric air N_2 (Air) or $^{17}O/^{16}O$ and $^{18}O/^{16}O$ in O_2 normalized to Vienna Standard Mean Ocean Water (VSMOW). The $\delta^{15}N$ values were calibrated against two international reference materials, USGS32 ($\delta^{15}N = 180$‰) and USGS34 ($\delta^{15}N = -1.8$‰). The $\delta^{17}O$ and $\delta^{18}O$ values were calibrated against USGS34 ($\delta^{17}O = -14.5$ ‰, $\delta^{18}O = -27.9$ ‰) and USGS35 ($\delta^{17}O = 51.3$ ‰, $\delta^{18}O = 57.5$ ‰). The $\Delta^{17}O$ values were then calculated using the linear equation $\Delta^{17}O = \delta^{17}O - 0.52 * \delta^{18}O$.

Analytical accuracy verified using replicate measurements of the international reference material IAEA-NO3 ($\delta^{15}N = 4.7$‰, $\delta^{18}O = +25.6$‰, $\Delta^{17}O = -0.2$‰,) was ±0.1‰, ±0.5‰, and

±0.5‰ for $\delta^{15}N$, $\delta^{18}O$, and $\Delta^{17}O$ respectively (1SD, n = 84). Precision calculated using duplicates from each analytical session was estimated to be ±0.2‰, ±0.5‰, and ±0.7‰ for $\delta^{15}N$, $\delta^{18}O$ and $\Delta^{17}O$, respectively (1SD, n = 181).

3.3.4 End-Member Mixing Analysis

The triple isotope analysis approach using $^{18}O/^{16}O$ and $^{17}O/^{16}O$ ratios enables the exclusive quantification of unprocessed atmospheric NO_3^- (Kaiser et al., 2007; Michalski et al., 2004; Sigman et al., 2001). This is due to the mass dependency of terrestrial fractionations, where $\delta^{17}O$ tracks $\delta^{18}O$ by a consistent factor of 0.52 (i.e., the terrestrial fractionation line is $\delta^{17}O \approx 0.52 \times \delta^{18}O$). In contrast, the production of atmospheric NO_3^- involves NOx oxidation by ozone, which bears excess ^{17}O. As a result, samples with atmospheric NO_3^- are enriched in $\delta^{17}O$ relative to $\delta^{18}O$, causing a positive deviation from the terrestrial fractionation line (Bourgeois, Savarino, Caillon, et al., 2018; Hundey et al., 2016b; Michalski et al., 2004). This deviation, quantified as $\Delta^{17}O$ ($\Delta^{17}O = \delta^{17}O - 0.52 \times \delta^{18}O$), provides an unambiguous tracer of atmospheric NO_3^-.

The proportion of atmospherically derived NO_3^- can be determined by a simple mixing calculation (eq. 1). $\Delta^{17}O$ values of atmospherically oxidized NO_3^- generally range between 20 and 35‰ in temperate latitudes (Bourgeois, Savarino, Caillon, et al., 2018; Bourgeois, Savarino, Némery, et al., 2018b; Clark et al., 2021; Sebestyen et al., 2019), whereas $\Delta^{17}O$ values of NO_3^- from terrestrially derived sources are zero (including NO_3^- from fertilizers, sewage, and soils) (Kendall et al., 2007; Michalski et al., 2004). To quantify the relative contributions of unprocessed atmospheric NO_3^- in the Puget Sound river NO_3^- samples, we used the known terrestrial $\Delta^{17}O$-NO_3^- value (i.e., 0‰) and measured $\Delta^{17}O$- NO_3^- values from the NADP

deposition water samples as end members in a two source mixing model (Bourgeois, Savarino, Caillon, et al., 2018; Bourgeois, Savarino, Némery, et al., 2018b; Clark et al., 2021; Liu et al., 2013). Because the terrestrial $\Delta^{17}O\text{-}NO_3^-$ value equals 0‰, the calculation of atmospheric contribution, termed f_{atm}, simplifies to the following equation:

$$f_{atm} = \left(\Delta^{17}O_{sample}/\Delta^{17}O_{atm}\right) \quad (1)$$

where $\Delta^{17}O_{sample}$ is the $\Delta^{17}O$ value of NO_3^- measured in the Puget Sound river water samples and $\Delta^{17}O_{atm}$ refers to the $\Delta^{17}O$ value of NO_3^- measured in the NADP deposition water samples. To account for seasonal oscillations in $\Delta^{17}O_{atm}$ (Bourgeois, Savarino, Caillon, et al., 2018; Clark et al., 2021) and to capture the winter and spring accumulation available for transport downstream during snowmelt, we used the wet season mean (October – April) of $\Delta^{17}O\text{-}NO_3^-$ in the NADP samples as the atmospheric value ($\Delta^{17}O_{atm}$) in our calculations of f_{atm} in samples taken from October to mid-July. Conversely, we used the dry season mean (June – August) of the NADP $\Delta^{17}O\text{-}NO_3^-$ values to calculate f_{atm} in samples collected from late July to September.

Because atmospheric values of $\delta^{18}O\text{-}NO_3^-$ are strongly enriched compared to terrestrial values of $\delta^{18}O\text{-}NO_3^-$, even a small proportion of atmospheric NO_3^- can obscure the isotopic identification of terrestrial NO_3^- sources and of the biological processes that affect $\delta^{15}N$ and $\delta^{18}O$ of NO_3^- (e.g., denitrification, assimilation) (Kendall et al., 2007). To improve our interpretation of terrestrial sources and biological transformation processes, we used the atmospheric fraction (f_{atm}) and the terrestrial fraction of NO_3^- ($f_{ter} = 1 - f_{atm}$) to remove the isotopic influence of atmospheric NO_3^- from the Puget Sound river $\delta^{15}N\text{-}NO_3^-$ and $\delta^{18}O\text{-}NO_3^-$ values. Following Riha

et al. 2014 and others (Bourgeois, Savarino, Caillon, et al., 2018; Bourgeois, Savarino, Némery, et al., 2018b), the equations are:

$$\delta^{18}O_{ter} = \left(\delta^{18}O_{sample} - \delta^{18}O_{atm} * f_{atm}\right)/f_{ter} \quad (2)$$

and

$$\delta^{15}N_{ter} = \left(\delta^{15}N_{sample} - \delta^{15}N_{atm} * f_{atm}\right)/f_{ter} \quad (3)$$

where $\delta^{18}O_{sample}$ and $\delta^{15}N_{sample}$ are the $\delta^{18}O$ and $\delta^{15}N$ values of NO_3^- measured in the Puget Sound river water samples, and $\delta^{18}O_{atm}$ and $\delta^{15}N_{atm}$ refers to the $\delta^{18}O$ and $\delta^{15}N$ values of NO_3^- measured in the NADP deposition water samples. For $\delta^{18}O_{atm}$ and $\delta^{15}N^-_{atm}$, we calculated the wet and dry seasonal means of the $\delta^{15}N$-NO_3^- and $\delta^{18}O$-NO_3^- values from the NADP samples and applied them in our calculations in the same fashion as we did above for $\Delta^{17}O_{atm}$.

3.3.5 Watershed and landscape characteristics

We compiled watershed-scale landscape metrics for each of the watersheds corresponding to our 21 river sites using the Environmental Protection Agency's StreamCat data library (Table 1). These metrics included watershed area, mean watershed elevation, mean watershed soil depth, mean water table depth, and percent urban, wetland, agricultural, and forested land. We also included mean watershed slope in our analyses as it captures aspects of watershed topography and stream geomorphology that may influence NO_3^- retention, loss, or transfer, such as water residence times, floodplain area, and hydrologic connectivity. We calculated watershed slope as the average of all slope raster pixels within the boundaries of each individual river's watershed using ArcGIS (v10.8).

3.3.6 Statistical Analyses

We used a combination of multivariate statistics and linear mixed effects models to evaluate the effects of landscape variation and climate interactions on NO_3^- concentrations, $\delta^{15}N\text{-}NO_3^-$, $\delta^{18}O\text{-}NO_3^-$, and $\Delta^{17}O\text{-}NO_3^-$ values across the Puget Sound rivers. First, to summarize the dominant gradients of environmental variability among river sites and their watersheds, we used principal component analysis (PCA) to reduce the dimensionality of watershed land use and topographic features, which were highly colinear across our study sites. We then used linear mixed effects models to investigate the association between watershed characteristics (as described by principal component scores) and river NO_3^- concentrations and isotopic composition ($\delta^{15}N$, $\delta^{18}O$, and $\Delta^{17}O$ of NO_3^-) from our downstream sampling stations (n = 13). In the same model, we used interaction terms to investigate whether these spatial relationships varied across hydrologic conditions (i.e., seasons and contrasting hydrologic years), and to identify differences in the overall mean across seasons and hydrologic years. Seasons were defined as winter (October – March) and summer (April – September). Per each response variable, the model fixed effects were specified as follows:

$$NO_3^-, \delta^{15}N, \delta^{18}O, \text{or } \Delta^{17}O = \text{PC1} \times \text{Season} \times \text{Year} \quad (4)$$

In a separate but related analysis, we evaluated spatial variation in river NO_3^- concentrations, $\delta^{15}N\text{-}NO_3^-$, $\delta^{18}O\text{-}NO_3^-$, and $\Delta^{17}O\text{-}NO_3^-$ values among the 6 different rivers that included downstream and upstream sampling sites. In these models, we used the same interaction terms to evaluate whether hydrologic conditions obscured or amplified differences among downstream and upstream sites. The models fixed effects were specified as follows:

$$NO_3^-, \delta^{15}N, \delta^{18}O, \text{or } \Delta^{17}O = \text{River position} \times \text{Season} \times \text{Year} \quad (5)$$

We log-transformed the NO_3^- concentration and $\Delta^{17}O$-NO_3^- response variables to meet the assumptions of normality. To address heteroscedasticity, we incorporated a variance function as a weighting factor for each response variable. For both sets of models, we included random intercepts for each river site and used an autoregressive correlation structure of order 1 (corAR1) to account for the temporal autocorrelation in our model errors.

We compared models with different combinations of fixed effects and interaction terms using Akaike Information Criterion corrected for small sample sizes (AICc; Burnham & Anderson, 2002) and the dredge function from the **MuMIn** package in R. We performed pairwise comparisons among seasons nested within water years and river positions nested within each watershed (i.e., downstream vs. upstream) using the **emmeans** package which calculates estimated mean differences from model outputs (Lenth, 2018). All multivariate data analyses were conducted using the **vegan** and **biostats** packages in R (R Development Core Team, 2011).

3.4 RESULTS

3.4.1 Watershed physical and land use characteristics

Principal component analysis (PCA) summarized a large proportion of variance (83.6%) in the river and watershed characteristics (PC1 = 68.3%, PC2 = 15.2%). PC1 was statistically significant according to a Monte Carlo randomization test (PC1, p = 0), and all variables except watershed area had significant loadings on PC1 (Table S1, Fig. 1c). Notably, watershed slope had a particularly high loading on PC1, with a linear correlation between the PC1 vector loadings of 0.98 (Table S1). Rivers with increased human activity and wetland areas were found in low-elevation, low-gradient watersheds (Fig. 1c). Conversely, rivers with greater forest cover were grouped in watersheds with higher elevations and steeper gradients (Fig. 1c). These river

groupings also corresponded to average mean annual temperatures, likely reflecting precipitation form and river hydrologic regimes. This indicates that rain-dominant rivers are prevalent in low-elevation, low-gradient watersheds with increased human activity, while snow-dominant rivers are more common in higher, steeper watersheds with greater forest cover. The second PCA axis was primarily explained by watershed area and was not statistically significant (PC2, $p = 1$).

3.4.2 NO_3^- Concentrations

River NO_3^- concentrations ranged from below the detection limit (< 0.01 mg/L) to a maximum of 1.06 mg/L across all river sampling stations and study months, with a basin-wide mean of 0.22 ± 0.21 mg/L (1SD) across the full period of study (Table 1). The highest study mean was observed in the Deschutes River (0.75 ± 0.1 mg/L), a river located along the southern Cascade Range. The lowest study means were observed in the Elwha and Duckabush rivers (0.03 ± 0.02 mg/L), which are both located in the Olympic Mountain Range.

Looking across downstream river sampling stations, we found that average river NO_3^- concentrations covaried strongly with watershed characteristics, but that the strength of this relationship across rivers varied between winter and summer seasons. The best supported models ($\Delta AIC < 2$) included a negative effect of PC1 and an interaction between PC1 and season (Table 2), indicating that river NO_3^- concentrations were higher in low gradient watersheds with increased human activity than in higher sloped, more forested watersheds, but the difference across rivers was stronger in the winter than in the summer season (Fig. 2a). When comparing NO_3^- concentrations across upstream and downstream sampling stations within watersheds, we observed a similar interaction between river sampling position and season (Table 3). Downstream stations had higher average NO_3^- concentrations compared to river stations located upstream, but the relative difference in NO_3^- concentrations between downstream and upstream

stations was more pronounced during the winter than in the summer (Table S2, Fig. 3a). In both analyses, the top models included an effect of hydrologic year and season nested within hydrologic year. On average, NO_3^- concentrations exhibited a small, but statistically identifiable increase during the summer season of the dry year (2015) but remained statistically unchanged between the wet and dry year winter seasons (Table 4).

3.4.3 NO_3^- Isotopic Composition: $\delta^{15}N$, $\delta^{18}O$, and $\Delta^{17}O$ of NO_3^-

$\Delta^{17}O$-NO_3^- values varied considerably across rivers in the Puget Sound Basin, ranging from 0 to 15.7‰, with a basin-wide study mean value of 0.68 ± 1.0‰. The Elwha River had the highest mean of $\Delta^{17}O$-NO_3^- values (2.76 ± 3.76‰). The Deschutes River had the lowest study $\Delta^{17}O$-NO_3^- mean (0.24 ± .20‰). The atmospherically corrected $\delta^{15}N{-}NO_3^-$ values across rivers ranged between −5.24 and 13.74‰, with a basin-wide study mean of 2.93 ± 2.92‰. For $\delta^{18}O$-NO_3^-, atmospherically corrected values ranged between −17.78 and 11.21‰ and the study average was -2.52 ± 3.05‰. The highest mean values for both $\delta^{15}N$-NO_3^- and $\delta^{18}O$-NO_3^- were found in the Puyallup river (8.66 ± 2.91‰. and 0.37 ± 1.72‰, respectively), and the lowest mean values for $\delta^{15}N$-NO_3^- and $\delta^{18}O$-NO_3^- were found upper Skagit River (-0.42 ± 0.56‰. and -7.68 ± 2.83‰, respectively). These findings are in the same range of previously measured NO_3^- isotopic values in temperate and high elevation, mountainous rivers (Bourgeois, Savarino, Caillon, et al., 2018; Hundey et al., 2016b; Jiang et al., 2022; Sebestyen et al., 2019; Tsunogai et al., 2014, 2016).

Comparison across downstream river sampling stations revealed average river NO_3^- isotopic composition ($\delta^{15}N$, $\delta^{18}O$, and $\Delta^{17}O$ of NO_3^-) covaried strongly with watershed characteristics, but that the strength of this relationship differed under contrasting hydrologic conditions (i.e., seasons and hydrologic years). For $\delta^{15}N$, $\delta^{18}O$, and $\Delta^{17}O$ of NO_3^-, the best

supported models (ΔAIC $\leq$ 2) included an effect of PC1 and, for $\Delta^{17}O\text{-}NO_3^-$ and $\delta^{15}N\text{-}NO_3^-$, top models also included an interaction between PC1 and season (Table 2). River $\Delta^{17}O\text{-}NO_3^-$ values were highest in steep, high elevation watersheds with greater forest cover compared to rivers draining lower gradient watersheds with more human activity (Fig. 2b). Conversely, $\delta^{15}N\text{-}NO_3^-$ and $\delta^{18}O\text{-}NO_3^-$ values were enriched in rivers with higher degrees of human disturbance relative to rivers draining more forested, steeper sloped watersheds (Fig. 2c). The relative differences in $\Delta^{17}O\text{-}NO_3^-$ and $\delta^{15}N\text{-}NO_3^-$ values across the downstream river stations, however, were most pronounced in the summer season, and, overall, both isotopes were more enriched in the summer than in the winter (Fig. 2b, c). In contrast to $\Delta^{17}O\text{-}NO_3^-$ and $\delta^{15}N\text{-}NO_3^-$ values, seasonal differences in $\delta^{18}O\text{-}NO_3^-$ values across the downstream river stations were not statistically supported (Table 2). Top models for $\delta^{18}O\text{-}NO_3^-$ values did however include an interaction between PC1 and hydrologic year, indicating the relationship between $\delta^{18}O\text{-}NO_3^-$ values and river watershed characteristics varied annually between normal and drought hydrologic conditions.

When comparing NO_3^- isotopic compositions across upstream and downstream sampling stations within watersheds, we again observed a similar interaction between hydrologic conditions and the relative influence of watershed conditions (in this case, river position) on $\delta^{15}N$, $\delta^{18}O$, and $\Delta^{17}O$ of NO_3^- values (Table 3). Specifically, we found that downstream and upstream stations were statistically distinct in their isotopic composition ($\delta^{15}N$, $\delta^{18}O$, and $\Delta^{17}O$ of NO_3^-), but the relative differences between downstream and upstream stations varied seasonally for $\Delta^{17}O\text{-}NO_3^-$ and $\delta^{15}N\text{-}NO_3^-$ values and annually for $\delta^{18}O\text{-}NO_3^-$ values (Fig. 3, Table S2). Downstream stations were more enriched in $\delta^{15}N\text{-}NO_3^-$ and $\delta^{18}O\text{-}NO_3^-$ values compared to upstream stations, while upstream stations were more enriched in $\Delta^{17}O\text{-}NO_3^-$ values compared to

downstream stations. The differences in $\Delta^{17}O\text{-}NO_3^-$ and $\delta^{15}N\text{-}NO_3^-$ values between downstream and upstream stations across rivers, however, were notably most pronounced during the summer than in the winter season. Seasonal differences between upstream and downstream station $\delta^{18}O\text{-}NO_3^-$ values were again not statistically supported (Table 3), but the relative difference in $\delta^{18}O\text{-}NO_3^-$ values between sites did vary across the two hydrologic years of study. We provide the annual relationships between $\delta^{18}O\text{-}NO_3^-$ values, watershed characteristics, and river position in Supplemental Figures 1 and 2.

For both across-watershed and within-watershed analyses, the top competing models for $\delta^{15}N\text{-}NO_3^-$ values included an effect of hydrologic year, and for $\Delta^{17}O\text{-}NO_3^-$ and $\delta^{18}O\text{-}NO_3^-$ values, the top competing models included an effect of hydrologic and season nested within hydrologic year (Table 2, Table 3). On average, $\Delta^{17}O\text{-}NO_3^-$ values were more enriched during the summer season of the wet year (2016) but remained statistically unchanged between the wet and dry year winter seasons (Table 4). $\delta^{15}N\text{-}NO_3^-$ and $\delta^{18}O\text{-}NO_3^-$ values were more enriched during the wet year (2016) across both the winter and summer seasons than in the dry year (2015) (Table 4).

3.5 DISCUSSION

We found broad spatial variation in NO_3^- concentration and isotopic composition among river systems in the Puget Sound Basin, primarily associated with land use and topographic gradients both across and within river watersheds. However, when examining these relationships in the context of seasonal climate, we found alternate hydrologic conditions either amplified or obscured variation in NO_3^- dynamics across rivers. Specifically, river sites exhibited more distinct isotopic compositions in summer compared to winter. This suggests that hydrologic connections with different NO_3^- source compartments strongly influence the relative

contributions of atmospheric and terrestrially derived NO_3^- sources to rivers (Briand et al., 2017; Rollinson et al., 2021b). Further, when comparing isotopic composition at the interannual scale across two highly contrasting water years, we found record drought conditions substantially altered NO_3^- mobilization from watersheds and affected the delivery of atmospheric and terrestrially derived NO_3^- sources to rivers. This underscores the importance of climate-landscape interactions in driving NO_3^- inputs to rivers, indicating that while landscape variation is a key driver of NO_3^- inputs, the consideration of climate is essential for a complete understanding of the NO_3^- sources entering and being delivered by rivers.

3.5.1 NO_3^- concentrations across and within river gradients

River NO_3^- concentrations were strongly associated with the first principal component axis (PC1), which represents a gradient of watershed land use and topography across the Puget Sound watersheds (Fig. 2a, Fig. 1c). NO_3^- concentrations were highest in rivers draining low gradient watersheds with increased human activity, whereas rivers draining steep, forested watersheds had far lower NO_3^- concentrations and were less developed (Fig. 2a). Downstream river stations also had significantly higher NO_3^- concentrations than river stations located upstream (Table S2), which drain steeper, primarily forested watershed areas (Table 1). The differences found across and within rivers, however, were most pronounced during the wet winter months compared to the dry summer season (Fig. 2a, Fig. 3a). The spatial variation in NO_3^- concentrations found across the Puget Sound rivers aligns with an extensive body of literature showing that river NO_3^- concentrations tend to vary with watershed characteristics (Bormann et al., 1968; Connolly et al., 2018b; Goyette et al., 2019a; Schiff et al., 2002), often increasing alongside human activity (Lewis & Grimm, 2007; Mulholland et al., 2008). Further, the increased winter variation in river NO_3^- concentrations provides more evidence to show that

precipitation interacts with landscapes to mobilize nutrients from watersheds to rivers, but often to varying degrees (Kaushal et al., 2014; Sinha & Michalak, 2016). Notably, while our results provide correlative associations between NO_3^- dynamics and the Puget Sound watershed characteristics, we cannot distinguish between the effects of land use and physical controls, which are fundamentally related in our mountainous and human influenced study system (Fig. 1c). Nevertheless, we discuss our results in the context of both watershed land use and topography and draw hypotheses regarding the dominant landscape-level physical and biogeochemical controls of Puget Sound river NO_3^-.

3.5.2 Atmospheric contributions to river NO_3^- vary across watersheds and with season

Enriched $\Delta^{17}O\text{-}NO_3^-$ values in river sites with greater montane influence clearly demonstrate the importance of watershed characteristics on atmospheric NO_3^- sources, and particularly highlight the role of topography in driving atmospheric NO_3^- inputs to aquatic ecosystems (Baron & Campbell, 1997; Bourgeois, Savarino, Némery, et al., 2018a; Clark et al., 2021). Atmospheric deposition contributed significantly more to NO_3^- pools in rivers draining steep, high elevation watersheds with increased forest cover compared to rivers draining lower gradient watersheds with increased human activity (Fig. 2b). Additionally, river sampling sites located at higher elevations within watersheds (Fig. 1a) exhibited notable increases in atmospheric NO_3^- signals relative to sampling sites located downstream near river mouths (Fig. 3b). Increased inputs of atmospheric NO_3^- to surface waters are well documented in other mountainous regions(Bourgeois, Savarino, Caillon, et al., 2018; Bourgeois, Savarino, Némery, et al., 2018b; Clark et al., 2021; Hundey et al., 2016b; Xia et al., 2019) and have been broadly attributed to the delivery of atmospheric NO_3^- from melting snowpack in high elevations, as well as landscape properties in high relief areas that expedite NO_3^- delivery. Steep slopes, reduced

soil development, and minimal vegetation, for example, promote the rapid infiltration of precipitation and low uptake of NO_3^- (Schiff et al., 2002; Sebestyen et al., 2019), such that atmospheric NO_3^- rapidly reaches streams and is transported downriver (Bourgeois, Savarino, Némery, et al., 2018b). The enriched $\Delta^{17}O\text{-}NO_3^-$ values found in the high relief and elevation river sites suggest that atmospheric NO_3^- inputs to rivers in the Puget Sound Basin are likely connected to similar topographic controls on snowpack, hydrologic connectivity, and water residence times. Reduced $\Delta^{17}O\text{-}NO_3^-$ values found in rivers draining low relief areas could also be influenced by topographic controls (e.g., increased residence times, soil development, and associated terrestrial loss or incorporation processes). Though in our study system, this is confounded by increased human activity in low relief areas, which can dilute atmospheric signals by dramatically enriching rivers with NO_3^- sources from urban and agricultural practices (Bostic et al., 2022).

Seasonal variations in $\Delta^{17}O\text{-}NO_3^-$ values at river sites with greater montane influence further highlight watershed topography as a potential driver of atmospheric NO_3^- contributions in rivers and their modulation by seasonal river hydrologic regimes. Atmospheric NO_3^- inputs in higher elevation rivers and upstream sites were most pronounced in the summer season (up to 55% in one of our highest elevation and sloped rivers, Fig. 2b, Fig. S3), clearly outlining the delivery of NO_3^- from snowmelt-driven flow in rivers with snow-dominant hydrologic regimes, as widely reported in other mountain-fed streams and rivers (Bourgeois, Savarino, Caillon, et al., 2018; Bourgeois, Savarino, Némery, et al., 2018b; Tsunogai et al., 2014, 2016; Xia et al., 2019). Conversely, in rivers draining lower relief areas with predominantly rain-driven hydrologic regimes, $\Delta^{17}O\text{-}NO_3^-$ values were lower and seasonally stable (Fig. 2b), suggesting that atmospheric NO_3^- inputs were unrelated to flow patterns and that rain-derived NO_3^- was either

retained in soils or as mentioned previously, diluted by anthropogenic NO_3^- sources (Bostic et al., 2022). These findings align with previous work showing that atmospheric NO_3^- contributions vary across river gradients (that is, across watersheds and within river networks) depending on topography and hydrologic regime. For example, in the French Alps, atmospheric deposition contributed significantly more to NO_3^- pools in streams at high elevations with snowmelt-driven flow relative to urban sites with smoother topography and mixed-rain-snow hydrologic regimes (Bourgeois, Savarino, Némery, et al., 2018b). Together, this suggests that spatial variation in atmospheric NO_3^- inputs is strongly influenced by watershed topography, with this variation predominately occurring in the summer due to the role of mountain snowpack in driving seasonal river hydrologic regimes.

3.5.3 Terrestrially derived river NO_3^- varies across watersheds and with hydrologic connectivity

The strong relationship found between watershed characteristics and the Puget Sound river $\delta^{15}N\text{-}NO_3^-$ values (Fig. 2c) indicates that rivers with low gradient, anthropogenically disturbed watersheds received a higher proportion of $\delta^{15}N$-enriched NO_3^- sources, such as septic and manure waste, compared to rivers with steeper watersheds and increased forest cover. The highest $\delta^{15}N\text{-}NO_3^-$ values were observed in the Puyallup River (up to 13.8‰), previously reported as one of the Puget Sound rivers most influenced by wastewater discharge (Wise & Johnson, 2011). Conversely, in rivers with the highest watershed forest cover, $\delta^{15}N\text{-}NO_3^-$ values were relatively depleted (ranging from -5.2‰ to 4.8‰) and fell within the range typical of soil N (Kendall et al., 2007). Enriched river $\delta^{15}N\text{-}NO_3^-$ values are widely documented in human-dominated watersheds elsewhere and often align with high river NO_3^- concentrations (Barnes & Raymond, 2010; Liu et al., 2013; Rose et al., 2015), linking downstream N exports to

wastewaters from human activities. However, despite the clear enrichment of $\delta^{15}N\text{-}NO_3^-$ values in rivers with human impacted watersheds, we observed that when NO_3^- concentrations increased with winter discharge, $\delta^{15}N\text{-}NO_3^-$ values declined, dampening the variation in $\delta^{15}N\text{-}NO_3^-$ values found across rivers (Fig. 2c, Fig. 4). The relatively depleted wintertime $\delta^{15}N\text{-}NO_3^-$ signals reflect soil N and microbial nitrification sources (including chemical fertilizers and rain-derived NH_4^+) (Barnes & Raymond, 2010; Kendall et al., 2007), implying that the majority of NO_3^- entering the Puget Sound rivers in winter had been reprocessed within the watershed prior to delivery. The seasonal depletion of river $\delta^{15}N\text{-}NO_3^-$ has been shown previously in the region (Elmstrom et al., 2024), however, by examining river $\delta^{15}N\text{-}NO_3^-$ values in the context of watershed characteristics, we show that rivers are enriched in $\delta^{15}N\text{-}NO_3^-$ to different degrees. This variation across rivers, however, largely occurs in the summer, with low gradient, human impacted rivers experiencing greater enrichment compared to rivers draining steeper, forested watersheds which are more pristine.

Corresponding $\delta^{15}N\text{-}NO_3^-$ values from upstream river stations provide further context to the dominant sources of river N in the region, indicating that wintertime NO_3^- concentrations in the Puget Sound rivers were strongly influenced by hydrologic connectivity with upland soils. Upstream stations, which drain large, primarily forested upland areas (93-96%), exhibited depleted $\delta^{15}N\text{-}NO_3^-$ values relative to downstream stations, with values predominantly within the range typical of mineralized and nitrified soil N (Kendall et al., 2007) (Fig. 3c). The isotopic distinction between river network positions, however, was most pronounced during the summer (Fig. 3c), implying more localized sources contributed to NO_3^- concentrations in downstream stations as river discharge declined. Conversely, in winter, when river flows were high, the relative difference in $\delta^{15}N\text{-}NO_3^-$ values between upstream and downstream stations decreased

(Fig. 3c), suggesting enhanced connectivity along the river network promoted leaching and the downstream delivery of soil N sources from forest organic matter. Although we cannot discount the potential influence of other depleted sources as drivers of downstream $\delta^{15}N\text{-}NO_3^-$ declines (e.g., chemical fertilizers, human legacy N in soils), our thinking aligns with previous research from the Puget Sound Basin watersheds, which identify upland forested areas as significant contributors to river N inputs and downstream water quality (J. Lin et al., 2020; McCarthy, 2019; Wise & Johnson, 2011). For example, a recent N budget study in the Nooksack River watershed found the upland watershed contributed 53% of annual NO_3^- export at the river mouth (J. Lin et al., 2020). Red alder plays an important role in adding fixed N to watershed soils in the Pacific Northwest (Binkley et al., 1992; Compton et al., 2003) and is prevalent in upland Puget Sound watersheds due to riparian disturbance and logging. This context, coupled with the overlapping winter $\delta^{15}N\text{-}NO_3^-$ values along the Puget Sound river networks, underscores the significance of upland forested landscapes as contributors to seasonal river NO_3^- exports, particularly through soil mineralization and the nitrification of soil NH_4^+ (Compton et al., 2003; S. Li et al., 2023; J. Lin et al., 2020).

When examining the differences between upstream and downstream stations of individual rivers, we further observed that the upstream-to-downstream differences in $\delta^{15}N\text{-}NO_3^-$ values varied across rivers, but this variation appeared predictable based on the dominant principal components axis (PC1). Specifically, we found that rivers draining lower sloped watersheds with greater human activity exhibited larger differences in $\delta^{15}N\text{-}NO_3^-$ between their up and downstream stations compared to rivers draining steeper sloped, more forested watersheds (Fig. 3c). This also held true for NO_3^- concentrations, with the exception of the lower sloped Cedar River, which had similar mean NO_3^- concentrations in its upstream and

downstream stations (Fig. 3a). Notably, rivers ordinated on the left of the PC1 axis (i.e., more disturbed, smoother watersheds) had the greatest differences in land use between their up and downstream river watershed areas (Table 1). This suggests the variation found across rivers was largely driven by the increased transfer of enriched $\delta^{15}N\text{-}NO_3^-$ sources from human activity in the downstream, flat areas of lower sloped watersheds. These differences, however, were once again confounded by the strong collinear relationship between watershed topography and land use cover in the Puget Sound Basin (Fig. 1c), indicating that river hydrology and slope-driven hydrologic connectivity could also play a role in the relative connection between NO_3^- dynamics in upstream and downstream river sites. For example, the Snohomish, Stillaguamish, and Skagit rivers all have drain relatively steep watersheds, which could expedite constituent movement down the river network, resulting in a more uniform NO_3^- source between the two river stations (Schiff et al., 2002). While we surmise that the upstream-downstream differences across rivers are predominately driven by contrasting land use across watersheds, we cannot disentangle the role of land use vs. the topography in driving terrestrially derived sources of NO_3^- downstream in our study system.

3.5.4 Drought affects NO_3^- runoff and the delivery of atmospheric and terrestrially derived NO_3^- sources to rivers

Interannual variation in Puget Sound river $\Delta^{17}O\text{-}NO_3^-$ values indicates that record drought conditions substantially decreased the seasonal delivery of atmospheric NO_3^- to rivers, with these effects varying strongly across different river types and locations within the Puget Sound Basin. Summer river $\Delta^{17}O\text{-}NO_3^-$ values were significantly lower on average during the 2015 hydrologic year (relative to 2016; Table 4, Fig. 5b), which was an exceptional year in the region characterized by high winter temperatures and reduced runoff and snow water equivalent

(SWE) (Marlier et al., 2017). However, despite a statistical decrease in the basin-wide mean $\Delta^{17}O\text{-}NO_3^-$ value for 2015 relative to 2016, decreases in $\Delta^{17}O\text{-}NO_3^-$ values varied among individual rivers, depending on their hydrologic regime and regional location (Fig. SI 3). The most prominent decreases in summer $\Delta^{17}O\text{-}NO_3^-$ values were observed in snow-dominant rivers in the Olympic Mountains and southern Cascade Range, whereas snow-dominant rivers in the North Cascade Range exhibited increases in summer $\Delta^{17}O\text{-}NO_3^-$ values during 2015 compared to 2016 (Fig SI 4). This regional variability aligns with recent climate research showing the impacts of the 2015 drought were differentially felt across the basin (Marlier et al., 2017). Specifically, the Olympic Mountains experienced their lowest SWE since 1950, and the southern Cascade Range recorded its second-lowest SWE on record. In contrast, the northern Cascade Range had its second warmest winter on record, but changes in precipitation and SWE were not extreme (Marlier et al., 2017).

Regardless of these locational specifics, the 2015 declines in river $\Delta^{17}O\text{-}NO_3^-$ values have broader implications for watershed ecosystem functioning in the Puget Sound Basin and in other mountainous regions. Specifically, as climate change intensifies and snowpack declines, these results suggest rivers draining steep, mountainous terrain will receive less NO_3^- from atmospheric deposition, which could lead to greater terrestrial N retention and further N enrichment of mountainous, high elevation environments (Bourgeois, Savarino, Némery, et al., 2018b). Elevated atmospheric N deposition has already been well documented in remote alpine ecosystems and has altered critical ecosystem processes, such as C:N:P stoichiometry, ecosystem primary productivity, and plant and microbial community structures (Baron & Campbell, 1997; Boot et al., 2016; Burns, 2004; Elser et al., 2009). Future effects on terrestrial ecosystems are complex and uncertain, but this is a critical area of study, particularly in high alpine

environments that are distinctly sensitive to climatic change and the broad ranging effects of anthropogenic N deposition (Burns, 2004).

River NO_3^- concentrations, along with $\delta^{15}N\text{-}NO_3^-$ and $\delta^{18}O\text{-}NO_3^-$ values, also exhibited notable changes during and following the 2015 water year, indicating that drought conditions substantially altered concentration-dilution patterns, landscape N retention, and the delivery of terrestrially derived NO_3^- sources from watersheds to rivers. River NO_3^- concentrations were statistically higher during the summer low-flow conditions of 2015 compared to 2016 (Table 4), suggesting that reductions in groundwater and snow-driven flow led to the concentration of NO_3^- in Puget Sound rivers. Although not statistically identifiable, winter NO_3^- concentrations also appeared to be influenced by drought conditions. Specifically, the winter of 2016, characterized by heavy precipitation, showed a much wider range of NO_3^- concentrations compared to the winter of 2015 (Fig. 5a). Drought can lead to the accumulation of N on land and in soils, and subsequent precipitation often triggers a pulse of NO_3^- in runoff and soil leaching (Greaver et al., 2016). For instance, the 2012 droughts in the US Midwest were followed by extremely high river NO_3^- concentrations in the spring of 2013 (Van Metre et al., 2016). The enriched $\delta^{15}N\text{-}NO_3^-$ and $\delta^{18}O\text{-}NO_3^-$ values in 2016 further indicate that wetter conditions and increased river discharge may have facilitated the transfer of previously accumulated anthropogenic NO_3^- sources, both in the winter and throughout the broader hydrologic year (Table 4, Fig. 5c, d). Wetter conditions can also facilitate rates of denitrification (Gomez-Velez et al., 2015; Sigler et al., 2022), which is a possible cause for the dual enrichment of river $\delta^{15}N\text{-}NO_3^-$ and $\delta^{18}O\text{-}NO_3^-$ values during 2016. Such biological processes should enrich residual $\delta^{15}N\text{-}NO_3^-$ and $\delta^{18}O\text{-}NO_3^-$ values along a positively 2:1 or 1:1 correlated line (F. Chen et al., 2009; Granger & Wankel, 2016; Kendall et al., 2007; Wells et al., 2019). However, largely weak correlations between $\delta^{15}N\text{-}NO_3^-$ and $\delta^{18}O$-

NO_3^- values at the individual river sites (Fig. S5) indicates that biological processes such as denitrification or N assimilation were largely not predominant in the Puget Sound rivers.

3.5.5 Conclusions

We found that spatial variation in the contribution of atmospheric vs. terrestrially derived river NO_3^- sources was strongly associated with a gradient of watershed characteristics, including differences in land use and topography, while also demonstrating the significance of climate-landscape interactions in driving NO_3^- inputs to rivers. By examining NO_3^- triple oxygen isotope variation across multiple river gradients—both across and within rivers—we demonstrate that measurable traces of atmospheric NO_3^- pollution exist in Puget Sound rivers and provide further evidence to show that river atmospheric NO_3^- contributions are strongly influenced by watershed topography and the balance of rain vs. snow that shape river hydrologic regimes. Additionally, by examining seasonal differences in terrestrially derived NO_3^- sources across rivers and along river networks, we highlight the importance of forested landscapes as significant contributors of soil N to wintertime concentrations of Puget Sound river NO_3^-. Finally, we show that climate substantially alters the delivery of atmospheric and terrestrially derived NO_3^- sources to Puget Sound rivers at the inter-annual scale, which has broader implications for the future of biogeochemical cycling in river and watershed ecosystems, particularly in mountainous landscapes. A major outcome of climate change will be the intensification of precipitation patterns, including increased winter runoff, rain-on-snow events, and reductions in snow in some regions (Hamlet et al., 2013; Seybold et al., 2022; Sinha et al., 2017). Here, we provide insight into how climate change may be expressed in terms of river N cycles and how this will not only affect the total amount of NO_3^- in rivers, but also the different sources of NO_3^-. Altogether, our study indicates that while landscape variation is a critical driver of atmospheric and terrestrially

derived NO_3^- inputs, the consideration of climate is essential for a complete understanding of current and future riverine NO_3^- source dynamics across rivers.

3.6 TABLES

Table 3.1. River and watershed characteristics of the Puget Sound Basin rivers of study. River and watershed characteristics are ordered by decreasing monthly mean NO_3^- concentration at the downstream station. Upstream river stations are listed below their corresponding downstream station. Other descriptors include stream order, watershed area, mean watershed elevation, mean watershed slope, and percent urban, agriculture, wetland, coniferous forest cover by area of the watershed. Downstream river water quality sampling sites are labeled on Figure 1 using the italicized abbreviations in the first column of the table.

Table 3-1 Watershed characteristics

Watershed	River name	Down or upstream	NO_3^- (mg L^{-1})	Stream order	Watershed area (km^2)	Watershed elevation (m)	Watershed slope (°)	% Urban	% Agriculture	% Wetland	% Coniferous
Deschutes (*De*)	Deschutes	down	0.75±0.1	3	409	288	8	15.4	8.4	5	44.1
Samish (*Sa*)	Samish	down	0.74±0.2	4	225	268	8	9.2	7.5	5.8	37.4
Green (Gr)	Green	down	0.39±0.2	5	1116	546	11	22.6	4.8	2.4	46.9
Green	Green	up	0.14±0.1	5	659	822	19	3	0.6	0.7	73.8
Nooksack (*No*)	Nooksack	down	0.33±0.2	5	2046	674	14	4.8	12.4	2.9	53.7
Nooksack	Nooksack	up	0.16±0.1	5	1543	868	19	1.9	1.5	2.1	65.3
Nisqually (*Ni*)	Nisqually	down	0.25±0.1	5	1853	556	9	8.4	6.4	5.6	49.7
Cedar (*Ce*)	Cedar	down	0.24±0.1	4	457	611	13	15.8	0.6	1.5	61.1
Cedar	Cedar	up	0.16±0.1	4	310	808	17	3.2	0	1	80.8
Puyallup (*Pu*)	Puyallup	down	0.23±0.1	6	2439	921	15	9.1	2.7	2.4	59.2
Snohomish (*Sno*)	Snohomish	down	0.22±0.1	6	4450	688	16	7.1	2.7	2.4	58
Snohomish	Skykomish	up	0.13±0.1	5	1987	905	21	2.3	0.9	1.1	71.1
Snohomish	Snoqualmie	up	0.19±0.1	5	947	898	18	3.3	0.3	0.9	70.3
Stillaguamish (*St*)	Stillaguamish	down	0.21±0.1	5	1457	604	14	4.3	2.9	1.7	68
Stillaguamish	N.F. Stillaguamish	up	0.15±0.1	3	222	714	19	2.7	1	0.6	78.3
Stillaguamish	S.F. Stillaguamish	up	0.10±0.1	3	308	769	21	2.4	0	0.7	78.1
Skagit (*Ska*)	Skagit	down	0.09±0.05	6	8035	1128	22	2	1.3	0.9	64.7
Skagit	Skagit	up	0.06±0.02	5	3601	1349	26	0.4	0.1	0.3	63.6
Skokomish (*Sko*)	Skokomish	down	0.06±0.03	5	592	609	21	5.5	1	1.3	70.8
Duckabush (*Du*)	Duckabush	down	0.03±0.02	3	179	1047	27	0.8	0	0.3	75.6
Elwha (*El*)	Elwha	down	0.03±0.02	4	757	1089	24	0.3	0	0.4	80.8

Table 3.2. Competing models with relative support (ΔAICc ≤ 2) for our **across river comparison** using AICc analysis for each response variable, where the most parsimonious models with the most support are shown in bold.

Response Variable	ΔAICc	Covariates included in model with relative support
NO_3^-	**0**	**PC1, Season, *PC1×Season***
NO_3^-	2.0	PC1, Season, Year, *PC1×Season*
$\Delta^{17}O\text{-}NO_3^-$	**0**	**PC1, Season, *PC1×Season***
$\Delta^{17}O\text{-}NO_3^-$	0.5	PC1, Season, Year, *PC1×Season, Season × Year*
$\delta^{15}N\text{-}NO_3^-$	**0**	**PC1, Season, Year, *PC1×Season***
$\delta^{15}N\text{-}NO_3^-$	0.9	PC1, Season, Year
$\delta^{18}O\text{-}NO_3^-$	**0**	**PC1, Year, *PC1×Year***
$\delta^{18}O\text{-}NO_3^-$	1.7	PC1, Year

Table 3-2 Across rivers

Table 3.3. Competing models with relative support (ΔAICc ≤ 2) for the **within river comparison** using AIC analysis for each response variable, where the most parsimonious models with the most support are shown in bold.

Response Variable	ΔAICc	Covariates included in model with relative support
NO_3^-	**0**	**Position, Season, Year, *Position* × *Season*, *Season* × *Year***
NO_3^-	1.5	Position, Season, Year, *Season* × *Year*
NO_3^-	2.0	Position, Season, Year, *Position* × *Season*, *Position* × *Year*, *Season* × *Year*
$\Delta^{17}O\text{-}NO_3^-$	**0**	**Position, Season, *Position* × *Season*,**
$\Delta^{17}O\text{-}NO_3^-$	1.8	Position, Season, Year, *Position* × *Season*
$\Delta^{17}O\text{-}NO_3^-$	1.9	Position, Season, Year, *Position* × *Season*, *Season* × *Year*
$\delta^{15}N\text{-}NO_3^-$	**0**	**Position, Season, Year, *Position* × *Season*,**
$\delta^{15}N\text{-}NO_3^-$	1.7	Position, Season, Year, *Position* × *Season*, *Position* × *Year*
$\delta^{15}N\text{-}NO_3^-$	1.8	Position, Season, Year, *Position* × *Season*, *Season* × *Year*
$\delta^{18}O\text{-}NO_3^-$	**0**	**Position, Season, Year**
$\delta^{18}O\text{-}NO_3^-$	1.5	Season, Year
$\delta^{18}O\text{-}NO_3^-$	1.8	Position, Season, Year, *Position* × *Year*
$\delta^{18}O\text{-}NO_3^-$	1.8	Position, Season, Year, *Season* × *Year*

Table 3-3 Within watersheds

Table 3.4. Pairwise comparisons assessing the basin-wide differences between seasons for each hydrologic year of study. “Dry” represents the 2015 hydrologic year and “wet” represents the 2016 hydrologic year. Significant comparisons are shown in bold.

Response variable	Year Contrast	Season	Sign	*p*
NO_3^-	Wet - Dry	Summer	−	***p* < 0.10**
NO_3^-	Wet - Dry	Winter	+	n.s.
$\Delta^{17}O\text{-}NO_3^-$	Wet - Dry	Summer	+	***p* < 0.05**
$\Delta^{17}O\text{-}NO_3^-$	Wet - Dry	Winter	−	n.s.
$\delta^{15}N\text{-}NO_3^-$	Wet - Dry	Summer	+	***p* < 0.01**
$\delta^{15}N\text{-}NO_3^-$	Wet - Dry	Winter	+	***p* < 0.05**
$\delta^{18}O\text{-}NO_3^-$	Wet - Dry	Summer	+	***p* < 0.01**
$\delta^{18}O\text{-}NO_3^-$	Wet - Dry	Winter	+	***p* < 0.001**

Table 3-4 Between years

3.7 FIGURES

Figure 3.1. Map and characteristics of the Puget Sound Basin watersheds of study. **a)** The watersheds of study shaded with their local slope in degrees. Black points represent the downstream river water quality sampling stations. Italicized abbreviations refer to the river names, which are provided in full in Table 2. Grey points represent the upstream river water quality sample stations. **b)** Location of the Puget Sound Basin within Washington state and British Columbia. **c)** Ordination plot showing principal component analysis (PCA) of watershed characteristics from the Puget Sound Basin rivers. Length and direction of arrows on the ordination are proportional to vector loading of watershed characteristics into each principal component (PC). Points are colored by the watershed 30-year average annual air temperature (PRISM Climate Group, 2015).

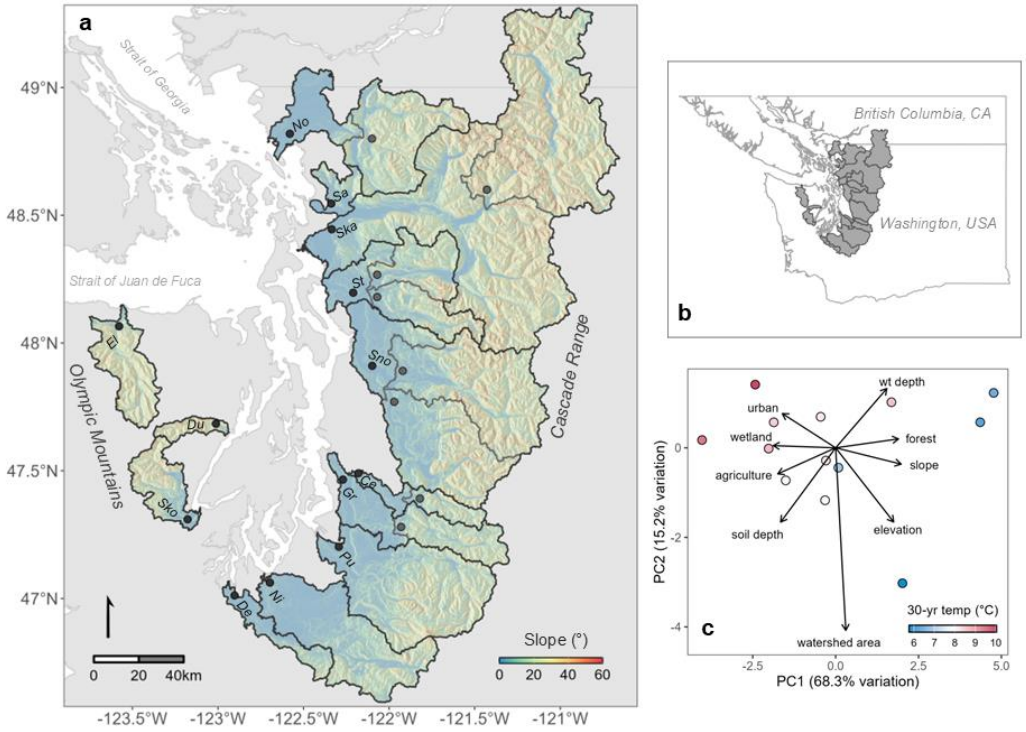

Figure 3-1 Study map

Figure 3.2. a) Average river NO_3^- concentrations modeled as a logarithmic function of principal component axis 1 for the winter and summer seasons. **b)** Average river $\Delta^{17}O\text{-}NO_3^-$ modeled as a logarithmic function of principal component axis 1 for the winter and summer seasons. **c)** Average river $\delta^{15}N\text{-}NO_3^-$ modeled as a linear function of principal component axis 1 for the winter and summer seasons.

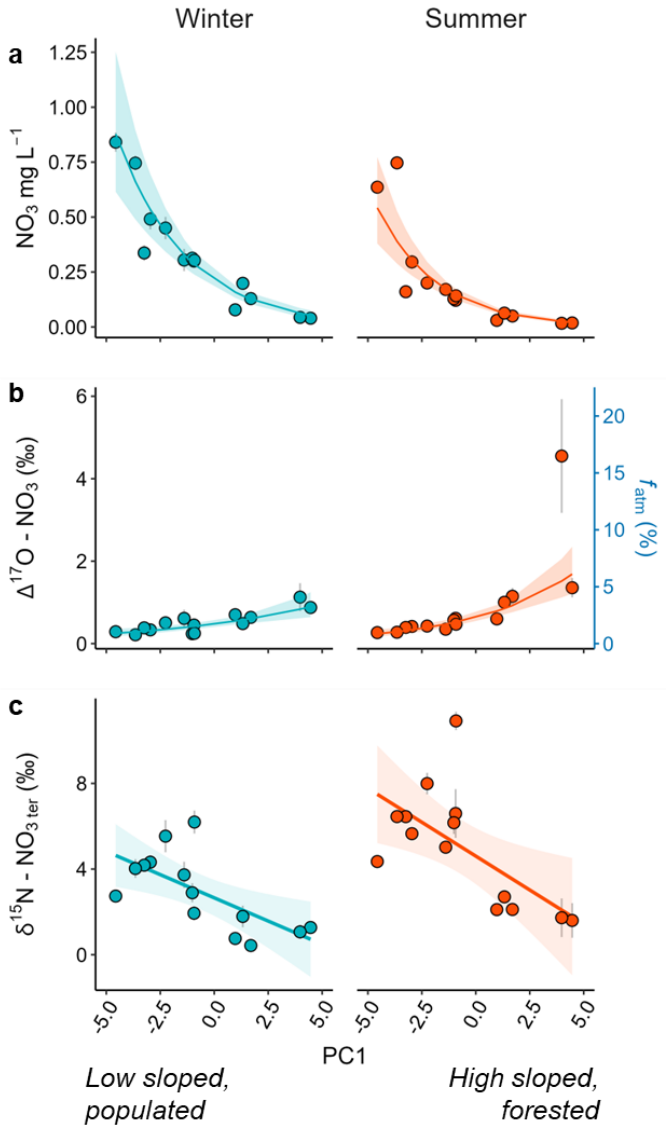

Figure 3-2 PC1 season

Figure 3.3. a) Average river NO_3^- concentration in downstream and upstream stations for the winter and summer seasons. **b)** Average river $\Delta^{17}O\text{-}NO_3^-$ in downstream and upstream stations for the winter and summer seasons. **c)** Average river $\delta^{15}N\text{-}NO_3^-$ in downstream and upstream stations for the winter and summer seasons. Downstream stations are colored grey. Upstream stations are colored blue and orange for the winter and summer seasons, respectively.

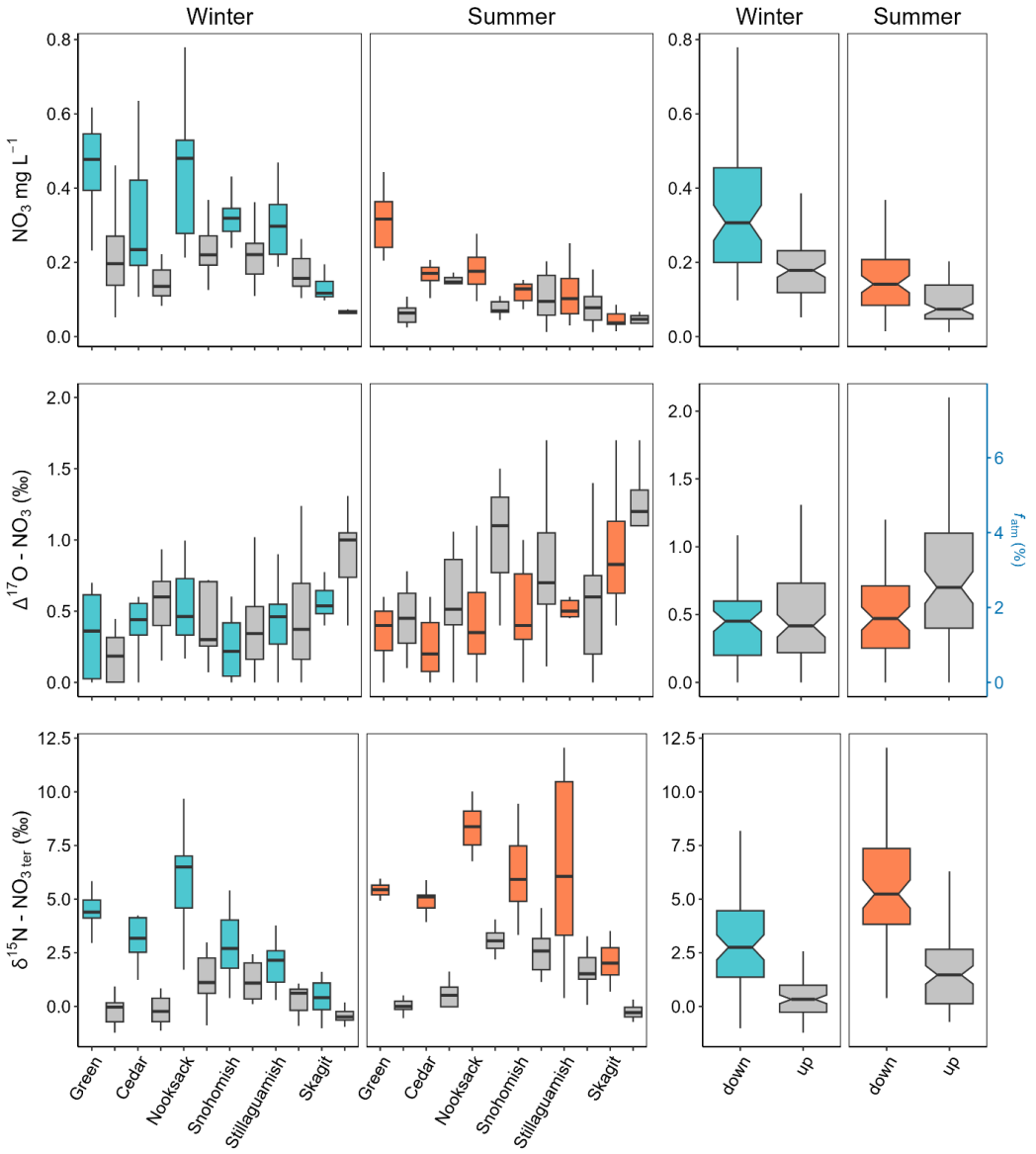

Figure 3-3 Up down season

Figure 3.4. δ^{15}N-NO_3^- values measured in the downstream Puget Sound river stations plotted versus river discharge on the logarithmic scale. Size and color of the points are proportional to the corresponding (but scaled) NO_3^- concentrations for each river sample.

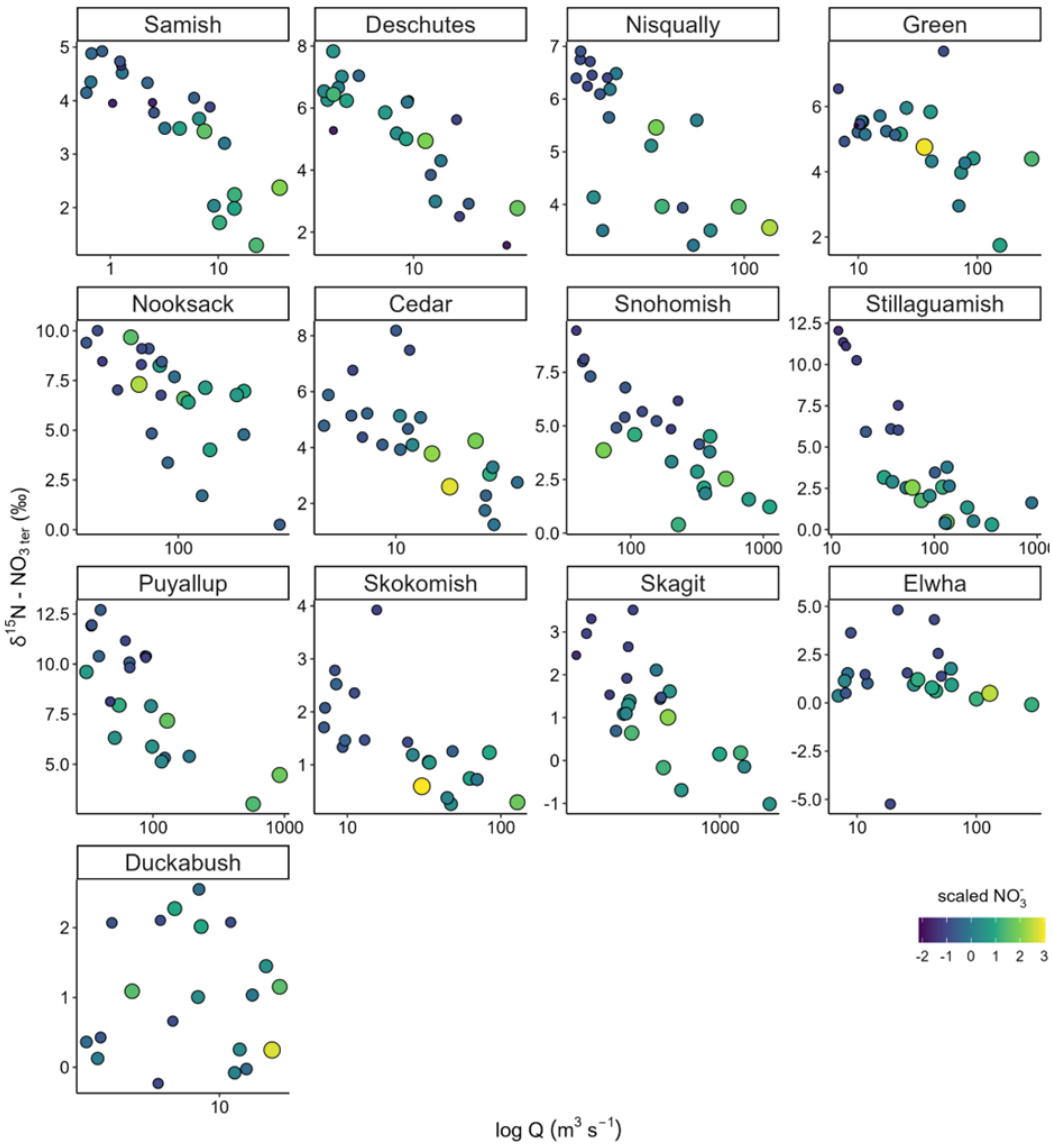

Figure 3-4 d15N vs. Q

Figure 3.5. a) Average river NO_3^- concentration in winter and summer seasons for the dry and wet year of study. **b)** Average river $\Delta^{17}O\text{-}NO_3^-$ in winter and summer seasons for the dry and wet year of study. **c)** Average river $\delta^{15}N\text{-}NO_3^-$ in winter and summer seasons for the dry and wet year of study. **d)** Average river $\delta^{18}O\text{-}NO_3^-$ in winter and summer seasons for the dry and wet year of study. Winter seasons are colored light blue and dark blue for 2015 and 2016, respectively. Summer seasons are colored light orange and dark orange for 2015 and 2016, respectively.

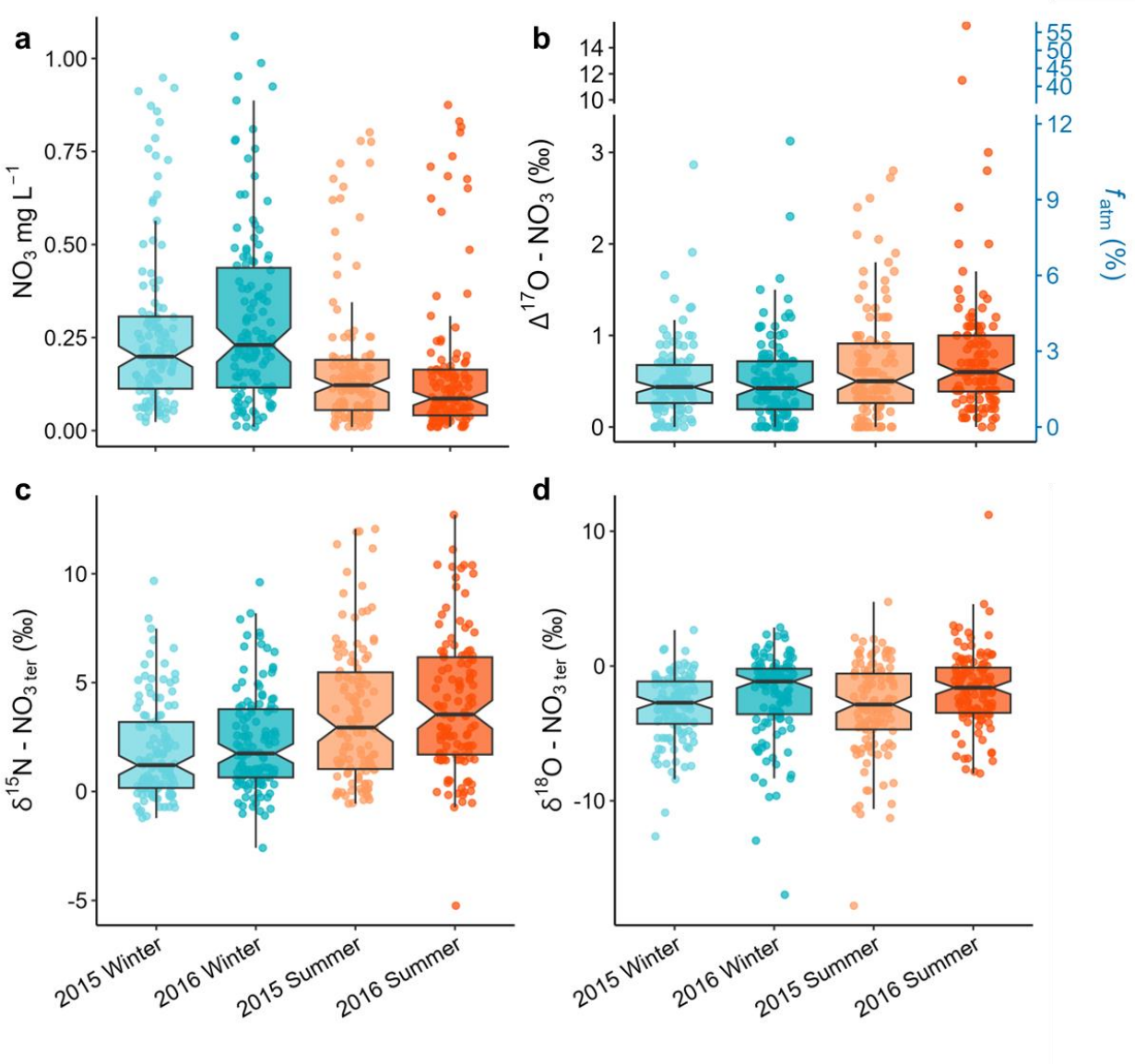

Figure 3-5 Between years

CONCLUSION

My dissertation research builds on foundational research in river ecosystems science showing rivers are fundamentally connected to their watersheds (Bormann et al., 1968; Bormann & Likens, 1967), while expanding on more recent work re-emphasizing this includes both watershed land cover and surrounding terrain (Cline et al., 2020; Connolly et al., 2018a; Harms et al., 2016; Holtgrieve et al., 2010; Jankowski et al., 2014; Jankowski & Schindler, 2019; Lisi et al., 2015; Schiff et al., 2002; Smits et al., 2017). Additionally, my research emphasizes the significance of hydroclimate as a key structuring variable of physical and ecological processes within watersheds (Poff et al., 1997) and highlights the importance of climate-landscape interactions in driving river nutrient processes and transport to the coastal ocean (Lewis & Grimm, 2007; Sinha & Michalak, 2016; Soranno et al., 2014). By employing cross-system comparisons (Levin, 1992), stable isotopes (Sigman et al., 2001), and time series statistical models (Holmes et al., 2021), my dissertation research ultimately shows that climate, landform, and hydrologic regime are dominant controls of river biogeochemical source and transport in the Puget Sound Basin, which has broader implications for the Pacific Northwest and other mountainous regions. Moreover, my research elucidates the major sources of reactive N to the Puget Sound rivers and indicates the need for future studies at finer scales to fully understand the confounding landscape-level controls that drive N sources and transport across human-influenced, mountainous landscapes. My conclusions are as follows:

Climate and the physical environment dominate changes in river nutrient concentration, source, and transport in a human-influenced, mountainous region:

Drivers of river nutrient concentration, source, and transport are numerous, with multiple interacting controls that are hierarchically nested at macro (e.g., PDO, ENSO), regional (e.g., temperature, precipitation), and watershed (e.g., topography, land use, hydrologic regime) scales (Frissell et al., 1986; Heffernan et al., 2014). When observing spatial and temporal variation through a broad, regional-scale lens, my dissertation research demonstrates that regional and macro-scale climate drivers dominate seasonal and decadal-scale changes in river nutrient sources, concentrations, and transport across the Puget Sound Basin. In Chapter 1, I show regional hydroclimate strongly influences the seasonality of river NO_3^- dynamics, largely synchronizing monthly variation in river NO_3^- yield, concentration, and isotopic composition across rivers within two mountain ranges. Given the strength of seasonal precipitation in the Pacific Northwest, I anticipated some degree of coherence in monthly river NO_3^- concentrations and yields, but coherence in monthly isotopic composition provides new evidence showing the importance of seasonal runoff and snowmelt in driving hydrologic connections with common watershed NO_3^- sources. In Chapter 2, I further demonstrate the importance of macro-scale climate phenomena, particularly the Pacific Decadal Oscillation, as drivers of long-term change in river hydrologic and nutrient transport regimes. Here, I specifically identify the largest changes in seasonal river DIN and DIP transport regimes were due to hydroclimate variation rather than nutrient mobilization or other biogeochemical shifts that would drive increases or decreases in nutrient concentration.

While the effects of climate are broad-reaching, individual rivers may vary in their hydrologic and biogeochemical responses to climate due to the spatial heterogeneity landscapes, which filter the effects of broad-scale processes like climate on river ecosystems (Cline et al., 2020; Jankowski et al., 2014; Lisi et al., 2015). When examining the river responses to regional

and macro-scale climate drivers through a more localized lens in Chapter 1 and 2, I found that watershed-scale variation in topography exerted strong control over the responses of Puget Sound river nutrient dynamics to hydroclimatic change. Specifically, I found variation in the response of river nutrient yields, concentrations, and isotopic compositions to seasonal and decadal-scale climate variables was explained by one simple topographic feature, watershed slope. This demonstrates that while climate exerts dominance over temporal patterns in Puget Sound river nutrient dynamics, watershed-scale variation in topography integrates landscape and climate variation to provide the clearest image of river hydrologic and biogeochemical responses to climatic change. Ultimately, this shows in the Puget Sound Basin, climate and the physical environment (in contrast to land use and land cover) interact to dominate spatiotemporal variation in river nutrient biogeochemistry and are primary controls of nutrients entering and leaving rivers to the coastal environment.

The strong relationships found between the Puget Sound river nutrient climate sensitivities and watershed slope also have broader implications for management in other human-influenced, mountainous regions. Findings from Chapter 1 and 2 show that NO_3^- yields from rivers draining lower sloped watersheds were most sensitive to the seasonal pulse of precipitation, while rivers draining steeper slopes are more likely to lose seasonality complexity in their DIN and DIP exports as snowpack diminishes under a warmer climate. These relationships build on previous work from more pristine mountainous regions that highlight watershed slope as a master predictor of physical and biogeochemical processes, ultimately modifying the response of river ecosystem function to climate (Cline et al., 2020; Connolly et al., 2018b; Harms et al., 2016; Jankowski et al., 2014; Jankowski & Schindler, 2019; Lisi et al., 2015; Smits et al., 2017). However, here, I relate watershed slope to river nutrient transport in a

human-dominated landscape, providing a reasonable framework with which to predict future biogeochemical change in mountainous regions with increasing human activity. This suggests that topographic features, such as watershed slope, could be used to improve future scenarios of river N and P transport in other regions, aiding river nutrient management and coastal modeling efforts in the context of future climate and anthropogenic change.

The forested landscape as a key contributor to seasonal N exports in a human-influenced, mountainous region:

The use of stable isotopes in river biogeochemical studies show that river NO_3^- concentrations and transport are driven by a diversity of natural and anthropogenically derived N sources, which can vary temporally and across watersheds (Bostic et al., 2022; Briand et al., 2017; Rose et al., 2015). My dissertation research elucidates those sources in a spatially and hydrologically complex region, supporting recent work showing the transfer of NO_3^- from watersheds to rivers is largely driven by hydrologic connections with different NO_3^- source compartments (e.g., soils, groundwater, see Briand et al., 2017). In Chapter 1, I demonstrate that during the winter months, when river NO_3^- concentrations and yields are high, $\delta^{15}N\text{-}NO_3^-$ values broadly deplete across the Puget Sound Basin rivers, reflecting soil N and microbial nitrification sources of NO_3^- (including chemical fertilizers and rain-derived NH_4^+) (Kendall et al., 2007). In Chapter 3, I expand on this finding by comparing $\delta^{15}N\text{-}NO_3^-$ values between downstream and upstream river sampling stations, the context of which identifies soil N from upland forests as a dominant contributor of winter river NO_3^- delivery. Although we cannot completely discount human derived NO_3^- sources (lower gradient rivers with increased human activity were still enriched in the winter relative to rivers draining steeper, more forested watersheds), findings

from these two chapters underscores the significance of forested landscapes as seasonal contributors to river NO_3^- exports and downstream coastal water quality. This has relevance to managers tasked with targeting sources of N pollution within the broader Puget Sound region, suggesting that, when rivers are most hydrologically connected to the Puget Sound estuary, a substantial proportion of riverine NO_3^- exports to the coastal environment are of natural origin, rather than from urban development or agricultural activity.

Findings from this dissertation are from a broad, regional-scale lens:

While the Puget Sound Basin is a spatially and hydrologically complex region, the individual watersheds within it are also heterogeneous and vary internally in their geomorphic features and land use composition. By studying the Puget Sound watersheds at the regional scale, my dissertation research inevitably masked some of this internal river and watershed heterogeneity. However, a key challenge in the future will be to manage our watersheds for the differential and interacting effects of climate and land use change. In reality, most management decisions are made at the watershed scale, which could benefit from localized, spatially targeted management efforts (Isaak et al., 2017). Further, a consistent challenge in drawing conclusions from my dissertation research was the confounding effects of watershed topography and human activity in the Puget Sound Basin, as watershed slope and land use cover were highly colinear across my study watersheds. River nutrient management in the Puget Sound Basin, as well as in other human-influenced, mountainous regions, would benefit from future river biogeochemical research that seeks to untangle these confounding controls, but within a local, watershed-scale context. This would further enhance our understanding of the different landscape properties that retain or release nutrient pollution to rivers, thereby informing where and how management

efforts should be focused. While my dissertation chapters expand our understanding of climate and physical controls on river nutrient source and transport across the Puget Sound Basin, findings from my research are ultimately a matter of scale, underscoring the importance of scale in ecology and the need to consider study grain and extent in designing future river research endeavors (Levin, 1992).

Chapter 1 Appendix

Supplementary Table 1. AICc (Akaike Information Criterion), number of trends and number of parameters for all **NO_3 yield** model structures considered comparing number of shared trends (**Z** matrices) and process error models (**Q** matrices).

Model (**Z**)	# Trends	**Q** matrix	Log likelihood	AICc	# of parameters	ΔAICc
Mountain	2	equal var-covar	-68.7	147.6	5	0
Mountain	2	unconstrained	-67.9	148.2	6	0.6
Geomorphology	3	unconstrained	-67.8	156.3	10	8.7
Geomorphology	3	equal var-covar	-75.4	163.1	6	15.5
Land use	3	unconstrained	-76.5	173.8	10	26.2
Land use	3	equal var-covar	-81.8	175.9	6	28.3
Mountain	2	diagonal and equal	-84.0	176.1	4	28.5
Mountain	2	diagonal and unequal	-83.8	177.8	5	30.2
Basin	1	diagonal and equal	-90.7	187.4	3	39.8
Basin	1	diagonal and unequal	-90.7	187.4	3	39.8
Basin	1	equal var-covar	-90.7	187.4	3	39.8
Basin	1	unconstrained	-90.7	187.4	3	39.8
Watershed	13	equal var-covar	-90.8	215.5	16	67.9
Geomorphology	3	diagonal and equal	-113.6	237.4	5	89.8
Geomorphology	3	diagonal and unequal	-113.3	240.9	7	93.3
Land use	3	diagonal and equal	-123.7	257.7	5	110.1
Land use	3	diagonal and unequal	-123.5	261.3	7	113.7
Watershed	13	unconstrained	24.5	269.1	105	121.5
Watershed	13	diagonal and equal	-271.6	574.9	15	427.3
Watershed	13	diagonal and unequal	-269.1	597.5	27	449.8

Supplementary Table 2. AICc (Akaike Information Criterion), number of trends and number of parameters for all **NO_3 concentration** model structures considered comparing number of shared trends (**Z** matrices) and process error models (**Q** matrices).

Model (**Z**)	# Trends	**Q** matrix	Log likelihood	AICc	# of parameters	ΔAICc
Mountain	2	equal var-covar	-331.3	672.7	5	0
Mountain	2	unconstrained	-331.3	674.8	6	2.1
Geomorphology	3	unconstrained	-327.6	676.0	10	3.2
Mountain	2	diagonal and equal	-334.2	676.6	4	3.9
Mountain	2	diagonal and unequal	-334.2	678.7	5	6.0
Geomorphology	3	equal var-covar	-335.8	683.8	6	11.1
Land use	3	equal var-covar	-338.7	689.8	6	17.1
Basin	1	diagonal and equal	-342.1	690.3	3	17.6
Basin	1	diagonal and unequal	-342.1	690.3	3	17.6
Basin	1	equal var-covar	-342.1	690.3	3	17.6
Basin	1	unconstrained	-342.1	690.3	3	17.6
Land use	3	unconstrained	-334.8	690.4	10	17.7
Geomorphology	3	diagonal and equal	-345.7	701.6	5	28.9
Geomorphology	3	diagonal and unequal	-345.4	705.2	7	32.5
Land use	3	diagonal and equal	-351.1	712.4	5	39.7
Land use	3	diagonal and unequal	-350.8	716.1	7	43.3
Watershed	13	equal var-covar	-342.3	718.4	16	45.7
Watershed	13	unconstrained	-240.6	802.4	105	129.7
Watershed	13	diagonal and equal	-393.0	817.7	15	145.0
Watershed	13	diagonal and unequal	-384.4	828.3	27	155.5

Supplementary Table 3. AICc (Akaike Information Criterion), number of trends and number of parameters for all δ^{15}**N** model structures considered comparing number of shared trends (**Z** matrices) and process error models (**Q** matrices).

Model (**Z**)	# Trends	**Q** matrix	Log likelihood	AICc	# of parameters	ΔAICc
Mountain	2	unconstrained	-360.4	733.0	6	0
Mountain	2	diagonal and unequal	-362.2	734.6	5	1.6
Mountain	2	diagonal and equal	-365.0	738.1	4	5.1
Mountain	2	equal var-covar	-364.4	738.9	5	5.9
Geomorphology	3	unconstrained	-360.3	741.3	10	8.3
Basin	1	diagonal and equal	-371.3	748.6	3	15.6
Basin	1	diagonal and unequal	-371.3	748.6	3	15.6
Basin	1	equal var-covar	-371.3	748.6	3	15.6
Basin	1	unconstrained	-371.3	748.6	3	15.6
Geomorphology	3	equal var-covar	-370.2	752.8	6	19.8
Land use	3	equal var-covar	-371.6	755.4	6	22.4
Land use	3	unconstrained	-369.1	758.9	10	25.9
Geomorphology	3	diagonal and unequal	-373.3	760.9	7	27.9
Geomorphology	3	diagonal and equal	-376.5	763.2	5	30.2
Watershed	13	equal var-covar	-371.5	776.9	16	43.9
Land use	3	diagonal and equal	-384.7	779.6	5	46.7
Land use	3	diagonal and unequal	-384.4	783.2	7	50.2
Watershed	13	diagonal and equal	-412.0	855.7	15	122.7
Watershed	13	diagonal and unequal	-410.6	880.8	27	147.8
Watershed	13	unconstrained	-315.1	953.2	105	220.2

Supplementary Table 4. AICc (Akaike Information Criterion), number of trends and number of parameters for all $\delta^{18}O$ model structures considered comparing number of shared trends (**Z** matrices) and process error models (**Q** matrices).

Model (**Z**)	# Trends	**Q** matrix	Log likelihood	AICc	# of parameters	ΔAICc
Mountain	2	equal var-covar	-372.7	755.6	5	0
Mountain	2	diagonal and equal	-374.4	757.0	4	1.4
Mountain	2	unconstrained	-372.6	757.5	6	1.9
Mountain	2	diagonal and unequal	-374.3	758.9	5	3.2
Geomorphology	3	equal var-covar	-376.3	764.9	6	9.3
Geomorphology	3	unconstrained	-372.6	766.0	10	10.3
Land use	3	unconstrained	-374.2	769.2	10	13.5
Basin	1	diagonal and equal	-381.8	769.8	3	14.1
Basin	1	diagonal and unequal	-381.8	769.8	3	14.1
Basin	1	equal var-covar	-381.8	769.8	3	14.1
Basin	1	unconstrained	-381.8	769.8	3	14.1
Land use	3	equal var-covar	-379.9	772.2	6	16.5
Geomorphology	3	diagonal and equal	-383.6	777.5	5	21.8
Geomorphology	3	diagonal and unequal	-383.3	780.9	7	25.3
Land use	3	diagonal and equal	-386.7	783.6	5	28.0
Land use	3	diagonal and unequal	-385.9	786.2	7	30.5
Watershed	13	equal var-covar	-382.6	799.1	16	43.5
Watershed	13	diagonal and equal	-415.3	862.2	15	106.6
Watershed	13	diagonal and unequal	-413.2	885.8	27	130.2
Watershed	13	unconstrained	-329.2	981.3	105	225.7

Supplementary Table 5. AICc (Akaike Information Criterion) values for the top twenty models considering the effects of covariates on watershed-specific **NO_3 yield trends**. "Scale of effect" column indicates whether the covariate effect size (i.e., the **C** coefficient) was shared among all rivers within the basin, within each mountain range, among rivers of similar land use, among rivers with similar geomorphic features, or for each watershed individually. The null model does not include covariates.

Covariate	Scale of effect	**Q** matrix	Log likelihood	AICc	# of parameters	ΔAICc
Precipitation	Mountain	equal var-covar	-67.6	173.5	18	0
Precipitation	Geomorphology	equal var-covar	-66.9	174.3	19	0.8
Precipitation	Land use	equal var-covar	-67.6	175.8	19	2.2
Temperature	Mountain	equal var-covar	-72.5	183.3	18	9.8
Temperature	Geomorphology	equal var-covar	-72.1	184.8	19	11.3
Precipitation	Basin	equal var-covar	-75.4	186.9	17	13.4
Precipitation	Watershed	equal var-covar	-62.1	188.3	29	14.8
Temperature	Watershed	equal var-covar	-68.8	201.8	29	28.3
Temperature	Land use	equal var-covar	-81.2	203.0	19	29.5
Snowmelt	Mountain	equal var-covar	-86.4	211.2	18	37.6
Snowmelt	Geomorphology	equal var-covar	-86.0	212.7	19	39.1
Null	Null	equal var-covar	-90.8	215.5	16	42.0
Snowmelt	Basin	equal var-covar	-90.8	217.7	17	44.2
Temperature	Basin	equal var-covar	-91.0	218.0	17	44.5
Snowmelt	Land use	equal var-covar	-89.2	219.1	19	45.6
SPI	Basin	equal var-covar	-93.3	222.6	17	49.1
SPI	Mountain	equal var-covar	-92.1	222.6	18	49.1
SPI	Geomorphology	equal var-covar	-92.1	224.9	19	51.3
SPI	Land use	equal var-covar	-92.5	225.6	19	52.1
SPI	Watershed	equal var-covar	-82.3	228.8	29	55.3

Supplementary Table 6. AICc (Akaike Information Criterion) values for the top twenty models considering the effects of covariates on watershed-specific **NO_3 concentration trends**. "Scale of effect" column indicates whether the covariate effect size (i.e., the **C** coefficient) was shared among all rivers within the basin, within each mountain range, among rivers of similar land use, among rivers with similar geomorphic features, or for each watershed individually. The null model does not include covariates.

Covariate	Scale of effect	**Q** matrix	Log likelihood	AICc	# of parameters	ΔAICc
Precipitation	Mountain	equal var-covar	-324.7	687.7	18	0
Temperature	Mountain	equal var-covar	-324.9	688.3	18	0.5
Temperature	Geomorphology	equal var-covar	-324.5	689.6	19	1.9
Precipitation	Geomorphology	equal var-covar	-324.7	690.0	19	2.3
Temperature	Watershed	equal var-covar	-313.3	691.0	29	3.2
Precipitation	Watershed	equal var-covar	-314.9	694.1	29	6.4
Q_{slow}	Geomorphology	equal var-covar	-332.3	705.2	19	17.5
Q_{slow}	Mountain	equal var-covar	-333.7	705.7	18	18.0
Snowmelt	Mountain	equal var-covar	-335.5	709.5	18	21.7
Snowmelt	Geomorphology	equal var-covar	-335.2	711.0	19	23.3
Temperature	Land use	equal var-covar	-335.4	711.5	19	23.8
Q_{slow}	Land use	equal var-covar	-336.2	713.1	19	25.4
Precipitation	Land use	equal var-covar	-337.2	715.1	19	27.4
Snowmelt	Basin	equal var-covar	-339.9	715.9	17	28.2
Snowmelt	Land use	equal var-covar	-338.0	716.6	19	28.8
Q_{quick}	Mountain	equal var-covar	-339.5	717.3	18	29.6
Q_{slow}	Basin	equal var-covar	-341.0	718.0	17	30.3
Null	Null	equal var-covar	-342.3	718.4	16	30.7
Precipitation	Basin	equal var-covar	-341.4	719.0	17	31.2
Temperature	Basin	equal var-covar	-341.6	719.3	17	31.6

Supplementary Table 7. AICc (Akaike Information Criterion) values for the top twenty models considering the effects of covariates on watershed-specific **δ^{15}N trends**. "Scale of effect" column indicates whether the covariate effect size (i.e., the **C** coefficient) was shared among all rivers within the basin, within each mountain range, among rivers of similar land use, among rivers with similar geomorphic features, or for each watershed individually. The null model does not include covariates.

Covariate	Scale of effect	**Q** matrix	Log likelihood	AICc	# of parameters	ΔAICc
Q_{quick}	Mountain	equal var-covar	-362.7	763.8	18	0
Q_{quick}	Geomorphology	equal var-covar	-362.5	765.7	19	1.9
Q_{quick}	Watershed	equal var-covar	-351.2	766.7	29	3.0
Q_{quick}	Basin	equal var-covar	-366.0	768.2	17	4.5
Precipitation	Mountain	equal var-covar	-366.0	770.5	18	6.7
Precipitation	Geomorphology	equal var-covar	-365.8	772.3	19	8.6
Q_{quick}	Land use	equal var-covar	-365.9	772.5	19	8.7
Precipitation	Basin	equal var-covar	-369.8	775.8	17	12.1
Null	Null	equal var-covar	-371.5	776.9	16	13.1
Precipitation	Watershed	equal var-covar	-356.7	777.7	29	14.0
SPI	Basin	equal var-covar	-370.9	778.0	17	14.3
Temperature	Basin	equal var-covar	-371.2	778.6	17	14.9
Snowmelt	Basin	equal var-covar	-371.4	779.0	17	15.3
Q_{slow}	Basin	equal var-covar	-371.5	779.1	17	15.3
SPI	Mountain	equal var-covar	-370.5	779.3	18	15.6
Precipitation	Land use	equal var-covar	-369.4	779.4	19	15.6
Q_{slow}	Land use	equal var-covar	-369.6	779.9	19	16.2
Temperature	Land use	equal var-covar	-369.7	780.0	19	16.3
Snowmelt	Geomorphology	equal var-covar	-369.9	780.4	19	16.7
Temperature	Mountain	equal var-covar	-371.2	780.8	18	17.0

Supplementary Table 8. AICc (Akaike Information Criterion) values for the top twenty models considering the effects of covariates on watershed-specific **$\delta^{18}O$ trends**. "Scale of effect" column indicates whether the covariate effect size (i.e., the **C** coefficient) was shared among all rivers within the basin, within each mountain range, among rivers of similar land use, among rivers with similar geomorphic features, or for each watershed individually. The null model does not include covariates.

Covariate	Scale of effect	**Q** matrix	Log likelihood	AICc	# of parameters	ΔAICc
Snowmelt	Mountain	equal var-covar	-369.8	777.9	18	0
Snowmelt	Geomorphology	equal var-covar	-369.7	780.1	19	2.2
Q_{quick}	Geomorphology	equal var-covar	-372.1	784.8	19	6.9
Q_{quick}	Mountain	equal var-covar	-373.6	785.6	18	7.7
Q_{quick}	Watershed	equal var-covar	-362.0	788.4	29	10.5
SPI	Basin	equal var-covar	-377.7	791.5	17	13.5
Precipitatoin	Mountain	equal var-covar	-377.1	792.6	18	14.7
SPI	Basin	equal var-covar	-376.1	792.9	19	15.0
Q_{slow}	Mountain	equal var-covar	-377.5	793.4	18	15.5
Q_{slow}	Geomorphology	equal var-covar	-376.5	793.7	19	15.8
SPI	Mountain	equal var-covar	-377.7	793.7	18	15.8
Q_{quick}	Land use	equal var-covar	-376.8	794.4	19	16.4
Precipitatoin	Geomorphology	equal var-covar	-376.9	794.4	19	16.5
SPI	Geomorphology	equal var-covar	-377.6	796.0	19	18.0
Q_{quick}	Basin	equal var-covar	-380.6	797.3	17	19.3
Temperature	Mountain	equal var-covar	-379.8	798.0	18	20.0
Null	Null	equal var-covar	-382.6	799.1	16	21.2
Temperature	Geomorphology	equal var-covar	-379.4	799.4	19	21.5
Q_{slow}	Land use	equal var-covar	-379.5	799.7	19	21.8
Temperature	Basin	equal var-covar	-382.1	800.3	17	22.4

Supplementary Figure 1. Monthly NO_3^- yield estimates plotted alongside the observed monthly hydrograph for each river of study. Green points represent NO_3^- yields from the Cascade Range rivers. Purple points represent NO_3^- yields from the Olympic Mountain rivers. NO_3^- yields were calculated using the linear composite method in the LOADFLEX package(Appling et al., 2015) and are expressed as a monthly rate in units of kg km^{-2} day^{-1}. Blue lines represent each individual river's mean monthly discharge.

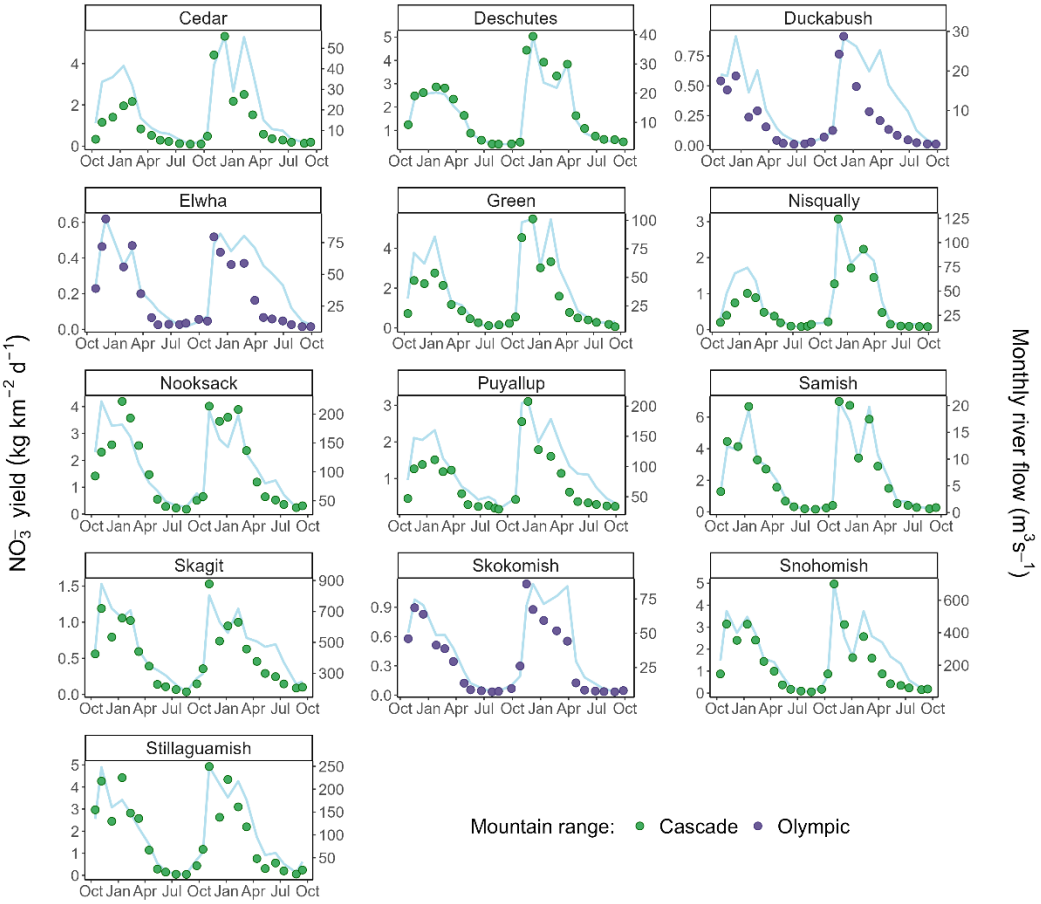

Supplementary Figure 2. Monthly NO_3^- concentration values plotted alongside the observed monthly hydrograph for each river of study. Green points represent NO_3^- concentration values from the Cascade Range rivers. Purple points represent NO_3^- concentration values from the Olympic Mountain rivers. Blue lines represent each individual river's mean monthly discharge.

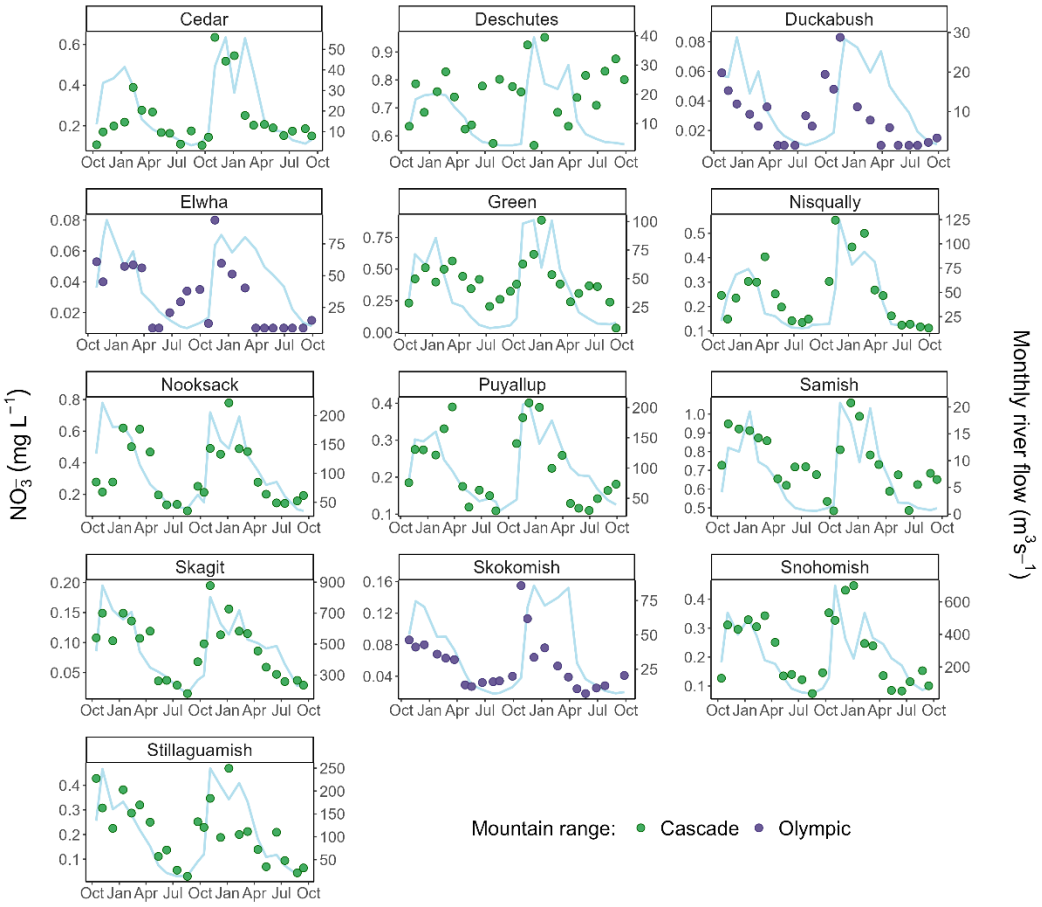

Supplementary Figure 3. Monthly $\delta^{15}N\text{-}NO_3^-$ values plotted alongside the observed monthly hydrograph for each river of study. Green points represent $\delta^{15}N\text{-}NO_3^-$ values from the Cascade Range rivers. Purple points represent $\delta^{15}N\text{-}NO_3^-$ values from the Olympic Mountain rivers. Blue lines represent each individual river's mean monthly discharge.

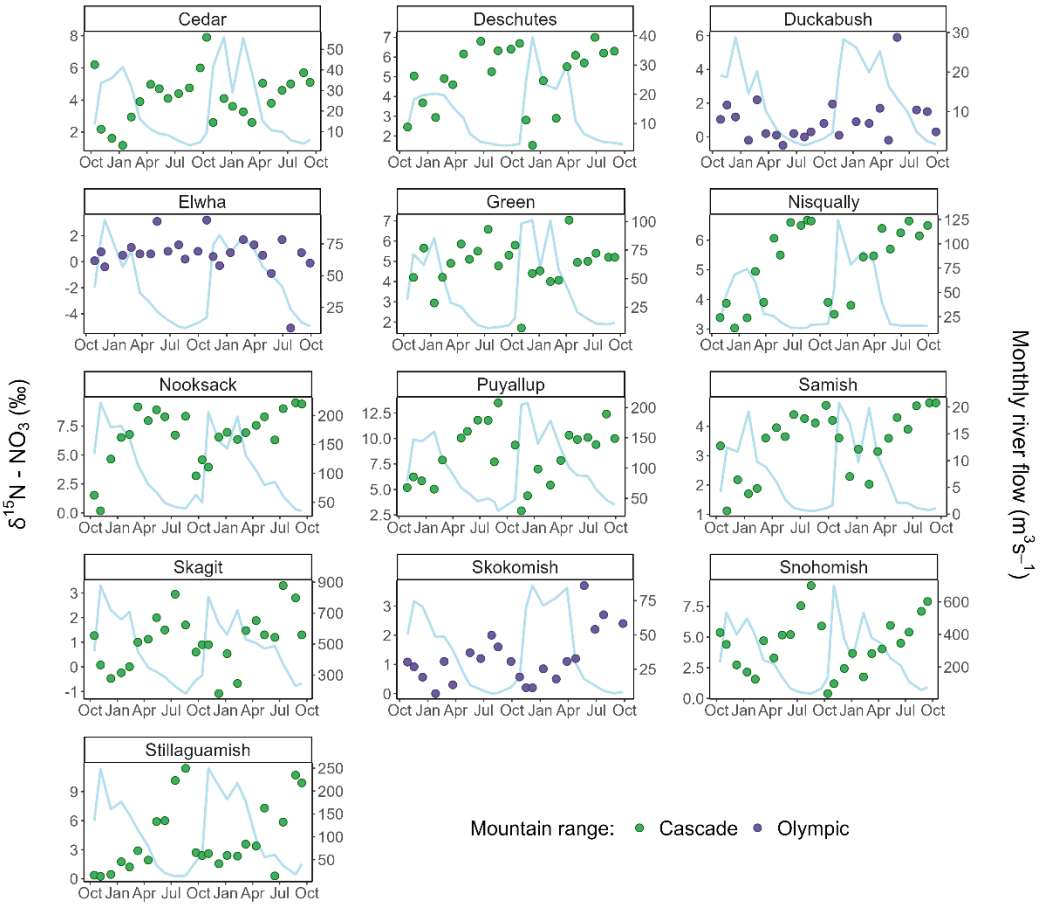

Supplementary Figure 4. Monthly $\delta^{18}O\text{-}NO_3^-$ values plotted alongside the observed monthly hydrograph for each river of study. Green points represent $\delta^{18}O\text{-}NO_3^-$ values from the Cascade Range rivers. Purple points represent $\delta^{18}O\text{-}NO_3^-$ values from the Olympic Mountain rivers. Blue lines represent each individual river's mean monthly discharge.

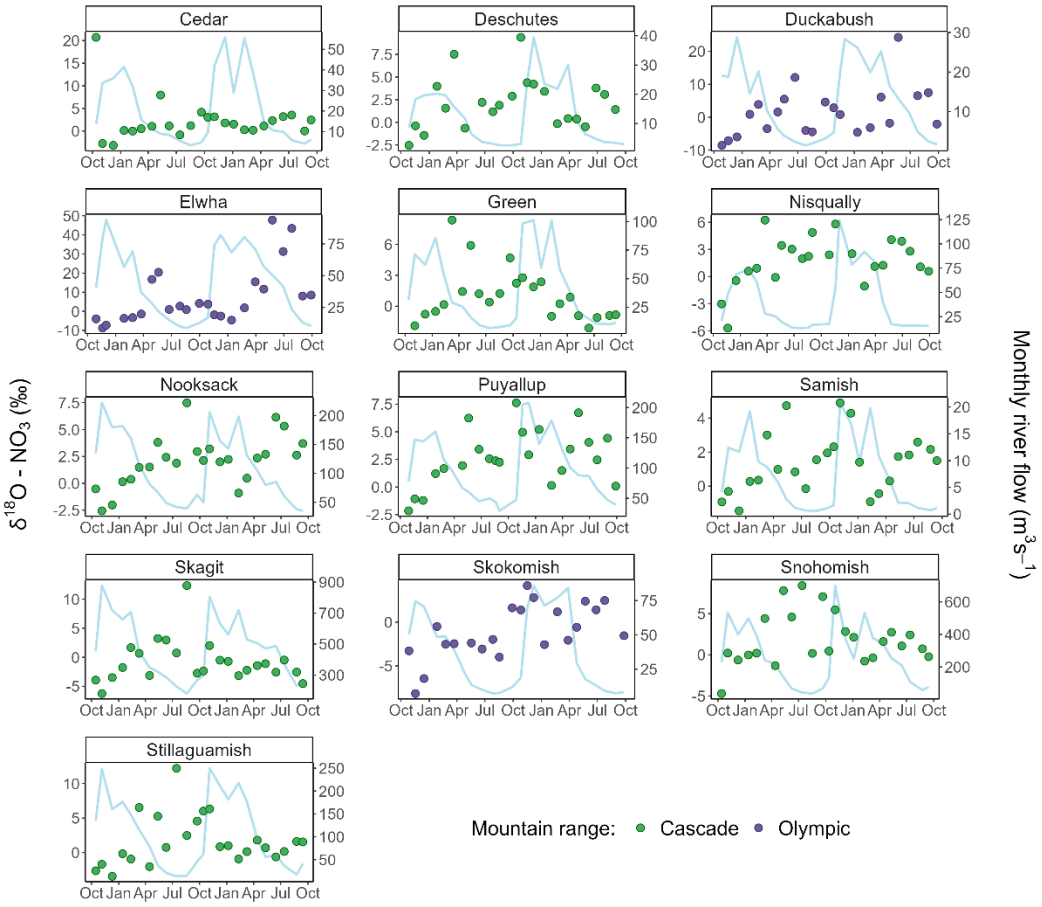

Supplementary Note 1. Calculation of seasonal and event-scale flow using a recursive digital filter.

In hydrology, it is common to separate river discharge hydrographs into two components: quick flow and baseflow(H. P. Duncan, 2019; Ladson et al., 2013; Nathan & McMahon, 1990; Xie et al., 2020). Baseflow is the slowest decaying, longest lasting component of the river hydrograph. It is usually associated with delayed water inputs or groundwater processes, and depicts the slow, seasonal pulse of river discharge(H. P. Duncan, 2019; Tallaksen, 1995). Quick flow instead represents the "flashy" component of the hydrograph and describes a combination of runoff and interflow though the vadose zone during storm events(Minaudo et al., 2019; Tallaksen, 1995). We included metrics of both discharge components as potential predictors in our MARSS analysis. By doing so, we hoped to reveal the role of flashy, event-scale flow vs. the sustained, seasonal pulse of river discharge in driving river NO_3^- variation.

To separate quick flow and baseflow, we obtained, and applied the Lyne and Hollick method (LH method) to each river hydrograph, a widely used recursive digital filter for baseflow separation(Lyne & Hollick, 1979). The LH method estimates quick flow using the following equation:

$$Q_{q(i)} = \alpha Q_{q(i-1)} + \frac{1+\alpha}{2}\left(Q_{(i)} - Q_{(i-1)}\right) \text{ for } Q_{q(i)} \geq 0$$

where Q_q is the quick flow at time *i*, *Q* is the original river flow at time *i*, and α (a recession constant) is the filter parameter that dictates the shape of the separation. Baseflow (Q_b) is subsequently calculated as:

$$Q_{b(i)} = Q_{(i)} - Q_{q(i)}$$

Following Nathan and McMahon (1990) and others(Ladson et al., 2013; Minaudo et al., 2019; Xie et al., 2020), we set the filter parameter to 0.925 and applied the digital recursive filter to each river hydrograph with three passes. This gave us a daily value for the quick flow and baseflow components of the hydrograph, represented in Supplementary Figure 5.

To include metrics of storm-event and seasonal-scale flow as predictors in our time series models, we converted the daily quick flow and baseflow values to monthly time steps. Previous work has shown that discharge lags precipitation events, roughly capturing an antecedent window of 24 to 72 hours(McGuire & McDonnell, 2006; Wilusz et al., 2017). To preserve the scale of individual storm events, we included quick flow as the raw daily value specific to the sample date (referred to in this paper as Q_{quick}). To capture the slower, seasonal scale of river discharge, we calculated baseflow as the previous week sum of daily river baseflow values (referred to in this paper as Q_{slow}). It is worth noting that we also considered including previous monthly or two-week sums as our Q_{slow} metric. However, we found that this artificially lagged the seasonal curve forward, past actual values of raw daily discharge.

Supplementary Figure 5. Daily discharge hydrographs in m^3/s for each river of study with the calculated flow components represented by color. Estimated daily quick flow values for each river are represented in red. Estimated daily baseflow values are represented in blue.

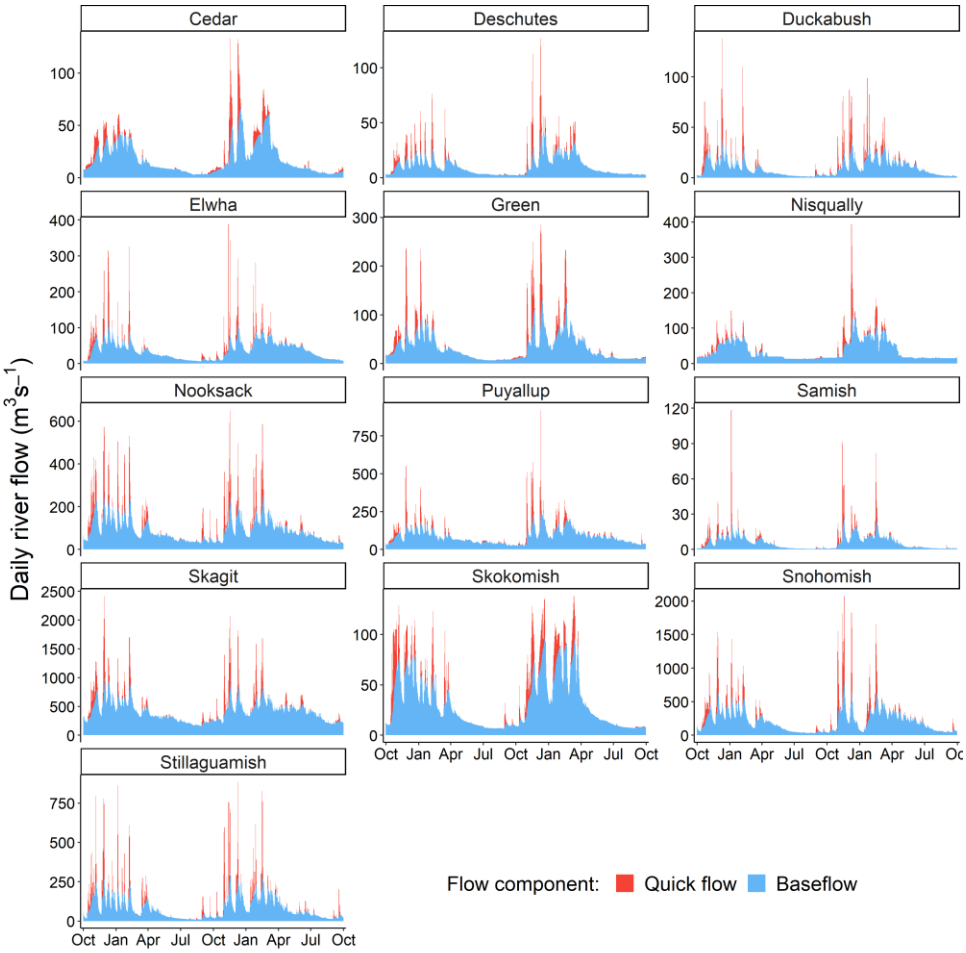

Chapter 2 Appendix

Supplementary Figure 1. Average monthly discharge (m^3 s^{-1}) plotted through time for each river of study.

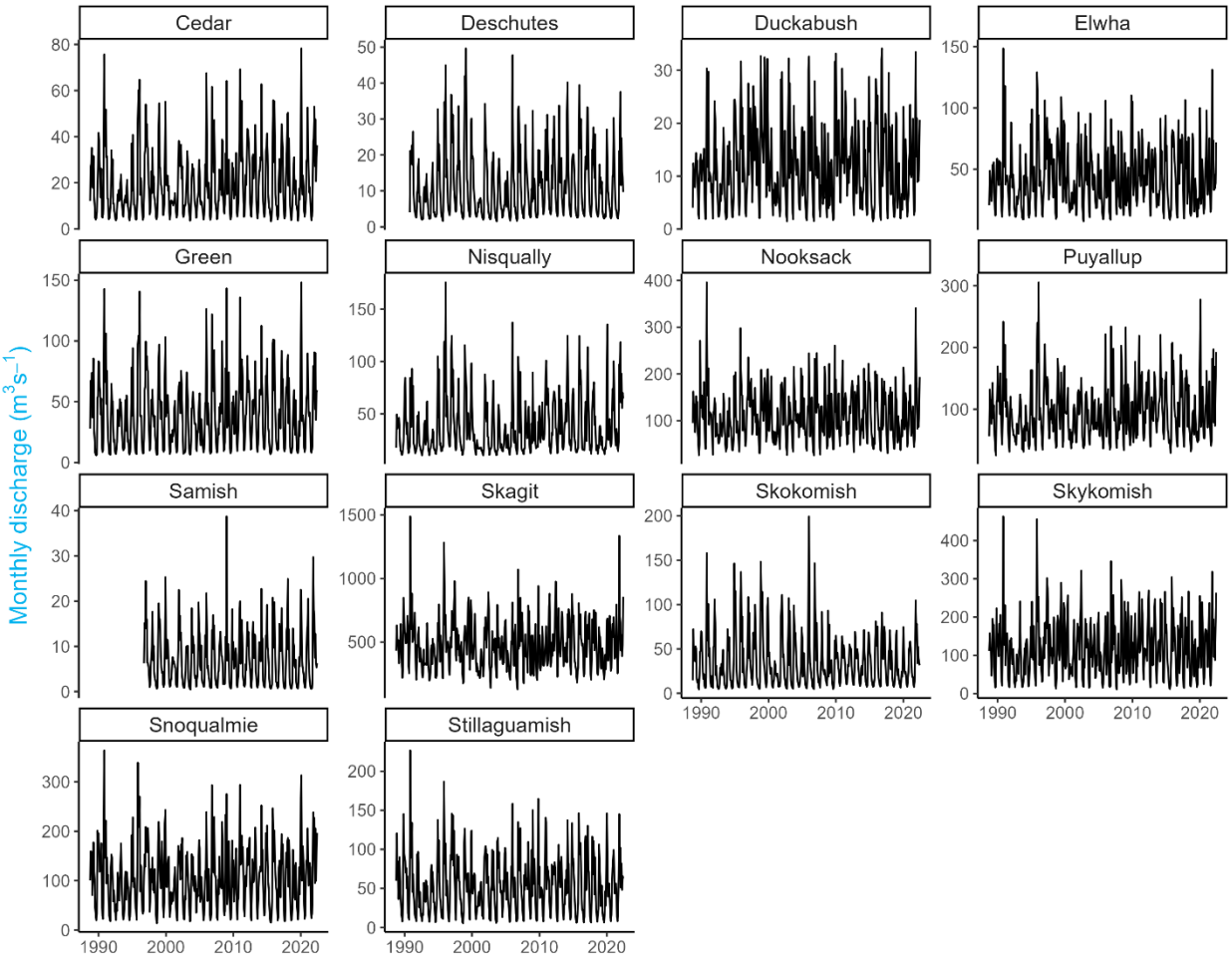

Supplementary Figure 2. Observed monthly DIN concentrations (mg L^{-1}) plotted through time for each river of study.

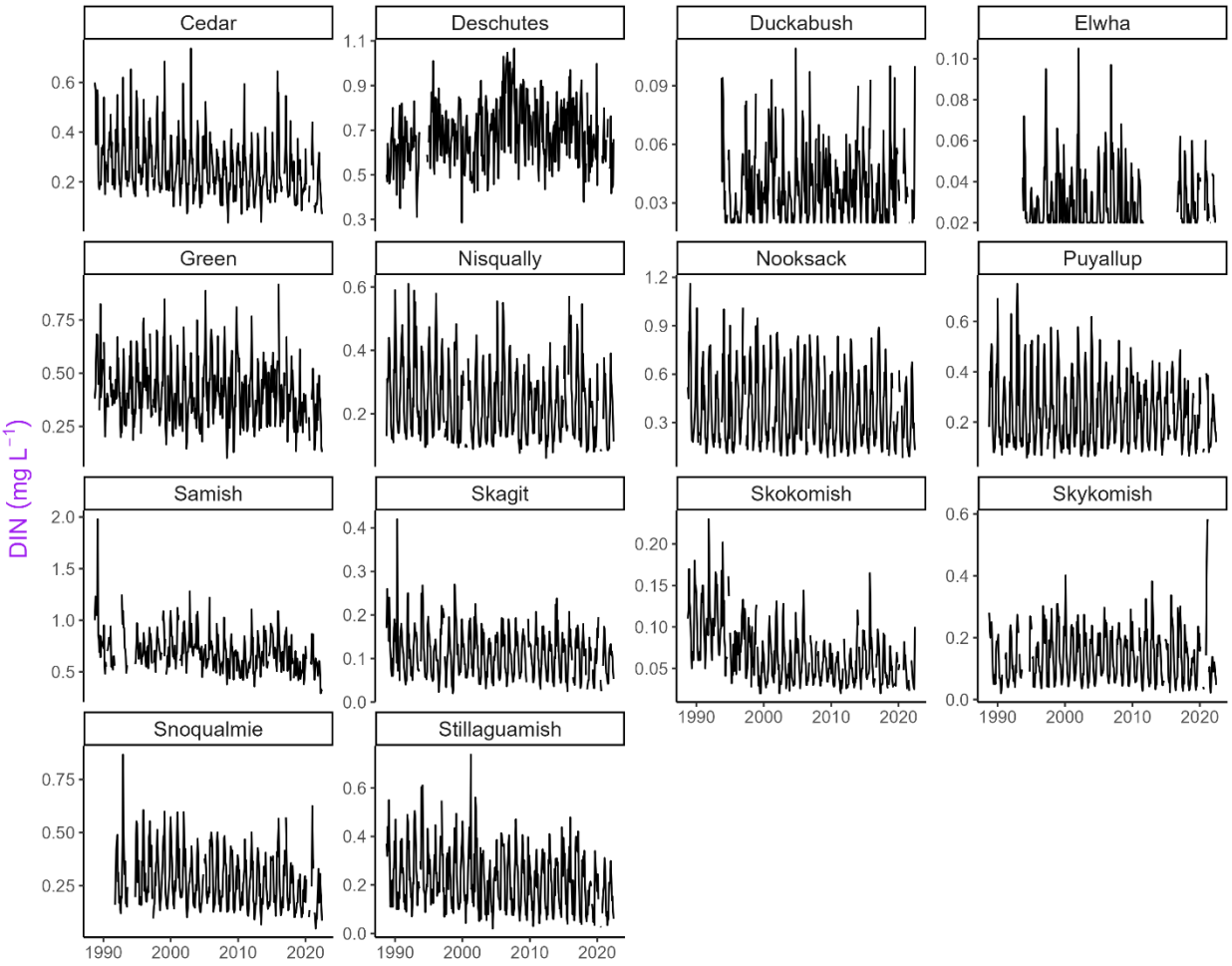

Supplementary Figure 3. Monthly DIN yield estimates plotted through time for each river of study. DIN yields were calculated using Weighted Regression on Time, Discharge, and Season model with the Kalman filter (WRTDS-K) in the EGRET R package (Hirsch et al., 2023) and are expressed as a monthly rate in units of kg km^{-2} day^{-1}.

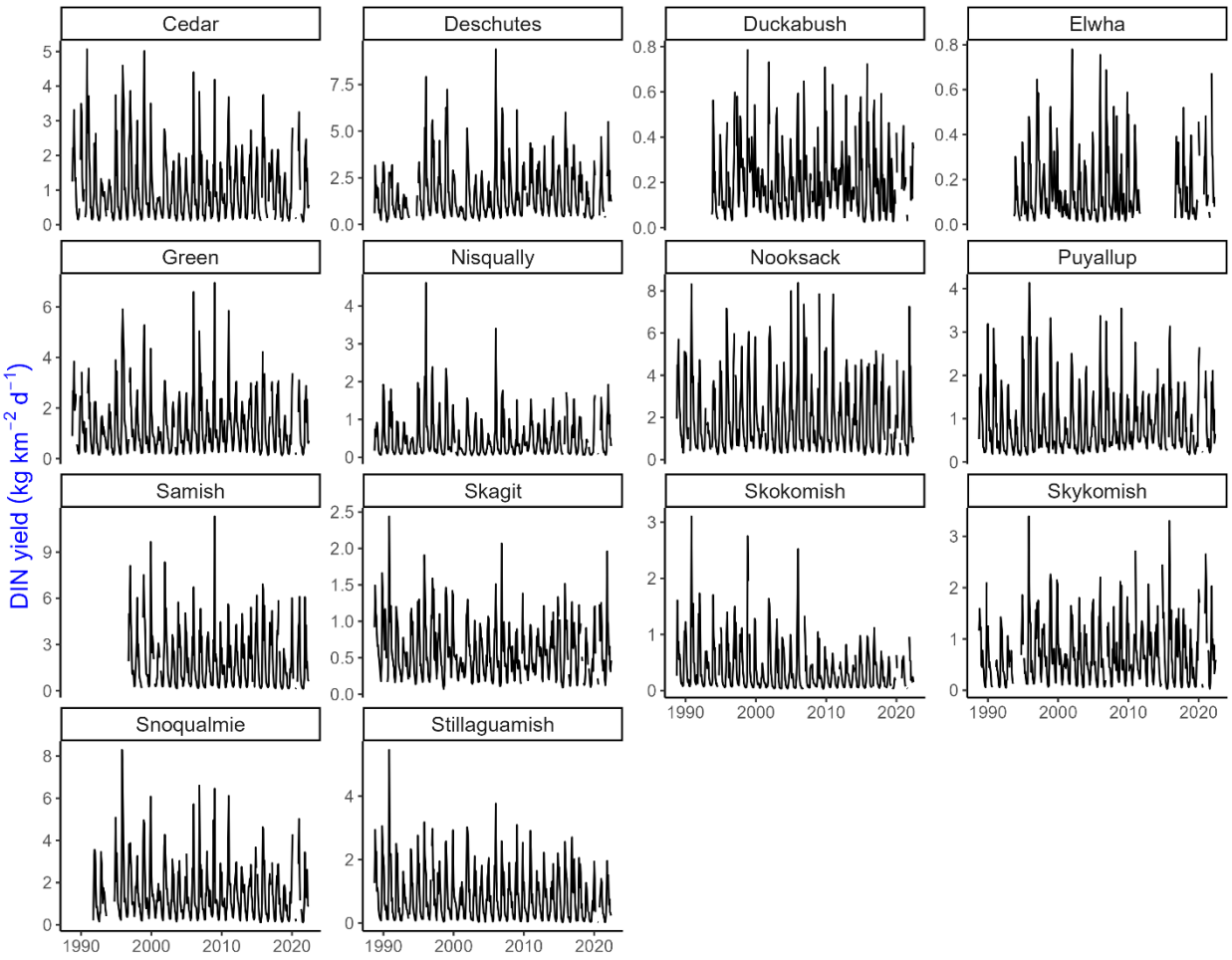

Supplementary Figure 4. Observed monthly DIP concentrations (mg L^{-1}) plotted through time for each river of study.

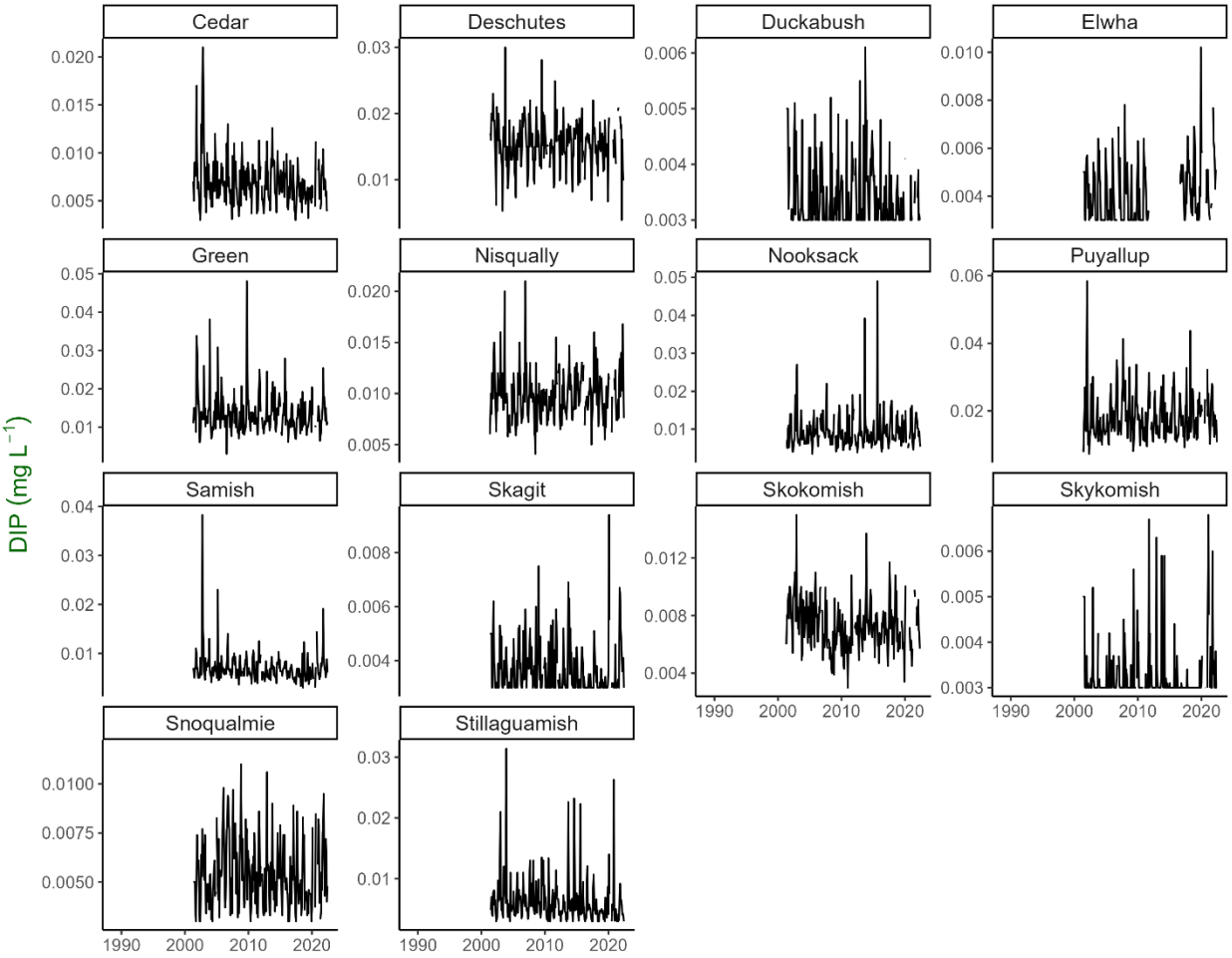

Supplementary Figure 5. Monthly DIP yield estimates plotted through time for each river of study. DIP yields were calculated using Weighted Regression on Time, Discharge, and Season model with the Kalman filter (WRTDS-K) in the EGRET R package (Hirsch et al., 2023) and are expressed as a monthly rate in units of kg km^{-2} day^{-1}.

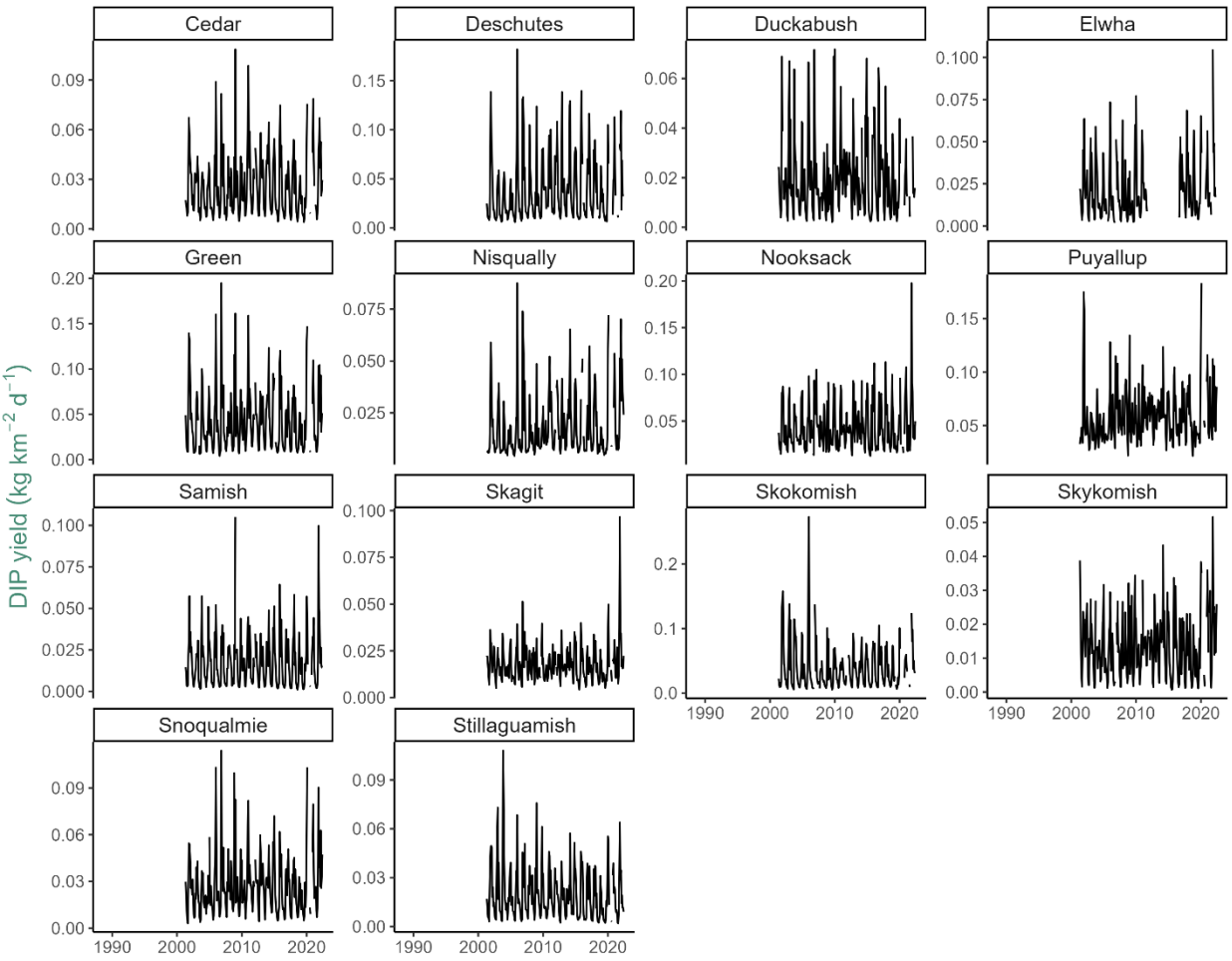

Supplementary Figure 6. DIN:DIP molar ratio plotted through time for each river of study. The red dashed line represents the Redfield ratio of 16:1 (N:P), which is mostly applicable to marine waters (Redfield, 1958). The blue dashed line represents a proposed ratio of 25:1 for freshwaters (Maranger et al., 2018).

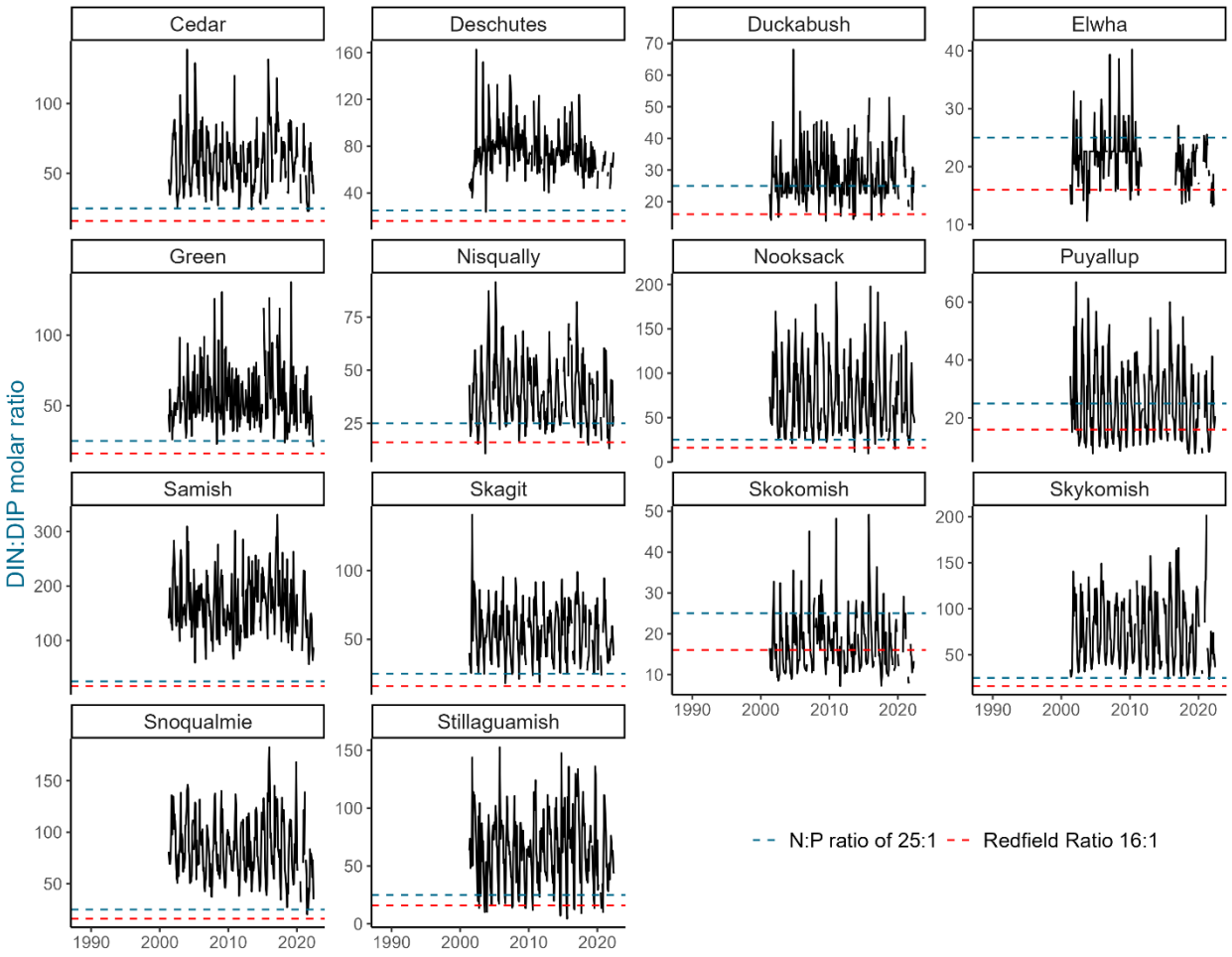

Supplemental Table 1. Linear correlations between original variables and the principal component scores (vector loadings). Correlations above 0.5 are highlighted in bold.

River and watershed variables	PC1 (61.1% variation)	PC2 (23.9% variation)
Watershed slope	**0.96**	0.07
Watershed area	0.35	**-0.81**
Watershed elevation	**0.93**	-0.27
% Ice	0.42	**-0.86**
% Agriculture	**-0.84**	-0.40
% Forested	**0.76**	0.47
% Wetland	**-0.92**	-0.23
% Urban	**-0.84**	0.09

Supplementary Table 2. AICc (Akaike Information Criterion) values for all six response variable models structures considered comparing shared or independent states (**Z** matrices) and process error correlations (**Q** matrices).

River discharge					
Shared or independent state	**Q matrix**	**Log likelihood**	**AICc**	**# of parameters**	**ΔAICc**
Independent	equal variance covariance	-1697.7	3932.3	256	0
Independent	diagonal and equal	-1712.28	3959.2	255	27.0
Shared		-1859.06	4224.3	242	292.0
Dissolved inorganic nitrogen					
Shared or independent state	**Q matrix**	**Log likelihood**	**AICc**	**# of parameters**	**ΔAICc**
Independent	equal variance covariance	-4419.9	9378.6	256	0.0
Independent	diagonal and equal	-4429.9	9396.3	255	17.7
Shared		-4704.8	9917.3	242	538.7
DIN yield					
Shared or independent state	**Q matrix**	**Log likelihood**	**AICc**	**# of parameters**	**ΔAICc**
Independent	equal variance covariance	-1030.5	2599.7	256	0
Independent	diagonal and equal	-1035.7	2607.8	255	8.1
Shared		-1398.2	3304.2	242	704.5
Dissolved inorganic phosphorus					
Shared or independent state	**Q matrix**	**Log likelihood**	**AICc**	**# of parameters**	**ΔAICc**
Independent	equal variance covariance	-3841.7	8238.0	256	0
Independent	diagonal and equal	-3849.4	8251.0	255	13.0
Shared		-3866.2	8254.4	242	16.4
DIP yield					
Shared or independent state	**Q matrix**	**Log likelihood**	**AICc**	**# of parameters**	**ΔAICc**
Independent	diagonal and equal	-1508.4	3569.0	255	0
Independent	equal variance covariance	-1507.7	3570.0	256	1.0
Shared		-1631.5	3784.8	242	215.8
DIN:DIP ratio					
Shared or independent state	**Q matrix**	**Log likelihood**	**AICc**	**# of parameters**	**ΔAICc**
Independent	equal variance covariance	-3245.82	7046.837	256	0
Independent	diagonal and equal	-3260.63	7074.112	255	27.3
Shared		-3277.34	7077.107	242	30.3

Supplementary Table 3. AICc (Akaike Information Criterion) values for the models considering the effects of climate covariates on **river discharge**. All models include a fixed effect of month to deal with the high autocorrelative nature of our monthly time series. The null model does not include climate covariates but does include the fixed effect of month.

Model covariates	Log likelihood	AICc	# of parameters	ΔAICc
Precipitation, 4-Season PDO	-1697.7	3932.3	256	0
Precipitation, 3-Season PDO	-1722.4	3951.0	242	18.8
Precipitation, 4-Season MEI	-1745.0	4026.9	256	94.6
Precipitation, PDO	-1798.2	4041.7	214	109.5
Precipitation, 3-Season MEI	-1778.6	4063.3	242	131.1
Precipitation	-1826.4	4067.8	200	135.5
Precipitation, MEI	-1818.6	4082.4	214	150.2
Temperature, 4-Season PDO	-2151.3	4839.5	256	907.3
Temperature, 3-Season PDO	-2166.8	4839.7	242	907.4
Temperature, PDO	-2221.1	4887.4	214	955.1
Temperature	-2246.7	4908.4	200	976.1
Temperature, 4-Season MEI	-2185.9	4908.7	256	976.5
Temperature, MEI	-2240.8	4926.9	214	994.6
Temperature, 3-Season MEI	-2211.4	4928.9	242	996.7
PDO	-2317.5	5050.0	200	1117.7
Null	-2354.8	5094.6	186	1162.3
MEI	-2348.0	5110.9	200	1178.7

Supplementary Table 4. AICc (Akaike Information Criterion) values for the models considering the effects of covariates on **dissolved inorganic nitrogen (DIN)**. All models include a fixed effect of month to deal with the high autocorrelative nature of our monthly time series. The null model does not include climate covariates but does include the fixed effect of month.

Model covariates	Log likelihood	AICc	# of parameters	ΔAICc
Precipitation, 3-Season PDO	-4427.3	9362.3	242	0
Precipitation, 4-Season PDO	-4419.9	9378.6	256	16.3
Precipitation, 4-Season SEAS	-4482.2	9380.5	200	18.2
Precipitation, 3-Season MEI	-4438.4	9384.7	242	22.4
Precipitation, MEI	-4473.5	9393.5	214	31.2
Precipitation, PDO	-4474.4	9395.3	214	33.0
Precipitation, 4-Season MEI	-4428.4	9395.5	256	33.2
Discharge, 3-Season PDO	-4457.1	9422.0	242	59.7
Discharge	-4503.8	9423.8	200	61.5
Discharge, 3-Season MEI	-4461.6	9430.9	242	68.6
Discharge, MEI	-4495.8	9438.1	214	75.7
Discharge, 4-Season PDO	-4451.0	9440.6	256	78.3
Discharge, 4-Season MEI	-4452.2	9443.0	256	80.7
Discharge, PDO	-4498.3	9443.1	214	80.8
Temperature, 3-Season PDO	-4505.9	9519.5	242	157.2
Temperature, 3-Season MEI	-4510.9	9529.5	242	167.2
Temperature	-4556.8	9529.7	200	167.4
Temperature, 4-Season PDO	-4496.9	9532.4	256	170.1
Temperature, 4-Season MEI	-4500.5	9539.7	256	177.4
Temperature, MEI	-4547.6	9541.8	214	179.5
Temperature, PDO	-4549.4	9545.3	214	183.0
Null	-4579.9	9545.8	186	183.5
MEI	-4570.8	9557.7	200	195.4
PDO	-4572.3	9560.7	200	198.4

Supplementary Table 5. AICc (Akaike Information Criterion) values for the models considering the effects of covariates on **DIN yield**. All models include a fixed effect of month to deal with the high autocorrelative nature of our monthly time series. The null model does not include climate covariates but does include a fixed effect of month.

Model covariates	Log likelihood	AICc	# of parameters	ΔAICc
Precipitation, 3-Season PDO	-1045.6	2599.0	242	0
Precipitation, 4-Season PDO	-1030.5	2599.7	256	0.7
Precipitation	-1122.9	2661.8	200	62.8
Precipitation, PDO	-1108.8	2664.1	214	65.1
Precipitation, MEI	-1117.0	2680.6	214	81.6
Precipitation, 4-Season MEI	-1074.8	2688.2	256	89.2
Precipitation, 3-Season MEI	-1092.2	2692.2	242	93.2
Temperature, 3-Season PDO	-1366.1	3239.8	242	640.8
Temperature, 4-Season PDO	-1354.6	3247.9	256	648.9
Temperature, PDO	-1424.9	3296.2	214	697.2
Temperature	-1440.8	3297.8	200	698.7
Temperature, MEI	-1435.7	3317.9	214	718.9
Temperature, 3-Season MEI	-1406.0	3319.8	242	720.8
Temperature, 4-Season MEI	-1391.7	3322.1	256	723.1
PDO	-1471.9	3359.8	200	760.8
Null	-1493.7	3373.3	186	774.3
MEI	-1488.6	3393.4	200	794.4

Supplementary Table 6. AICc (Akaike Information Criterion) values for the models considering the effects of covariates on **dissolved inorganic phosphorus (DIP)**. All models include a fixed effect of month to deal with the high autocorrelative nature of our monthly time series. The null model does not include climate covariates but does include a fixed effect of month.

Model covariates	Log likelihood	AICc	# of parameters	ΔAICc
Precipitation, PDO	-3875.7	8208.8	214	0
Precipitation	-3892.8	8211.1	200	2.4
Discharge, PDO	-3878.2	8213.8	214	5.1
Discharge	-3894.3	8214.2	200	5.4
Precipitation, 3-Season PDO	-3849.7	8221.3	242	12.6
Discharge, 3-Season PDO	-3853.5	8229.0	242	20.3
Precipitation, MEI	-3888.5	8234.5	214	25.7
Precipitation, 4-Season PDO	-3841.7	8238.0	256	29.3
Discharge, MEI	-3890.3	8238.0	214	29.3
Discharge, 4-Season PDO	-3845.6	8245.9	256	37.1
Null	-3933.8	8261.7	186	53.0
PDO	-3918.3	8262.3	200	53.5
Precipitation, 3-Season MEI	-3873.9	8269.8	242	61.0
Temperature	-3922.3	8270.2	200	61.5
Discharge, 3-Season MEI	-3874.9	8271.8	242	63.1
Temperature, PDO	-3910.6	8278.6	214	69.8
Precipitation, 4-Season MEI	-3863.1	8280.9	256	72.2
Discharge, 4-Season MEI	-3863.7	8282.0	256	73.2
MEI	-3929.2	8284.0	200	75.3
Temperature, 3-Season PDO	-3883.9	8289.8	242	81.0
Temperature, MEI	-3918.6	8294.6	214	85.9
Temperature, 4-Season PDO	-3875.9	8306.5	256	97.7
Temperature, 3-Season MEI	-3903.5	8329.0	242	120.3
Temperature, 4-Season MEI	-3894.3	8343.2	256	134.4

Supplementary Table 7. AICc (Akaike Information Criterion) values for the models considering the effects of covariates on **DIP yield**. All models include a fixed effect of month to deal with the high autocorrelative nature of our monthly time series. The null model does not include climate covariates but does include a fixed effect of month.

Model covariates	Log likelihood	AICc	# of parameters	ΔAICc
Precipitation, 3-Season PDO	-1522.2	3566.3	242	0
Precipitation, 4-Season PDO	-1507.7	3570.0	256	3.7
Precipitation, 4-Season MEI	-1540.6	3635.7	256	69.3
Precipitation, PDO	-1592.2	3641.8	214	75.4
Precipitation, 3-Season MEI	-1561.0	3643.9	242	77.6
Precipitation	-1616.7	3659.0	200	92.7
Precipitation, MEI	-1605.3	3668.0	214	101.7
Temperature, 3-Season PDO	-1732.4	3986.6	242	420.3
Temperature, 4-Season PDO	-1720.7	3996.0	256	429.6
Temperature, PDO	-1795.8	4048.9	214	482.6
Temperature, 4-Season MEI	-1751.3	4057.1	256	490.8
Temperature, 3-Season MEI	-1768.2	4058.2	242	491.8
Temperature	-1817.7	4060.9	200	494.5
Temperature, MEI	-1808.6	4074.6	214	508.3
PDO	-1828.9	4083.3	200	516.9
Null	-1862.1	4118.3	186	551.9
MEI	-1850.6	4126.7	200	560.4

Supplementary Table 8. AICc (Akaike Information Criterion) values for the models considering the effects of covariates on **DIN:DIP ratios**. All models include a fixed effect of month to deal with the high autocorrelative nature of our monthly time series. The null model does not include climate covariates but does include a fixed effect of month.

Model covariates	Log likelihood	AICc	# of parameters	ΔAICc
Precipitation	-3303.5	7032.9	200	0
Precipitation, 3-Season PDO	-3256.0	7034.5	242	1.6
Discharge	-3310.0	7045.8	200	12.9
Precipitation, 4-Season PDO	-3245.8	7046.8	256	13.9
Precipitation, PDO	-3295.7	7049.2	214	16.3
Precipitation, MEI	-3296.5	7050.9	214	18.0
Discharge, 3-Season PDO	-3267.1	7056.6	242	23.7
Precipitation, 3-Season MEI	-3268.7	7059.9	242	27.0
Precipitation, 4-Season MEI	-3253.7	7062.6	256	29.8
Discharge, MEI	-3303.9	7065.7	214	32.8
Discharge, PDO	-3304.8	7067.4	214	34.5
Discharge, 4-Season PDO	-3256.7	7068.5	256	35.6
Discharge, 3-Season MEI	-3277.5	7077.5	242	44.6
Discharge, 4-Season MEI	-3262.6	7080.4	256	47.5
Null	-3375.2	7144.6	186	111.8
Temperature	-3360.0	7146.0	200	113.1
Temperature, 3-Season PDO	-3312.0	7146.5	242	113.6
MEI	-3366.3	7158.6	200	125.7
Temperature, 3-Season MEI	-3318.5	7159.5	242	126.6
Temperature, 4-Season PDO	-3302.6	7160.5	256	127.6
PDO	-3368.1	7162.1	200	129.2
Temperature, MEI	-3352.7	7163.2	214	130.3
Temperature, 4-Season MEI	-3305.1	7165.4	256	132.5
Temperature, PDO	-3355.9	7169.6	214	136.7

Chapter 3 Appendix

Table S1. Linear correlations between original variables and the principal component scores (vector loadings). Correlations above 0.5 are highlighted in bold.

Environmental variable	PC1 (68.3% variation)	PC2 (15.2% variation)
Watershed area	0.15	**-0.95**
Watershed elevation	**0.87**	-0.39
Watershed slope	**0.98**	-0.09
Water table depth	**0.77**	0.31
Soil depth	**-0.82**	-0.39
% Urban	**-0.80**	0.18
% Agriculture	**-0.87**	-0.14
% Wetland	**-0.93**	0.01
% Coniferous forest	**0.94**	0.05

Table S2. Pairwise comparisons assessing the differences between downstream and upstream river sampling stations for each season. Significant comparisons are shown in bold.

Response variable	River position contrast	Season	Sign	*p*
NO_3^-	Down - Up	Summer	+	n.s.
NO_3^-	Down - Up	Winter	+	**$p < 0.05$**
$\Delta^{17}O\text{-}NO_3^-$	Down - Up	Summer	–	**$p < 0.05$**
$\Delta^{17}O\text{-}NO_3^-$	Down - Up	Winter	–	n.s.
$\delta^{15}N\text{-}NO_3^-$	Down - Up	Summer	+	**$p < 0.001$**
$\delta^{15}N\text{-}NO_3^-$	Down - Up	Winter	+	**$p < 0.01$**
$\delta^{18}O\text{-}NO_3^-$	Down - Up	Summer	+	**$p < 0.10$**
$\delta^{18}O\text{-}NO_3^-$	Down - Up	Winter	+	**$p < 0.10$**

Figure S1. Average river $\delta^{18}O\text{-}NO_3^-$ as a function of principal component axis 1 for the dry (2015) and wet (2016) hydrologic years. Slopes for the linear relationships are presented in the bottom left corner of each plot panel.

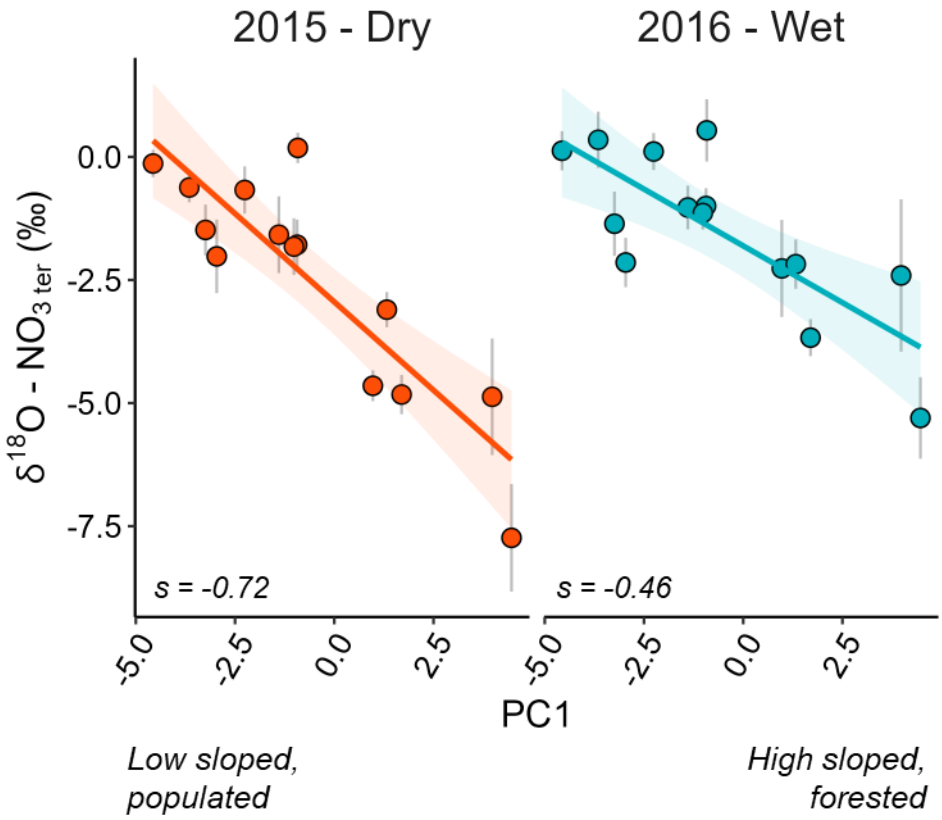

Figure S2. Average river $\delta^{18}O\text{-}NO_3^-$ in downstream and upstream stations for the dry (2015) and wet (2016) hydrologic years. Downstream stations are colored grey. Upstream stations are colored orange and blue for the dry and wet years, respectively.

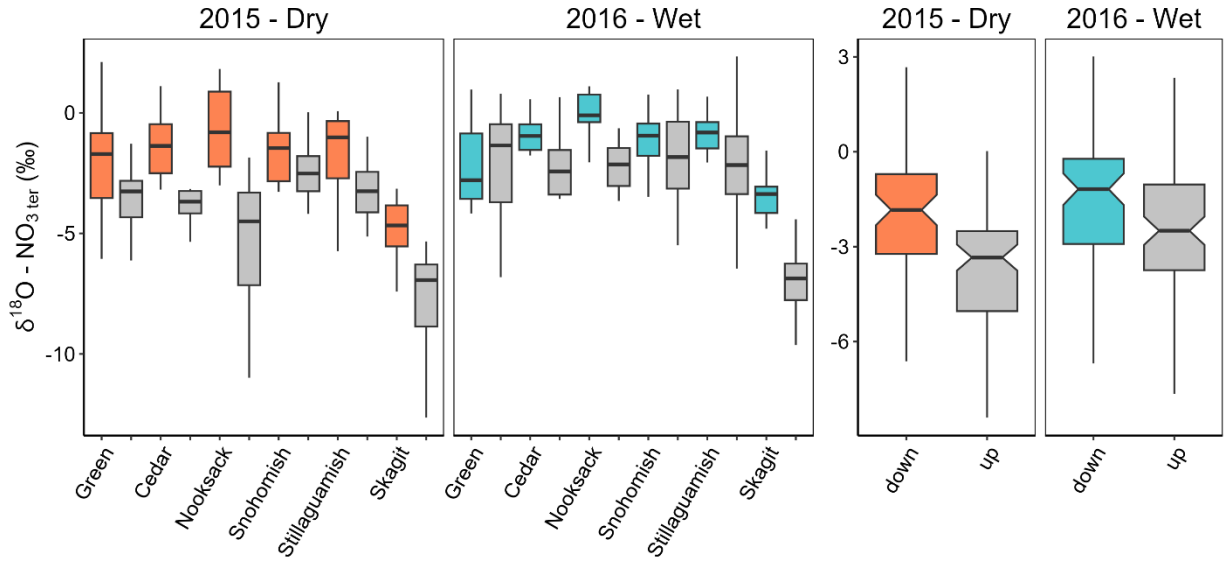

Figure S3. a) Average river NO_3^- concentration in winter and summer seasons for the dry and wet year of study. **b)** Average river $\Delta^{17}O\text{-}NO_3^-$ in winter and summer seasons for the dry and wet year of study. **c)** Average river $\delta^{15}N\text{-}NO_3^-$ in winter and summer seasons for the dry and wet year of study. **d)** Average river $\delta^{18}O\text{-}NO_3^-$ in winter and summer seasons for the dry and wet year of study. Winter seasons are colored light blue and dark blue for 2015 and 2016, respectively. Summer seasons are colored light orange and dark orange for 2015 and 2016, respectively.

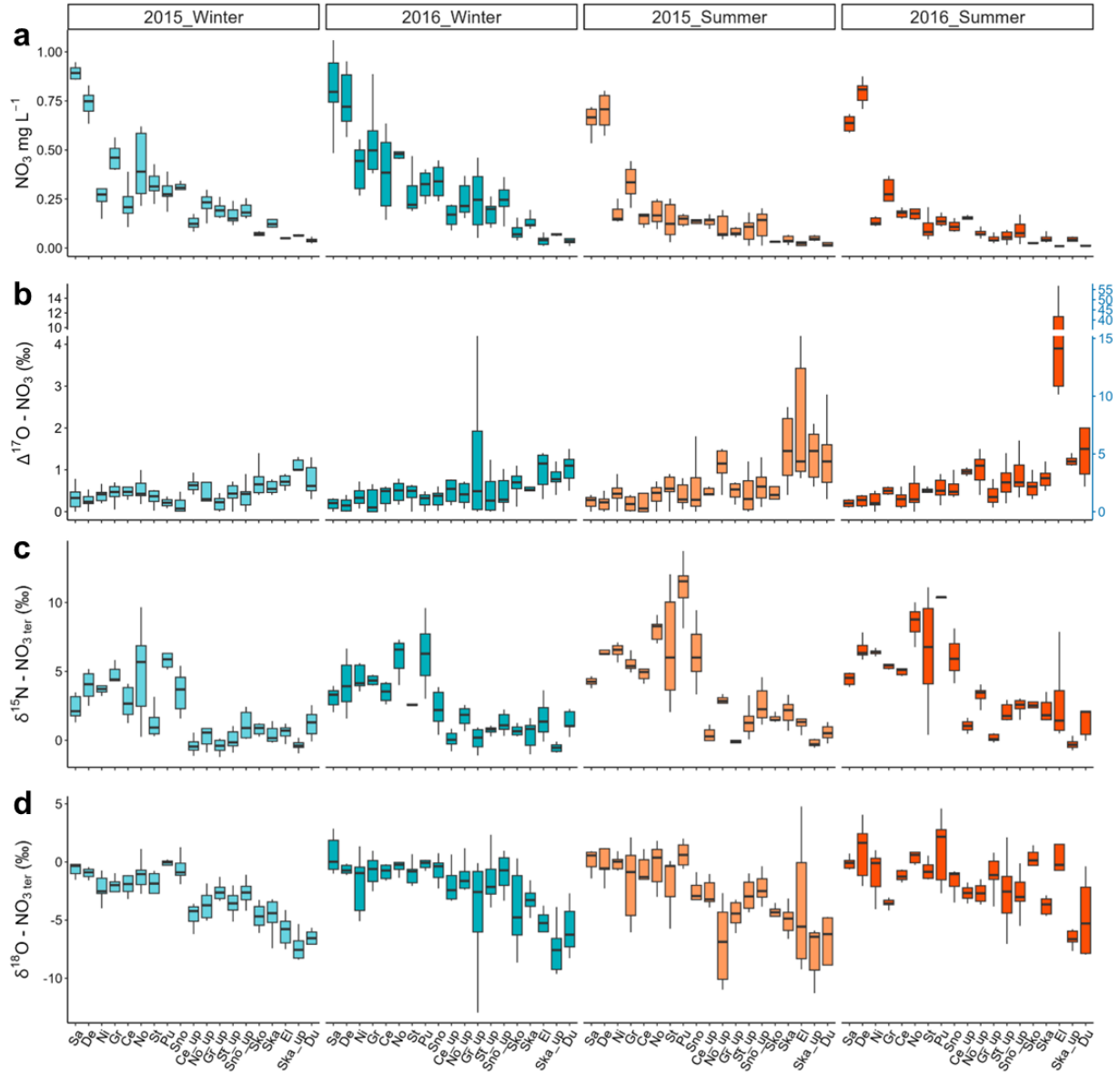

Figure S4. Average river $\Delta^{17}O\text{-}NO_3^-$ in winter and summer seasons for the dry and wet year of study for each region within the broader Puget Sound Basin. Winter seasons are colored light blue and dark blue for 2015 and 2016, respectively. Summer seasons are colored light orange and dark orange for 2015 and 2016, respectively.

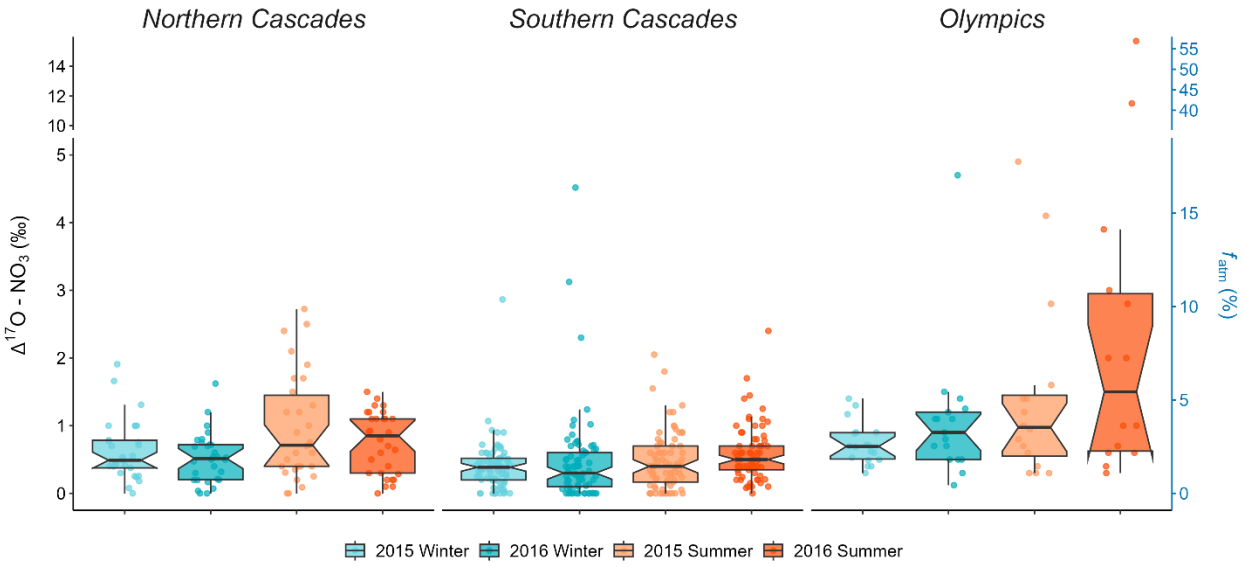

REFERENCES

2015 WSDA agricultural land use. (2022). [Dataset].

Albers, S. (2023). *rsoi: Import Various Northern and Southern Hemisphere Climate Indices* (Version R package version 0.5.5) [Computer software]. https://boshek.github.io/rsoi/

Alexander, R. B., Böhlke, J. K., Boyer, E. W., David, M. B., Harvey, J. W., Mulholland, P. J., Seitzinger, S. P., Tobias, C. R., Tonitto, C., & Wollheim, W. M. (2009). Dynamic modeling of nitrogen losses in river networks unravels the coupled effects of hydrological and biogeochemical processes. *Biogeochemistry*, *93*(1), 91–116. https://doi.org/10.1007/s10533-008-9274-8

Appling, A. P., Leon, M. C., & McDowell, W. H. (2015). Reducing bias and quantifying uncertainty in watershed flux estimates: The R package loadflex. *Ecosphere*, *6*(12), 1–25. https://doi.org/10.1890/ES14-00517.1

Aravena, R., & Robertson, W. D. (1998). Use of Multiple Isotope Tracers to Evaluate Denitrification in Ground Water: Study of Nitrate from a Large-Flux Septic System Plume. *Groundwater*, *36*(6), 975–982. https://doi.org/10.1111/j.1745-6584.1998.tb02104.x

Arnell, N. W., & Gosling, S. N. (2013). The impacts of climate change on river flow regimes at the global scale. *Journal of Hydrology*, *486*, 351–364. https://doi.org/10.1016/j.jhydrol.2013.02.010

Aufdenkampe, A. K., Mayorga, E., Raymond, P. A., Melack, J. M., Doney, S. C., Alin, S. R., Aalto, R. E., & Yoo, K. (2011). Riverine coupling of biogeochemical cycles between land, oceans, and atmosphere. *Frontiers in Ecology and the Environment*, *9*(1), 53–60. https://doi.org/10.1890/100014

Aulenbach, B. T. (2013). Improving regression-model-based streamwater constituent load estimates derived from serially correlated data. *Journal of Hydrology*, *503*, 55–66. https://doi.org/10.1016/j.jhydrol.2013.09.001

Aulenbach, B. T., & Hooper, R. P. (2006). The composite method: An improved method for stream-water solute load estimation. *Hydrological Processes*, *20*(14), 3029–3047. https://doi.org/10.1002/hyp.6147

Barnes, R. T., & Raymond, P. A. (2010). Land-use controls on sources and processing of nitrate in small watersheds: Insights from dual isotopic analysis. *Ecological Applications*, *20*(7), 1961–1978. https://doi.org/10.1890/08-1328.1

Baron, J. S., & Campbell, D. H. (1997). Nitrogen fluxes in a high elevation colorado rocky mountain basin. *Hydrological Processes*, *11*(7), 783–799. https://doi.org/10.1002/(SICI)1099-1085(199706)11:7<783::AID-HYP519>3.0.CO;2-U

Basu, N. B., Destouni, G., Jawitz, J. W., Thompson, S. E., Loukinova, N. V., Darracq, A., Zanardo, S., Yaeger, M., Sivapalan, M., Rinaldo, A., & Rao, P. S. C. (2010). Nutrient loads exported from managed catchments reveal emergent biogeochemical stationarity. *Geophysical Research Letters*, *37*(23). https://doi.org/10.1029/2010GL045168

Battye, W., Aneja, V. P., & Schlesinger, W. H. (2017). Is nitrogen the next carbon? *Earth's Future*, *5*(9), 894–904. https://doi.org/10.1002/2017EF000592

Bechtold, J. S., Edwards, R. T., & Naiman, R. J. (2003). *Biotic versus hydrologic control over seasonal nitrate leaching in a floodplain forest*. *63*, 53–72.

Beechie, T., Buhle, E., Ruckelshaus, M., Fullerton, A., & Holsinger, L. (2006). Hydrologic regime and the conservation of salmon life history diversity. *Biological Conservation*, *130*(4), 560–572. https://doi.org/10.1016/j.biocon.2006.01.019

Bennett, E. M., Carpenter, S. R., & Caraco, N. F. (2001). Human Impact on Erodable Phosphorus and Eutrophication: A Global Perspective: Increasing accumulation of phosphorus in soil threatens rivers, lakes, and coastal oceans with eutrophication. *BioScience*, *51*(3), 227–234. https://doi.org/10.1641/0006-3568(2001)051[0227:HIOEPA]2.0.CO;2

Binkley, D., Sollins, P., Bell, R., Sachs, D., & Myrold, D. (1992). Biogeochemistry of Adjacent Conifer and Alder-Conifer Stands. *Ecology*, *73*(6), 2022–2033. https://doi.org/10.2307/1941452

Blaszczak, J. R., Koenig, L. E., Mejia, F. H., Gómez-Gener, L., Dutton, C. L., Carter, A. M., Grimm, N. B., Harvey, J. W., Helton, A. M., & Cohen, M. J. (2022). Extent, patterns, and drivers of hypoxia in the world's streams and rivers. *Limnology and Oceanography Letters*, *n/a*(n/a). https://doi.org/10.1002/lol2.10297

Boot, C. M., Hall, E. K., Denef, K., & Baron, J. S. (2016). Long-term reactive nitrogen loading alters soil carbon and microbial community properties in a subalpine forest ecosystem. *Soil Biology and Biochemistry*, *92*, 211–220. https://doi.org/10.1016/j.soilbio.2015.10.002

Bormann, F. H., & Likens, G. E. (1967). Nutrient cycling: Small watersheds can provide invaluable information about terrestrial ecosystems. *Science (New York, N.Y.)*, *155*(3761), 424–429. https://doi.org/10.1126/science.155.3761.424

Bormann, F. H., Likens, G. E., Fisher, D. W., & Pierce, R. S. (1968). Nutrient Loss Accelerated by Clear-Cutting of a Forest Ecosystem. *Science*, *159*(3817), 882–884.

Bostic, J. T., Nelson, D. M., Sabo, R. D., & Eshleman, K. N. (2022). Terrestrial Nitrogen Inputs Affect the Export of Unprocessed Atmospheric Nitrate to Surface Waters: Insights from

Triple Oxygen Isotopes of Nitrate. *Ecosystems*, *25*(6), 1384–1399. https://doi.org/10.1007/s10021-021-00722-9

Böttcher, J., Strebel, O., Voerkelius, S., & Schmidt, H.-L. (1990). Using isotope fractionation of nitrate-nitrogen and nitrate-oxygen for evaluation of microbial denitrification in a sandy aquifer. *Journal of Hydrology*, *114*(3), 413–424. https://doi.org/10.1016/0022-1694(90)90068-9

Bourgeois, I., Savarino, J., Caillon, N., Angot, H., Barbero, A., Delbart, F., Voisin, D., & Clément, J.-C. (2018). Tracing the Fate of Atmospheric Nitrate in a Subalpine Watershed Using Δ17O. *Environmental Science & Technology*, *52*(10), 5561–5570. https://doi.org/10.1021/acs.est.7b02395

Bourgeois, I., Savarino, J., Némery, J., Caillon, N., Albertin, S., Delbart, F., Voisin, D., & Clément, J.-C. (2018a). Atmospheric nitrate export in streams along a montane to urban gradient. *Science of The Total Environment*, *633*, 329–340. https://doi.org/10.1016/j.scitotenv.2018.03.141

Bourgeois, I., Savarino, J., Némery, J., Caillon, N., Albertin, S., Delbart, F., Voisin, D., & Clément, J.-C. (2018b). Atmospheric nitrate export in streams along a montane to urban gradient. *The Science of the Total Environment*, *633*, 329–340. https://doi.org/10.1016/j.scitotenv.2018.03.141

Boyer, E. W., Howarth, R. W., Galloway, J. N., Dentener, F. J., Green, P. A., & Vörösmarty, C. J. (2006). Riverine nitrogen export from the continents to the coasts. *Global Biogeochemical Cycles*, *20*(1). https://doi.org/10.1029/2005GB002537

Briand, C., Sebilo, M., Louvat, P., Chesnot, T., Vaury, V., Schneider, M., & Plagnes, V. (2017). Legacy of contaminant N sources to the NO3− signature in rivers: A combined isotopic

(δ15N-NO3−, δ18O-NO3−, δ11B) and microbiological investigation. *Scientific Reports*, *7*(1), 41703. https://doi.org/10.1038/srep41703

Burnham, K. P., & Anderson, D. R. (Eds.). (2004). *Model Selection and Multimodel Inference*. Springer. https://doi.org/10.1007/b97636

Burns, D. A. (2004). The effects of atmospheric nitrogen deposition in the Rocky Mountains of Colorado and southern Wyoming, USA—a critical review. *Environmental Pollution*, *127*(2), 257–269. https://doi.org/10.1016/S0269-7491(03)00264-1

Burns, D. A., Boyer, E. W., Elliott, E. M., & Kendall, C. (2009). Sources and Transformations of Nitrate from Streams Draining Varying Land Uses: Evidence from Dual Isotope Analysis. *Journal of Environmental Quality*, *38*(3), 1149–1159. https://doi.org/10.2134/jeq2008.0371

Chen, F., Jia, G., & Chen, J. (2009). Nitrate sources and watershed denitrification inferred from nitrate dual isotopes in the Beijiang River, south China. *Biogeochemistry*, *94*(2), 163–174. https://doi.org/10.1007/s10533-009-9316-x

Chen, Z., & Grasby, S. E. (2009). Impact of decadal and century-scale oscillations on hydroclimate trend analyses. *Journal of Hydrology*, *365*(1), 122–133. https://doi.org/10.1016/j.jhydrol.2008.11.031

Clark, S. C., Barnes, R. T., Oleksy, I. A., Baron, J. S., & Hastings, M. G. (2021). Persistent Nitrate in Alpine Waters with Changing Atmospheric Deposition and Warming Trends. *Environmental Science & Technology*, *55*(21), 14946–14956. https://doi.org/10.1021/acs.est.1c02515

Cline, T. J., Schindler, D. E., Walsworth, T. E., French, D. W., & Lisi, P. J. (2020). Low snowpack reduces thermal response diversity among streams across a landscape. *Limnology and Oceanography Letters*, *5*(3), 254–263. https://doi.org/10.1002/lol2.10148

Compton, J. E., Church, M. R., Larned, S. T., & Hogsett, W. E. (2003). Nitrogen Export from Forested Watersheds in the Oregon Coast Range: The Role of N2-fixing Red Alder. *Ecosystems*, *6*(8), 773–785. https://doi.org/10.1007/s10021-002-0207-4

Compton, J. E., Goodwin, K. E., Sobota, D. J., & Lin, J. (2020). Seasonal Disconnect Between Streamflow and Retention Shapes Riverine Nitrogen Export in the Willamette River Basin, Oregon. *Ecosystems*, *23*(1), 1–17. https://doi.org/10.1007/s10021-019-00383-9

Connolly, C. T., Khosh, M. S., Burkart, G. A., Douglas, T. A., Holmes, R. M., Jacobson, A. D., Tank, S. E., & McClelland, J. W. (2018a). Watershed slope as a predictor of fluvial dissolved organic matter and nitrate concentrations across geographical space and catchment size in the Arctic. *Environmental Research Letters*, *13*(10), 104015. https://doi.org/10.1088/1748-9326/aae35d

Connolly, C. T., Khosh, M. S., Burkart, G. A., Douglas, T. A., Holmes, R. M., Jacobson, A. D., Tank, S. E., & McClelland, J. W. (2018b). Watershed slope as a predictor of fluvial dissolved organic matter and nitrate concentrations across geographical space and catchment size in the Arctic. *Environmental Research Letters*, *13*(10), 104015. https://doi.org/10.1088/1748-9326/aae35d

De Cicco, L. A., Hirsch, R. M., Lorenze, D., Watkins, W. D., & Johnson, M. (2024). *dataRetrieval: R packages for discovering and retrieving water data available from Federal hydrologic web services* (Version v.2.7.15) [Computer software]. doi:10.5066/P9X4L3GE

Divers, M. T., Elliott, E. M., & Bain, D. J. (2014). Quantification of Nitrate Sources to an Urban Stream Using Dual Nitrate Isotopes. *Environmental Science & Technology*, *48*(18), 10580–10587. https://doi.org/10.1021/es404880j

Duncan, H. P. (2019). Baseflow separation – A practical approach. *Journal of Hydrology*, *575*, 308–313. https://doi.org/10.1016/j.jhydrol.2019.05.040

Duncan, J. M., Band, L. E., & Groffman, P. M. (2017). Variable nitrate concentration–discharge relationships in a forested watershed. *Hydrological Processes*, *31*(9), 1817–1824. https://doi.org/10.1002/hyp.11136

Elmstrom, E. J., Holtgrieve, G. W., Scheuerell, M. D., Schauer, A. J., & Leazer, K. (2024). Climate and landform interact to control the source and transport of nitrate in Pacific Northwest rivers. *Communications Earth & Environment*, *5*(1), 1–13. https://doi.org/10.1038/s43247-024-01235-8

Elser, J. J., Andersen, T., Baron, J. S., Bergström, A.-K., Jansson, M., Kyle, M., Nydick, K. R., Steger, L., & Hessen, D. O. (2009). Shifts in Lake N:P Stoichiometry and Nutrient Limitation Driven by Atmospheric Nitrogen Deposition. *Science*, *326*(5954), 835–837. https://doi.org/10.1126/science.1176199

Fleming, S. W., Hood, E., Dahlke, H. E., & O'Neel, S. (2016). Seasonal flows of international British Columbia-Alaska rivers: The nonlinear influence of ocean-atmosphere circulation patterns. *Advances in Water Resources*, *87*, 42–55. https://doi.org/10.1016/j.advwatres.2015.10.007

Fleming, S. W., Whitfield, P. H., Moore, R. D., & Quilty, E. J. (2007). Regime-dependent streamflow sensitivities to Pacific climate modes cross the Georgia–Puget transboundary ecoregion. *Hydrological Processes*, *21*(24), 3264–3287. https://doi.org/10.1002/hyp.6544

Fowler, D., Coyle, M., Skiba, U., Sutton, M. A., Cape, J. N., Reis, S., Sheppard, L. J., Jenkins, A., Grizzetti, B., Galloway, J. N., Vitousek, P., Leach, A., Bouwman, A. F., Butterbach-Bahl, K., Dentener, F., Stevenson, D., Amann, M., & Voss, M. (2013). The global nitrogen cycle in the twenty-first century. *Philosophical Transactions of the Royal Society B: Biological Sciences*, *368*(1621), 20130164. https://doi.org/10.1098/rstb.2013.0164

Frissell, C. A., Liss, W. J., Warren, C. E., & Hurley, M. D. (1986). A hierarchical framework for stream habitat classification: Viewing streams in a watershed context. *Environmental Management*, *10*(2), 199–214. https://doi.org/10.1007/BF01867358

Galloway, J. N., Dentener, F. J., Capone, D. G., Boyer, E. W., Howarth, R. W., Seitzinger, S. P., Asner, G. P., Cleveland, C. C., Green, P. A., Holland, E. A., Karl, D. M., Michaels, A. F., Porter, J. H., Townsend, A. R., & Vöosmarty, C. J. (2004). Nitrogen Cycles: Past, Present, and Future. *Biogeochemistry*, *70*(2), 153–226. https://doi.org/10.1007/s10533-004-0370-0

Gomez-Velez, J. D., Harvey, J. W., Cardenas, M. B., & Kiel, B. (2015). Denitrification in the Mississippi River network controlled by flow through river bedforms. *Nature Geoscience*, *8*(12), Article 12. https://doi.org/10.1038/ngeo2567

Goodale, C. L., Thomas, S. A., Fredriksen, G., Elliott, E. M., Flinn, K. M., Butler, T. J., & Walter, M. T. (2009). Unusual seasonal patterns and inferred processes of nitrogen retention in forested headwaters of the Upper Susquehanna River. *Biogeochemistry*, *93*(3), 197–218. https://doi.org/10.1007/s10533-009-9298-8

Goyette, J.-O., Bennett, E. M., & Maranger, R. (2019a). Differential influence of landscape features and climate on nitrogen and phosphorus transport throughout the watershed. *Biogeochemistry*, *142*(1), 155–174. https://doi.org/10.1007/s10533-018-0526-y

Goyette, J.-O., Bennett, E. M., & Maranger, R. (2019b). Differential influence of landscape features and climate on nitrogen and phosphorus transport throughout the watershed. *Biogeochemistry*, *142*(1), 155–174. https://doi.org/10.1007/s10533-018-0526-y

Granger, J., & Wankel, S. D. (2016). Isotopic overprinting of nitrification on denitrification as a ubiquitous and unifying feature of environmental nitrogen cycling. *Proceedings of the National Academy of Sciences*, *113*(42), E6391–E6400. https://doi.org/10.1073/pnas.1601383113

Greaver, T. L., Clark, C. M., Compton, J. E., Vallano, D., Talhelm, A. F., Weaver, C. P., Band, L. E., Baron, J. S., Davidson, E. A., Tague, C. L., Felker-Quinn, E., Lynch, J. A., Herrick, J. D., Liu, L., Goodale, C. L., Novak, K. J., & Haeuber, R. A. (2016). Key ecological responses to nitrogen are altered by climate change. *Nature Climate Change*, *6*(9), Article 9. https://doi.org/10.1038/nclimate3088

Hale, S. S., Cicchetti, G., & Deacutis, C. F. (2016). Eutrophication and Hypoxia Diminish Ecosystem Functions of Benthic Communities in a New England Estuary. *Frontiers in Marine Science*, *3*. https://www.frontiersin.org/articles/10.3389/fmars.2016.00249

Hall, J. E., Greene, C. M., Stefankiv, O., Anderson, J. H., Timpane-Padgham, B., Beechie, T. J., & Pess, G. R. (2018). Large river habitat complexity and productivity of Puget Sound Chinook salmon. *PLOS ONE*, *13*(11), e0205127. https://doi.org/10.1371/journal.pone.0205127

Hamlet, A. F., Elsner, M. M., Mauger, G. S., Lee, S.-Y., Tohver, I., & Norheim, R. A. (2013). An Overview of the Columbia Basin Climate Change Scenarios Project: Approach, Methods, and Summary of Key Results. *Atmosphere-Ocean*, *51*(4), 392–415. https://doi.org/10.1080/07055900.2013.819555

Hanson, G. C., Groffman, P. M., & Gold, A. J. (1994). Denitrification in Riparian Wetlands Receiving High and Low Groundwater Nitrate Inputs. *Journal of Environmental Quality*, *23*(5), 917–922. https://doi.org/10.2134/jeq1994.00472425002300050011x

Hao, Y., & Lu, J. (2021). Teleconnection between climate oscillations and riverine nutrient dynamics in Southeast China based on wavelet analysis. *Environmental Science and Pollution Research*, *28*(31), 41807–41820. https://doi.org/10.1007/s11356-021-13715-x

Harms, T. K., Edmonds, J. W., Genet, H., Creed, I. F., Aldred, D., Balser, A., & Jones, J. B. (2016). Catchment influence on nitrate and dissolved organic matter in Alaskan streams across a latitudinal gradient. *Journal of Geophysical Research: Biogeosciences*, *121*(2), 350–369. https://doi.org/10.1002/2015JG003201

Hart, S. C., Binkley, D., & Perry, D. A. (1997). Influence of red alder on soil nitrogen transformations in two conifer forests of contrasting productivity. *Soil Biology and Biochemistry*, *29*(7), 1111–1123. https://doi.org/10.1016/S0038-0717(97)00004-7

Hattermann, F. F., Krysanova, V., Gosling, S. N., Dankers, R., Daggupati, P., Donnelly, C., Flörke, M., Huang, S., Motovilov, Y., Buda, S., Yang, T., Müller, C., Leng, G., Tang, Q., Portmann, F. T., Hagemann, S., Gerten, D., Wada, Y., Masaki, Y., … Samaniego, L. (2017). Cross-scale intercomparison of climate change impacts simulated by regional and global hydrological models in eleven large river basins. *Climatic Change*, *141*(3), 561–576. https://doi.org/10.1007/s10584-016-1829-4

Heffernan, J. B., Soranno, P. A., Angilletta, M. J., Buckley, L. B., Gruner, D. S., Keitt, T. H., Kellner, J. R., Kominoski, J. S., Rocha, A. V., Xiao, J., Harms, T. K., Goring, S. J., Koenig, L. E., McDowell, W. H., Powell, H., Richardson, A. D., Stow, C. A., Vargas, R., & Weathers, K. C. (2014). Macrosystems ecology: Understanding ecological patterns and processes at continental scales. *Frontiers in Ecology and the Environment*, *12*(1), 5–14. https://doi.org/10.1890/130017

Hill, R. A., Weber, M. H., Leibowitz, S. G., Olsen, A. R., & Thornbrugh, D. J. (2016). The Stream-Catchment (StreamCat) Dataset: A Database of Watershed Metrics for the Conterminous United States. *JAWRA Journal of the American Water Resources Association*, *52*(1), 120–128. https://doi.org/10.1111/1752-1688.12372

Hirsch, R. M., DeCicco, L. A., & Murphy, J. C. (2023). *EGRET* [Computer software]. U.S. Geological Survey. https://doi.org/10.5066/P9CC9JEX

Holmes, Ward, Eric J., & Scheuerell, Mark D. (2021). *Analysis of multivariate time series using the MARSS package. Version 3.11.4*. https://doi.org/10.5281/ZENODO.5781847

Holtgrieve, G. W., Schindler, D. E., Gowell, C. P., Ruff, C. P., & Lisi, P. J. (2010). Stream geomorphology regulates the effects on periphyton of ecosystem engineering and nutrient enrichment by Pacific salmon. *Freshwater Biology*, *55*(12), 2598–2611. https://doi.org/10.1111/j.1365-2427.2010.02489.x

Holtgrieve, G. W., Schindler, D. E., Hobbs, W. O., Leavitt, P. R., Ward, E. J., Bunting, L., Chen, G., Finney, B. P., Gregory-Eaves, I., Holmgren, S., Lisac, M. J., Lisi, P. J., Nydick, K., Rogers, L. A., Saros, J. E., Selbie, D. T., Shapley, M. D., Walsh, P. B., & Wolfe, A. P. (2011). A Coherent Signature of Anthropogenic Nitrogen Deposition to Remote

Watersheds of the Northern Hemisphere. *Science*, *334*(6062), 1545–1548. https://doi.org/10.1126/science.1212267

Howarth, R., Swaney, D., Billen, G., Garnier, J., Hong, B., Humborg, C., Johnes, P., Mörth, C.-M., & Marino, R. (2012). Nitrogen fluxes from the landscape are controlled by net anthropogenic nitrogen inputs and by climate. *Frontiers in Ecology and the Environment*, *10*(1), 37–43. https://doi.org/10.1890/100178

Howarth, R. W., & Marino, R. (2006). Nitrogen as the limiting nutrient for eutrophication in coastal marine ecosystems: Evolving views over three decades. *Limnology and Oceanography*, *51*(1part2), 364–376. https://doi.org/10.4319/lo.2006.51.1_part_2.0364

Hrycik, A. R., Isles, P. D. F., Pierson, D. C., & Stockwell, J. D. (2024). Winter/Spring Runoff Is Earlier, More Protracted, and Increasing in Volume in the Laurentian Great Lakes Basin. *Water Resources Research*, *60*(3), e2023WR035773. https://doi.org/10.1029/2023WR035773

Huang, Y., Huang, J., Ervinia, A., Duan, S., & Kaushal, S. S. (2021). Land use and climate variability amplifies watershed nitrogen exports in coastal China. *Ocean & Coastal Management*, *207*, 104428. https://doi.org/10.1016/j.ocecoaman.2018.02.024

Hundey, E. J., Russell, S. D., Longstaffe, F. J., & Moser, K. A. (2016a). Agriculture causes nitrate fertilization of remote alpine lakes. *Nature Communications*, *7*(1), Article 1. https://doi.org/10.1038/ncomms10571

Hundey, E. J., Russell, S. D., Longstaffe, F. J., & Moser, K. A. (2016b). Agriculture causes nitrate fertilization of remote alpine lakes. *Nature Communications*, *7*(1), Article 1. https://doi.org/10.1038/ncomms10571

Hynes, H. B. N. (1970). *The Ecology of Running Waters*. University of Toronto Press.

Isaak, D. J., Ver Hoef, J. M., Peterson, E. E., Horan, D. L., & Nagel, D. E. (2017). Scalable population estimates using spatial-stream-network (SSN) models, fish density surveys, and national geospatial database frameworks for streams. *Canadian Journal of Fisheries and Aquatic Sciences*, *74*(2), 147–156. https://doi.org/10.1139/cjfas-2016-0247

Jaeger, K. L., Anderson, S. W., & Dunn, S. B. (2023). Changes in suspended-sediment yields under divergent land-cover disturbance histories: A comparison of two large watersheds, Olympic Mountains, USA. *Earth Surface Processes and Landforms*, *48*(7), 1398–1413. https://doi.org/10.1002/esp.5556

Jankowski, K. J., Houser, J. N., Scheuerell, M. D., & Smits, A. P. (2021). Warmer Winters Increase the Biomass of Phytoplankton in a Large Floodplain River. *Journal of Geophysical Research: Biogeosciences*, *126*(9), e2020JG006135. https://doi.org/10.1029/2020JG006135

Jankowski, K. J., Johnson, K., Sethna, L., Julian, P., Wymore, A. S., Shogren, A. J., Thomas, P. K., Sullivan, P. L., McKnight, D. M., McDowell, W. H., Heindel, R., Jones, J. B., Wollheim, W., Abbott, B., Deegan, L., & Carey, J. C. (2023). Long-Term Changes in Concentration and Yield of Riverine Dissolved Silicon From the Poles to the Tropics. *Global Biogeochemical Cycles*, *37*(9), e2022GB007678. https://doi.org/10.1029/2022GB007678

Jankowski, K. J., & Schindler, D. E. (2019). Watershed geomorphology modifies the sensitivity of aquatic ecosystem metabolism to temperature. *Scientific Reports*, *9*(1), 17619. https://doi.org/10.1038/s41598-019-53703-3

Jankowski, K. J., Schindler, D. E., & Holtgrieve, G. W. (2012). Assessing nonpoint-source nitrogen loading and nitrogen fixation in lakes using δ15N and nutrient stoichiometry.

Limnology and Oceanography, *57*(3), 671–683. https://doi.org/10.4319/lo.2012.57.3.0671

Jankowski, K. J., Schindler, D. E., & Lisi, P. J. (2014). Temperature sensitivity of community respiration rates in streams is associated with watershed geomorphic features. *Ecology*, *95*(10), 2707–2714. https://doi.org/10.1890/14-0608.1

Jiang, H., Liu, W., Li, Y., Zhang, J., & Xu, Z. (2022). Multiple Isotopes Reveal a Hydrology Dominated Control on the Nitrogen Cycling in the Nujiang River Basin, the Last Undammed Large River Basin on the Tibetan Plateau. *Environmental Science & Technology*, *56*(7), 4610–4619. https://doi.org/10.1021/acs.est.1c07102

Johnson, K., Jankowski, K. J., Carey, J., Lyon, N. J., McDowell, W. H., Shogren, A., Wymore, A., Sethna, L., Wollheim, W. M., Poste, A. E., Kortelainen, P., Heindel, R., Laudon, H., Räike, A., Jones, J. B., McKnight, D., Julian, P., Bush, S., & Sullivan, P. L. (2024). Establishing fluvial silicon regimes and their stability across the Northern Hemisphere. *Limnology and Oceanography Letters*, *n/a*(n/a). https://doi.org/10.1002/lol2.10372

Johnston, S. E., Gunawardana, P. V. S. L., Rood, S. B., & Bogard, M. J. (2022). Multidecadal Trends in Organic Carbon Flux Through a Grassland River Network Shaped by Human Controls and Climatic Cycles. *Geophysical Research Letters*, *49*(4), e2021GL096885. https://doi.org/10.1029/2021GL096885

Kaiser, J., Hastings, M. G., Houlton, B. Z., Röckmann, T., & Sigman, D. M. (2007). Triple Oxygen Isotope Analysis of Nitrate Using the Denitrifier Method and Thermal Decomposition of N2O. *Analytical Chemistry*, *79*(2), 599–607. https://doi.org/10.1021/ac061022s

Kaushal, S. S., Mayer, P. M., Vidon, P. G., Smith, R. M., Pennino, M. J., Newcomer, T. A., Duan, S., Welty, C., & Belt, K. T. (2014). Land Use and Climate Variability Amplify Carbon, Nutrient, and Contaminant Pulses: A Review with Management Implications. *JAWRA Journal of the American Water Resources Association*, *50*(3), 585–614. https://doi.org/10.1111/jawr.12204

Keener, V. W., Feyereisen, G. W., Lall, U., Jones, J. W., Bosch, D. D., & Lowrance, R. (2010). El-Niño/Southern Oscillation (ENSO) influences on monthly NO3 load and concentration, stream flow and precipitation in the Little River Watershed, Tifton, Georgia (GA). *Journal of Hydrology*, *381*(3), 352–363. https://doi.org/10.1016/j.jhydrol.2009.12.008

Kelly, C. N., McGuire, K. J., Miniat, C. F., & Vose, J. M. (2016). Streamflow response to increasing precipitation extremes altered by forest management. *Geophysical Research Letters*, *43*(8), 3727–3736. https://doi.org/10.1002/2016GL068058

Kendall, C., Elliott, E. M., & Wankel, S. D. (2007). Tracing Anthropogenic Inputs of Nitrogen to Ecosystems. In R. Michener & K. Lajtha (Eds.), *Stable Isotopes in Ecology and Environmental Science* (pp. 375–449). Blackwell Publishing Ltd. https://doi.org/10.1002/9780470691854.ch12

Knapp, J. L. A., von Freyberg, J., Studer, B., Kiewiet, L., & Kirchner, J. W. (2020). Concentration–discharge relationships vary among hydrological events, reflecting differences in event characteristics. *Hydrology and Earth System Sciences*, *24*(5), 2561–2576. https://doi.org/10.5194/hess-24-2561-2020

Kumar, P., Le, P. V. V., Papanicolaou, A. N. T., Rhoads, B. L., Anders, A. M., Stumpf, A., Wilson, C. G., Bettis, E. A., Blair, N., Ward, A. S., Filley, T., Lin, H., Keefer, L., Keefer,

D. A., Lin, Y.-F., Muste, M., Royer, T. V., Foufoula-Georgiou, E., & Belmont, P. (2018). Critical transition in critical zone of intensively managed landscapes. *Anthropocene, 22*, 10–19. https://doi.org/10.1016/j.ancene.2018.04.002

Ladson, A. R., Brown, R., Neal, B., & Nathan, R. (2013). A Standard Approach to Baseflow Separation Using The Lyne and Hollick Filter. *Australasian Journal of Water Resources, 17*(1), 25–34. https://doi.org/10.7158/13241583.2013.11465417

Levin, S. A. (1992). The Problem of Pattern and Scale in Ecology: The Robert H. MacArthur Award Lecture. *Ecology*, *73*(6), 1943–1967. https://doi.org/10.2307/1941447

Lewis, D. B., & Grimm, N. B. (2007). Hierarchical Regulation of Nitrogen Export from Urban Catchments: Interactions of Storms and Landscapes. *Ecological Applications*, *17*(8), 2347–2364. https://doi.org/10.1890/06-0031.1

Li, L., Knapp, J. L. A., Lintern, A., Ng, G.-H. C., Perdrial, J., Sullivan, P. L., & Zhi, W. (2024). River water quality shaped by land–river connectivity in a changing climate. *Nature Climate Change, 14*(3), 225–237. https://doi.org/10.1038/s41558-023-01923-x

Li, S., Jiang, H., Guo, W., Zhang, W., & Zhang, Q. (2023). From Soil to River: Revealing the Mechanisms Underlying the High Riverine Nitrate Levels in a Forest Dominated Catchment. *Water Research, 241*, 120155. https://doi.org/10.1016/j.watres.2023.120155

Likens, G. E. (1984). Beyond the shoreline: A watershed-ecosystem approach. *SIL Proceedings, 1922-2010*, *22*(1), 1–22. https://doi.org/10.1080/03680770.1983.11897264

Lin, J., Böhlke, J. K., Huang, S., Gonzalez-Meler, M., & Sturchio, N. C. (2019). Seasonality of nitrate sources and isotopic composition in the Upper Illinois River. *Journal of Hydrology, 568*, 849–861. https://doi.org/10.1016/j.jhydrol.2018.11.043

Lin, J., Compton, J. E., Clark, C., Bittman, S., Schwede, D., Homann, P. S., Kiffney, P., Hooper, D., Bahr, G., & Baron, J. S. (2020). Key Components and Contrasts in the Nitrogen Budget Across a U.S.-Canadian Transboundary Watershed. *Journal of Geophysical Research: Biogeosciences*, *125*(9), e2019JG005577. https://doi.org/10.1029/2019JG005577

Lin, X., Yu, S., Yang, D., Hutchins, M. G., Ding, J., Hong, B., Chen, P., & Liu, X. (2020). Discriminating surface soil inorganic nitrogen cycling under various land uses in a watershed with simulations of energy balanced temperature and slope introduced moisture. *Journal of Hydrology*, *587*, 124950. https://doi.org/10.1016/j.jhydrol.2020.124950

Lisi, P. J., Schindler, D. E., Cline, T. J., Scheuerell, M. D., & Walsh, P. B. (2015). Watershed geomorphology and snowmelt control stream thermal sensitivity to air temperature. *Geophysical Research Letters*, *42*(9), 3380–3388. https://doi.org/10.1002/2015GL064083

Litzow, M. A., Malick, M. J., Bond, N. A., Cunningham, C. J., Gosselin, J. L., & Ward, E. J. (2020). Quantifying a Novel Climate Through Changes in PDO-Climate and PDO-Salmon Relationships. *Geophysical Research Letters*, *47*(16), e2020GL087972. https://doi.org/10.1029/2020GL087972

Liu, T., Wang, F., Michalski, G., Xia, X., & Liu, S. (2013). Using 15N, 17O, and 18O To Determine Nitrate Sources in the Yellow River, China. *Environmental Science & Technology*, *47*(23), 13412–13421. https://doi.org/10.1021/es403357m

Lohse, K. A., Sanderman, J., & Amundson, R. (2013). Identifying sources and processes influencing nitrogen export to a small stream using dual isotopes of nitrate. *Water Resources Research*, *49*(9), 5715–5731. https://doi.org/10.1002/wrcr.20439

Lottig, N. R., Tan, P.-N., Wagner, T., Cheruvelil, K. S., Soranno, P. A., Stanley, E. H., Scott, C. E., Stow, C. A., & Yuan, S. (2017). Macroscale patterns of synchrony identify complex relationships among spatial and temporal ecosystem drivers. *Ecosphere*, *8*(12), e02024. https://doi.org/10.1002/ecs2.2024

Lyne, V., & Hollick, M. (1979). Stochastic Time-Variable Rainfall-Runoff Modeling. In *Australian National Conference Publication* (Vol. 79).

Maranger, R., Jones, S. E., & Cotner, J. B. (2018). Stoichiometry of carbon, nitrogen, and phosphorus through the freshwater pipe. *Limnology and Oceanography Letters*, *3*(3), 89–101. https://doi.org/10.1002/lol2.10080

Marcé, R., von Schiller, D., Aguilera, R., Martí, E., & Bernal, S. (2018). Contribution of Hydrologic Opportunity and Biogeochemical Reactivity to the Variability of Nutrient Retention in River Networks. *Global Biogeochemical Cycles*, *32*(3), 376–388. https://doi.org/10.1002/2017GB005677

Marlier, M. E., Xiao, M., Engel, R., Livneh, B., Abatzoglou, J. T., & Lettenmaier, D. P. (2017). The 2015 drought in Washington State: A harbinger of things to come? *Environmental Research Letters*, *12*(11), 114008. https://doi.org/10.1088/1748-9326/aa8fde

Matiatos, I., Wassenaar, L. I., Monteiro, L. R., Venkiteswaran, J. J., Gooddy, D. C., Boeckx, P., Sacchi, E., Yue, F.-J., Michalski, G., Alonso-Hernández, C., Biasi, C., Bouchaou, L., Edirisinghe, N. V., Fadhullah, W., Fianko, J. R., García-Moya, A., Kazakis, N., Li, S.-L., Luu, M. T. N., … Welti, N. (2021). Global patterns of nitrate isotope composition in rivers and adjacent aquifers reveal reactive nitrogen cascading. *Communications Earth & Environment*, *2*(1), 1–10. https://doi.org/10.1038/s43247-021-00121-x

Mauger, G. S., Casola, H. A., Morgan, R. L., Strauch, B., Jones, B., & Curry, T. M. (2015). State of Knowledge: Climate Change in Puget Sound. In *Encyclopedia of Puget Sound*. https://doi.org/10.7915/CIG93777D

McCarthy, S. (2019). *Puget Sound Nutrient Synthesis Report, Part 2*.

McCluney, K. E., Poff, N. L., Palmer, M. A., Thorp, J. H., Poole, G. C., Williams, B. S., Williams, M. R., & Baron, J. S. (2014). Riverine macrosystems ecology: Sensitivity, resistance, and resilience of whole river basins with human alterations. *Frontiers in Ecology and the Environment*, *12*(1), 48–58. https://doi.org/10.1890/120367

McGill, L. M., Brooks, J. R., & Steel, E. A. (2021). Spatiotemporal dynamics of water sources in a mountain river basin inferred through $\Delta^{2}H$ and $\Delta^{18}O$ of water. *Hydrological Processes*, *35*(3). https://doi.org/10.1002/hyp.14063

McGuire, K. J., & McDonnell, J. J. (2006). A review and evaluation of catchment transit time modeling. *Journal of Hydrology*, *330*(3), 543–563. https://doi.org/10.1016/j.jhydrol.2006.04.020

Metson, G. S., Lin, J., Harrison, J. A., & Compton, J. E. (2020). Where Have All the Nutrients Gone? Long-Term Decoupling of Inputs and Outputs in the Willamette River Watershed, Oregon, United States. *Journal of Geophysical Research: Biogeosciences*, *125*(10), e2020JG005792. https://doi.org/10.1029/2020JG005792

Michalski, G., Meixner, T., Fenn, M., Hernandez, L., Sirulnik, A., Allen, E., & Thiemens, M. (2004). Tracing Atmospheric Nitrate Deposition in a Complex Semiarid Ecosystem Using Δ17O. *Environmental Science & Technology*, *38*(7), 2175–2181. https://doi.org/10.1021/es034980+

Minaudo, C., Dupas, R., Gascuel-Odoux, C., Roubeix, V., Danis, P.-A., & Moatar, F. (2019). Seasonal and event-based concentration-discharge relationships to identify catchment controls on nutrient export regimes. *Advances in Water Resources*, *131*, 103379. https://doi.org/10.1016/j.advwatres.2019.103379

Mulholland, P. J., Helton, A. M., Poole, G. C., Hall, R. O., Hamilton, S. K., Peterson, B. J., Tank, J. L., Ashkenas, L. R., Cooper, L. W., Dahm, C. N., Dodds, W. K., Findlay, S. E. G., Gregory, S. V., Grimm, N. B., Johnson, S. L., McDowell, W. H., Meyer, J. L., Valett, H. M., Webster, J. R., … Thomas, S. M. (2008). Stream denitrification across biomes and its response to anthropogenic nitrate loading. *Nature*, *452*(7184), Article 7184. https://doi.org/10.1038/nature06686

Murphy, J., & Sprague, L. (2019). Water-quality trends in US rivers: Exploring effects from streamflow trends and changes in watershed management. *Science of The Total Environment*, *656*, 645–658. https://doi.org/10.1016/j.scitotenv.2018.11.255

Nathan, R. J., & McMahon, T. A. (1990). Evaluation of automated techniques for base flow and recession analyses. *Water Resources Research*, *26*(7), 1465–1473. https://doi.org/10.1029/WR026i007p01465

Nijssen, B., O'Donnell, G. M., Hamlet, A. F., & Lettenmaier, D. P. (2001). Hydrologic Sensitivity of Global Rivers to Climate Change. *Climatic Change*, *50*(1), 143–175. https://doi.org/10.1023/A:1010616428763

Noe, G. B., & Hupp, C. R. (2007). Seasonal variation in nutrient retention during inundation of a short-hydroperiod floodplain. *River Research and Applications*, *23*(10), 1088–1101. https://doi.org/10.1002/rra.1035

Ockenden, M. C., Hollaway, M. J., Beven, K. J., Collins, A. L., Evans, R., Falloon, P. D., Forber, K. J., Hiscock, K. M., Kahana, R., Macleod, C. J. A., Tych, W., Villamizar, M. L., Wearing, C., Withers, P. J. A., Zhou, J. G., Barker, P. A., Burke, S., Freer, J. E., Johnes, P. J., … Haygarth, P. M. (2017). Major agricultural changes required to mitigate phosphorus losses under climate change. *Nature Communications*, *8*(1), Article 1. https://doi.org/10.1038/s41467-017-00232-0

Perakis, S. S. (2002). Nutrient limitation, hydrology and watershed nitrogen loss. *Hydrological Processes*, *16*(17), 3507–3511. https://doi.org/10.1002/hyp.5078

Perakis, S. S., Matkins, J. J., & Hibbs, D. E. (2012). N2-Fixing Red Alder Indirectly Accelerates Ecosystem Nitrogen Cycling. *Ecosystems*, *15*(7), 1182–1193. https://doi.org/10.1007/s10021-012-9579-2

Poff, N. L. (1992). Regional Hydrologic Response to Climate Change: An Ecological Perspective. In P. Firth & S. G. Fisher (Eds.), *Global Climate Change and Freshwater Ecosystems* (pp. 88–115). Springer. https://doi.org/10.1007/978-1-4612-2814-1_5

Poff, N. L., Allan, J. D., Bain, M. B., Karr, J. R., Prestegaard, K. L., Richter, B. D., Sparks, R. E., & Stromberg, J. C. (1997). The Natural Flow Regime. *BioScience*, *47*(11), 769–784. https://doi.org/10.2307/1313099

PRISM Climate Group. (2015). *PRISM Gridded Climate Data* [Dataset]. https://www.prism.oregonstate.edu/recent/

R Core Team. (2023). *R: A language and environment for statistical computing.* [Computer software]. R Foundation for Statistical Computing. https://www.R-project.org/

Redfield, A. C. (1958). The Biological Control of Chemical Factors in the Environment. *American Scientist*, *46*(3), 230A – 221.

Regional Data Profile: Population and Households. (2017, March 27). Puget Sound Regional Council. https://www.psrc.org/rdp-population

Reidy Liermann, C. A., Olden, J. D., Beechie, T. J., Kennard, M. J., Skidmore, P. B., Konrad, C. P., & Imaki, H. (2012). Hydrogeomorphic Classification of Washington State Rivers to Support Emerging Environmental Flow Management Strategies. *River Research and Applications*, *28*(9), 1340–1358. https://doi.org/10.1002/rra.1541

Reiter, M., Heffner, J. T., Beech, S., Turner, T., & Bilby, R. E. (2009). Temporal and Spatial Turbidity Patterns Over 30 Years in a Managed Forest of Western Washington1. *JAWRA Journal of the American Water Resources Association*, *45*(3), 793–808. https://doi.org/10.1111/j.1752-1688.2009.00323.x

Rice, J. S., & Emanuel, R. E. (2017). How are streamflow responses to the El Nino Southern Oscillation affected by watershed characteristics? *Water Resources Research*, *53*(5), 4393–4406. https://doi.org/10.1002/2016WR020097

Rollinson, V. R., Granger, J., Clark, S. C., Blanusa, M. L., Koerting, C. P., Vaudrey, J. M. P., Treibergs, L. A., Westbrook, H. C., Matassa, C. M., Hastings, M. G., & Tobias, C. R. (2021a). Seasonality of nitrogen sources, cycling, and loading in a New England river discerned from nitrate isotope ratios. *Biogeosciences*, *18*(11), 3421–3444. https://doi.org/10.5194/bg-18-3421-2021

Rollinson, V. R., Granger, J., Clark, S. C., Blanusa, M. L., Koerting, C. P., Vaudrey, J. M. P., Treibergs, L. A., Westbrook, H. C., Matassa, C. M., Hastings, M. G., & Tobias, C. R. (2021b). Seasonality of nitrogen sources, cycling, and loading in a New England river discerned from nitrate isotope ratios. *Biogeosciences*, *18*(11), 3421–3444. https://doi.org/10.5194/bg-18-3421-2021

Rose, L. A., Elliott, E. M., & Adams, M. B. (2015). Triple Nitrate Isotopes Indicate Differing Nitrate Source Contributions to Streams Across a Nitrogen Saturation Gradient. *Ecosystems*, *18*(7), 1209–1223. https://doi.org/10.1007/s10021-015-9891-8

Schiff, S. L., Devito, K. J., Elgood, R. J., McCrindle, P. M., Spoelstra, J., & Dillon, P. (2002). Two adjacent forested catchments: Dramatically different NO3− export. *Water Resources Research*, *38*(12), 28-1-28–13. https://doi.org/10.1029/2000WR000170

Sebestyen, S. D., Ross, D. S., Shanley, J. B., Elliott, E. M., Kendall, C., Campbell, J. L., Dail, D. B., Fernandez, I. J., Goodale, C. L., Lawrence, G. B., Lovett, G. M., McHale, P. J., Mitchell, M. J., Nelson, S. J., Shattuck, M. D., Wickman, T. R., Barnes, R. T., Bostic, J. T., Buda, A. R., … Williard, K. W. J. (2019). Unprocessed Atmospheric Nitrate in Waters of the Northern Forest Region in the U.S. and Canada. *Environmental Science & Technology*, *53*(7), 3620–3633. https://doi.org/10.1021/acs.est.9b01276

Sebilo, M., Mayer, B., Nicolardot, B., Pinay, G., & Mariotti, A. (2013). Long-term fate of nitrate fertilizer in agricultural soils. *Proceedings of the National Academy of Sciences*, *110*(45), 18185–18189. https://doi.org/10.1073/pnas.1305372110

Seybold, E. C., Dwivedi, R., Musselman, K. N., Kincaid, D. W., Schroth, A. W., Classen, A. T., Perdrial, J. N., & Adair, E. C. (2022). Winter runoff events pose an unquantified continental-scale risk of high wintertime nutrient export. *Environmental Research Letters*, *17*(10), 104044. https://doi.org/10.1088/1748-9326/ac8be5

Sigler, W. A., Ewing, S. A., Wankel, S. D., Jones, C. A., Leuthold, S., Brookshire, E. N. J., & Payn, R. A. (2022). Isotopic signals in an agricultural watershed suggest denitrification is locally intensive in riparian areas but extensive in upland soils. *Biogeochemistry*, *158*(2), 251–268. https://doi.org/10.1007/s10533-022-00898-9

Sigman, D. M., Casciotti, K. L., Andreani, M., Barford, C., Galanter, M., & Böhlke, J. K. (2001). A Bacterial Method for the Nitrogen Isotopic Analysis of Nitrate in Seawater and Freshwater. *Analytical Chemistry*, *73*(17), 4145–4153. https://doi.org/10.1021/ac010088e

Sinha, E., & Michalak, A. M. (2016). Precipitation Dominates Interannual Variability of Riverine Nitrogen Loading across the Continental United States. *Environmental Science & Technology*, *50*(23), 12874–12884. https://doi.org/10.1021/acs.est.6b04455

Sinha, E., Michalak, A. M., & Balaji, V. (2017). Eutrophication will increase during the 21st century as a result of precipitation changes. *Science*, *357*(6349), 405–408. https://doi.org/10.1126/science.aan2409

Smits, A. P., Ruffing, C. M., Royer, T. V., Appling, A. P., Griffiths, N. A., Bellmore, R., Scheuerell, M. D., Harms, T. K., & Jones, J. B. (2019). Detecting Signals of Large-Scale Climate Phenomena in Discharge and Nutrient Loads in the Mississippi-Atchafalaya River Basin. *Geophysical Research Letters*, *46*(7), 3791–3801. https://doi.org/10.1029/2018GL081166

Smits, A. P., Schindler, D. E., Holtgrieve, G. W., Jankowski, K. J., & French, D. W. (2017). Watershed geomorphology interacts with precipitation to influence the magnitude and source of CO2 emissions from Alaskan streams. *Journal of Geophysical Research: Biogeosciences*, *122*(8), 1903–1921. https://doi.org/10.1002/2017JG003792

Sobota, D. J., Harrison, J. A., & Dahlgren, R. A. (2009). Influences of climate, hydrology, and land use on input and export of nitrogen in California watersheds. *Biogeochemistry*, *94*(1), 43–62. https://doi.org/10.1007/s10533-009-9307-y

Soranno, P. A., Cheruvelil, K. S., Bissell, E. G., Bremigan, M. T., Downing, J. A., Fergus, C. E., Filstrup, C. T., Henry, E. N., Lottig, N. R., Stanley, E. H., Stow, C. A., Tan, P.-N.,

Wagner, T., & Webster, K. E. (2014). Cross-scale interactions: Quantifying multi-scaled cause–effect relationships in macrosystems. *Frontiers in Ecology and the Environment*, *12*(1), 65–73. https://doi.org/10.1890/120366

Soranno, P. A., Wagner, T., Collins, S. M., Lapierre, J.-F., Lottig, N. R., & Oliver, S. K. (2019). Spatial and temporal variation of ecosystem properties at macroscales. *Ecology Letters*, *22*(10), 1587–1598. https://doi.org/10.1111/ele.13346

Stackpoole, S., Sabo, R., Falcone, J., & Sprague, L. (2021). Long-Term Mississippi River Trends Expose Shifts in the River Load Response to Watershed Nutrient Balances Between 1975 and 2017. *Water Resources Research*, *57*(11), e2021WR030318. https://doi.org/10.1029/2021WR030318

Stets, E. G., Sprague, L. A., Oelsner, G. P., Johnson, H. M., Murphy, J. C., Ryberg, K., Vecchia, A. V., Zuellig, R. E., Falcone, J. A., & Riskin, M. L. (2020). Landscape Drivers of Dynamic Change in Water Quality of U.S. Rivers. *Environmental Science & Technology*, *54*(7), 4336–4343. https://doi.org/10.1021/acs.est.9b05344

Strahler, A. (1952). HYPSOMETRIC (AREA-ALTITUDE) ANALYSIS OF EROSIONAL TOPOGRAPHY. *GSA Bulletin*, *63*(11), 1117–1142. https://doi.org/10.1130/0016-7606(1952)63[1117:HAAOET]2.0.CO;2

Tallaksen, L. M. (1995). A review of baseflow recession analysis. *Journal of Hydrology*, *165*(1), 349–370. https://doi.org/10.1016/0022-1694(94)02540-R

Thornton, M. M., Shrestha, R., Wei, Y., Thornton, P. E., Kao, S.-C., & Wilson, B. E. (2020). Daymet: Daily Surface Weather Data on a 1-km Grid for North America, Version 4. *ORNL DAAC*. https://doi.org/10.3334/ORNLDAAC/1840

Tsunogai, U., Komatsu, D. D., Ohyama, T., Suzuki, A., Nakagawa, F., Noguchi, I., Takagi, K., Nomura, M., Fukuzawa, K., & Shibata, H. (2014). Quantifying the effects of clear-cutting and strip-cutting on nitrate dynamics in a forested watershed using triple oxygen isotopes as tracers. *Biogeosciences*, *11*(19), 5411–5424. https://doi.org/10.5194/bg-11-5411-2014

Tsunogai, U., Miyauchi, T., Ohyama, T., Komatsu, D. D., Nakagawa, F., Obata, Y., Sato, K., & Ohizumi, T. (2016). Accurate and precise quantification of atmospheric nitrate in streams draining land of various uses by using triple oxygen isotopes as tracers. *Biogeosciences*, *13*(11), 3441–3459. https://doi.org/10.5194/bg-13-3441-2016

Turner, R. E. (2024). Water quality at the end of the Mississippi River for 120 years: The agricultural imperative. *Hydrobiologia*, *851*(5), 1219–1239. https://doi.org/10.1007/s10750-023-05383-4

U.S. Gridded Standardized Precipitation Index (SPI) from nClimGrid-Monthly | Drought.gov. (n.d.). Retrieved September 25, 2023, from https://www.drought.gov/data-maps-tools/us-gridded-standardized-precipitation-index-spi-nclimgrid-monthly

USGS. (2023). *National Water Information System Data (USGS Water Data for the Nation)* [Dataset]. http://waterdata.usgs.gov/nwis

USGS Water Data for the Nation. (n.d.). Retrieved December 22, 2023, from https://waterdata.usgs.gov/nwis/

Van Meter, K. J., Basu, N. B., Veenstra, J. J., & Burras, C. L. (2016). The nitrogen legacy: Emerging evidence of nitrogen accumulation in anthropogenic landscapes. *Environmental Research Letters*, *11*(3), 035014. https://doi.org/10.1088/1748-9326/11/3/035014

Van Meter, K. J., Chowdhury, S., Byrnes, D. K., & Basu, N. B. (2020). Biogeochemical asynchrony: Ecosystem drivers of seasonal concentration regimes across the Great Lakes Basin. *Limnology and Oceanography*, *65*(4), 848–862. https://doi.org/10.1002/lno.11353

Van Meter, K. J., Van Cappellen, P., & Basu, N. B. (2018). Legacy nitrogen may prevent achievement of water quality goals in the Gulf of Mexico. *Science*, *360*(6387), 427–430. https://doi.org/10.1126/science.aar4462

Van Metre, P. C., Frey, J. W., Musgrove, M., Nakagaki, N., Qi, S., Mahler, B. J., Wieczorek, M. E., & Button, D. T. (2016). High Nitrate Concentrations in Some Midwest United States Streams in 2013 after the 2012 Drought. *Journal of Environmental Quality*, *45*(5), 1696–1704. https://doi.org/10.2134/jeq2015.12.0591

Venkiteswaran, J. J., Boeckx, P., & Gooddy, D. C. (2019). Towards a global interpretation of dual nitrate isotopes in surface waters. *Journal of Hydrology X*, *4*, 100037. https://doi.org/10.1016/j.hydroa.2019.100037

Vitousek, P. M., Aber, J. D., Howarth, R. W., Likens, G. E., Matson, P. A., Schindler, D. W., Schlesinger, W. H., & Tilman, D. G. (1997). Human Alteration of the Global Nitrogen Cycle: Sources and Consequences. *Ecological Applications*, *7*(3), 737–750. https://doi.org/10.1890/1051-0761(1997)007[0737:HAOTGN]2.0.CO;2

Von Prause, M. (2021). *Quality Assurance Monitoring Plan: Statewide River and Stream Ambient Water Quality Monitoring* (Publication 21-03-109). Washington Department of Ecology. https://apps.ecology.wa.gov/publications/SummaryPages/2103109.html

Wadnerkar, P. D., Andrews, L., Wong, W. W., Chen, X., Correa, R. E., White, S., Cook, P. L. M., Sanders, C. J., & Santos, I. R. (2021). Land use and episodic rainfall as drivers of nitrogen exports in subtropical rivers: Insights from δ15N-NO3−, δ18O-NO3− and

222Rn. *Science of The Total Environment*, *758*, 143669. https://doi.org/10.1016/j.scitotenv.2020.143669

Washington Department of Ecology. (2023). *Environmental Information Management System* (AMS001) [Dataset]. http://www.ecology.wa.gov/eim/

Webster, A. J., Douglas, T. A., Regier, P., Scheuerell, M. D., & Harms, T. K. (2022). Multi-Scale Temporal Patterns in Stream Biogeochemistry Indicate Linked Permafrost and Ecological Dynamics of Boreal Catchments. *Ecosystems*, *25*(5), 1189–1206. https://doi.org/10.1007/s10021-021-00709-6

Weitzman, J. N., Brooks, J. R., Mayer, P. M., Rugh, W. D., & Compton, J. E. (2021). Coupling the dual isotopes of water ($\updelta$ 2H and $\updelta$ 18O) and nitrate ($\updelta$ 15N and $\updelta$ 18O): A new framework for classifying current and legacy groundwater pollution. *Environmental Research Letters*, *16*(4), 045008. https://doi.org/10.1088/1748-9326/abdcef

Wells, N. S., Clough, T. J., Johnson-Beebout, S. E., Elberling, B., & Baisden, W. T. (2019). Effects of denitrification and transport on the isotopic composition of nitrate (δ18O, δ15N) in freshwater systems. *Science of The Total Environment*, *651*, 2228–2234. https://doi.org/10.1016/j.scitotenv.2018.10.065

Wilkinson, G. M., Walter, J., Fleck, R., & Pace, M. L. (2020). Beyond the trends: The need to understand multiannual dynamics in aquatic ecosystems. *Limnology and Oceanography Letters*, *5*(4), 281–286. https://doi.org/10.1002/lol2.10153

Wilusz, D. C., Harman, C. J., & Ball, W. P. (2017). Sensitivity of Catchment Transit Times to Rainfall Variability Under Present and Future Climates. *Water Resources Research*, *53*(12), 10231–10256. https://doi.org/10.1002/2017WR020894

Wise, D. R., & Johnson, H. M. (2011). Surface-Water Nutrient Conditions and Sources in the United States Pacific Northwest. *Journal of the American Water Resources Association*, *47*(5), 1110–1135. https://doi.org/10.1111/j.1752-1688.2011.00580.x

Wollheim, W. M., Vörösmarty, C. J., Peterson, B. J., Seitzinger, S. P., & Hopkinson, C. S. (2006). Relationship between river size and nutrient removal. *Geophysical Research Letters*, *33*(6). https://doi.org/10.1029/2006GL025845

Xia, X., Li, S., Wang, F., Zhang, S., Fang, Y., Li, J., Michalski, G., & Zhang, L. (2019). Triple oxygen isotopic evidence for atmospheric nitrate and its application in source identification for river systems in the Qinghai-Tibetan Plateau. *Science of The Total Environment*, *688*, 270–280. https://doi.org/10.1016/j.scitotenv.2019.06.204

Xie, J., Liu, X., Wang, K., Yang, T., Liang, K., & Liu, C. (2020). Evaluation of typical methods for baseflow separation in the contiguous United States. *Journal of Hydrology*, *583*, 124628. https://doi.org/10.1016/j.jhydrol.2020.124628

Zargar, A., Sadiq, R., Naser, B., & Khan, F. I. (2011). A review of drought indices. *Environmental Reviews*, *19*(NA), 333–349. https://doi.org/10.1139/a11-013

Zhang, Q., & Hirsch, R. M. (2019). River Water-Quality Concentration and Flux Estimation Can be Improved by Accounting for Serial Correlation Through an Autoregressive Model. *Water Resources Research*, *55*(11), 9705–9723. https://doi.org/10.1029/2019WR025338

Zhang, T., Hoell, A., Perlwitz, J., Eischeid, J., Murray, D., Hoerling, M., & Hamill, T. M. (2019). Towards Probabilistic Multivariate ENSO Monitoring. *Geophysical Research Letters*, *46*(17–18), 10532–10540. https://doi.org/10.1029/2019GL083946

Zhang, Y., Wallace, J. M., & Battisti, D. S. (1997). ENSO-like Interdecadal Variability: 1900–93. *Journal of Climate*, *10*(5), 1004–1020. https://doi.org/10.1175/1520-0442(1997)010<1004:ELIV>2.0.CO;2